MEASUREMENT AND ANALYSIS OF COULOMB (d,p) STRIPPING TO STATES IN ^{117}Sn, ^{123}Sn, AND ^{125}Sn

by

Paul Langford Carson

A Dissertation Submitted to the Faculty of the

DEPARTMENT OF PHYSICS

In Partial Fulfillment of the Requirements
For the Degree of

DOCTOR OF PHILOSOPHY

In the Graduate College

THE UNIVERSITY OF ARIZONA

1 9 7 2

THE UNIVERSITY OF ARIZONA

GRADUATE COLLEGE

I hereby recommend that this dissertation prepared under my direction by Paul Langford Carson entitled Measurement and Analysis of Coulomb (d,p) Stripping to States in ^{117}Sn, ^{123}Sn, and ^{125}Sn be accepted as fulfilling the dissertation requirement of the degree of Doctor of Philosophy

L. C. McIntyre Jr. — Oct 6, 1971
Dissertation Director — Date

After inspection of the final copy of the dissertation, the following members of the Final Examination Committee concur in its approval and recommend its acceptance:*

Arnold J. Sherwood — Oct. 15, 1971

Chang-yun Fan — Oct. 15, 1971

[illegible] — Oct 15, 1971

[illegible] — Oct 15, 1971

*This approval and acceptance is contingent on the candidate's adequate performance and defense of this dissertation at the final oral examination. The inclusion of this sheet bound into the library copy of the dissertation is evidence of satisfactory performance at the final examination.

STATEMENT BY AUTHOR

This dissertation has been submitted in partial fulfillment of requirements for an advanced degree at The University of Arizona and is deposited in the University Library to be made available to borrowers under rules of the Library.

Brief quotations from this dissertation are allowable without special permission, provided that accurate acknowledgment of source is made. Requests for permission for extended quotation from or reproduction of this manuscript in whole or in part may be granted by the head of the major department or the Dean of the Graduate College when in his judgment the proposed use of the material is in the interests of scholarship. In all other instances, however, permission must be obtained from the author.

SIGNED: Paul L. Carson

ACKNOWLEDGMENTS

The author is deeply indebted to Professor Laurence C. McIntyre, Jr., for suggesting this research, and for his advice and assistance in all phases of the work. The author is also thankful to Professors Douglas J. Donahue, John D. McCullen, and Arnold Sherwood for many helpful discussions. Many people were helpful in furnishing results of their unpublished work. In particular, Professor P. D. Kunz of the University of Colorado, who furnished the program DWUCK and explained its use and contents.

The author wishes to acknowledge the help of his associate, D. L. Barker, who helped construct some of the equipment and assisted in data acquisition. In addition, the author is grateful to Drs. K. S. Burton, M. J. Wozniak, R. L. Hershberger, J. E. Cummings, and A. S. Goodman, and Messrs. D. Rickel, J. Tipton, and C. Ceccon. All participated in helpful discussions related to this research and helped develop equipment and techniques of use to us all. Professor Stanley Bashkin has been a driving force behind the Van de Graaff Laboratories, and Mr. Peter Stoss has kept the Van de Graaff and much of the other laboratory equipment in excellent working condition.

Very special thanks are due to my wife, Patricia, who has been a constant help and source of encouragement.

TABLE OF CONTENTS

TABLE OF CONTENTS--Continued

LIST OF TABLES

LIST OF ILLUSTRATIONS

LIST OF ILLUSTRATIONS--Continued

ABSTRACT

The nuclear reactions $^{116}Sn(d,p)^{117}Sn$, $^{122}Sn(d,p)^{123}Sn$, and $^{124}Sn(d,p)^{125}Sn$ have been studied at incident deuteron energies between 4.35 and 5.55 MeV. Below 5.2-MeV excitation energy, 52 levels are observed in ^{117}Sn, 49 in ^{123}Sn, and 49 in ^{125}Sn. Many of the upper levels in all three nuclei are previously unreported, as is the 0.859-MeV level in ^{125}Sn. Comparison is made between our results and those of other experiments to help establish the orbital angular momentum transfer and total angular momentum of the observed levels.

Angular distributions of the differential cross section at several incident deuteron energies have been measured for certain states of interest in ^{117}Sn, ^{123}Sn, and ^{125}Sn. Angular distributions are tabulated for all resolved levels in the $^{116}Sn(d,p)^{117}Sn$ reaction at 5.35 MeV, and the $^{124}Sn(d,p)^{125}Sn$ reaction at 5.55 MeV. Cross sections at 160° with E_d = 5.15 MeV are reported for all observed levels in ^{123}Sn. Excitation functions for the $^{116}Sn(d,p)^{117}Sn$ reaction at deuteron energies between 4.35 and 5.55 MeV in steps of 100 keV were measured at 160° for the first three states in ^{117}Sn.

A DWBA stripping analysis of the angular distributions and excitation functions is discussed, and values for the reduced width and spectroscopic factor are given. The spectroscopic factors are relatively insensitive to the optical-model parameters for the deuteron and proton. Values of the spectroscopic factor for a given level at all

incident deuteron energies are consistent to better than 10%. The spectroscopic factor, but not the reduced width, is quite sensitive to the method of calculating the neutron bound state wave function. The spectroscopic factors are estimated to be accurate to approximately 15%.

Comparison of the present spectroscopic factors with those obtained from other experiments reveals general agreement with most of the other experiments. Occupation parameters from the experimental spectroscopic factors are compared with results from recent pairing theory calculations. It is concluded that pairing theory can describe fairly accurately the filling of shell-model orbits in the ground state of even tin isotopes, and that the lowest levels of the odd tin isotopes can be described as predominantly one-quasi-particle states.

CHAPTER I

INTRODUCTION

The tin isotopes, with a closed shell of protons and a wide range of neutron numbers, offer special opportunities for studying nuclear structure and nuclear reactions. The nuclear structure is relatively simple and has been represented fairly accurately by shell-model calculations using pairing theory [1-7]. One is able to measure various quantities as the N=50 to 82 neutron shell is filled and compare them with experiment.

In a comprehensive study of (d,p) stripping and (d,t) pickup reactions at 15 MeV on the available isotopes from A=112 to 124, Schneid, Prakash, and Cohen [8] obtained, among other things, spectroscopic factors and corresponding occupation parameters for the active neutron orbits. The spectroscopic factors were obtained from the stripping cross sections by comparison with distorted-wave Born approximation (DWBA) calculations of the cross sections. For the three orbits which are filling most rapidly in the available tin isotopes, the $3s_{\frac{1}{2}}$, $2d_{\frac{3}{2}}$, and $1h_{11/2}$, the experimental values agree with recent calculations of occupation parameters [4,5,9] to within the rather large uncertainties present in DWBA analysis at the energy used by Schneid et al. [8].

Many uncertainties in DWBA theory for the (d,p) reaction on heavy nuclei like tin are reduced if the incident deuteron energy is

sufficiently below the Coulomb barrier, and if the Q value of the reaction is sufficiently small. Also it is possible under these conditions to extract a reduced width which is independent of the assumed bound state neutron wave function [10,11].

We have studied the reactions $^{116}Sn(d,p)^{117}Sn$, $^{122}Sn(d,p)^{123}Sn$, and $^{124}Sn(d,p)^{125}Sn$ at incident deuteron energies down to approximately one half the Coulomb barrier in order to obtain reduced widths and more accurate spectroscopic factors and to assess the reliability of these measurements. In Chapter V, spectroscopic factors and their change with neutron number are compared with occupation parameters from simple pairing theory and with results from other experiments, including those of Schneid et al. [8]. In the process of studying the reactions, we have observed new levels in ^{117}Sn, ^{123}Sn, and ^{125}Sn, and have associated levels not previously reported in stripping reactions with levels observed in pickup reactions [11,12] and gamma decay [13].

Much theoretical [11,14] and experimental effort has been devoted to investigating the possibility that more reliable spectroscopic factors may be obtained from DWBA analysis of neutron stripping reactions at incident energies below the Coulomb barrier than at the usual energies above the Coulomb barrier. There are several reasons for thinking that this might be the case, particularly when both the incident and outgoing particle energies are well below the Coulomb barrier so the distorted waves are attenuated rapidly near the nuclear surface. The bound state neutron wave function falls off slowly with radius, so the overlap with the incident and outgoing distorted waves occurs

predominantly outside the nuclear radius in a region where many of the uncertainties in the DWBA method are minimized. The Born approximation is more valid since the reaction channels are very weak compared to the incident elastic channel. The neglect of compound nucleus effects is less serious, and simplifying assumptions about the internal structure of multinucleon projectiles should be more valid. Most importantly, the distorted waves are relatively insensitive at the low energies to the uncertain nuclear optical-model potentials. Under very favorable conditions of low bombarding energy, near zero Q value, and heavy targets, the nuclear potentials for the distorted waves may be omitted.

The effect of these advantages has been demonstrated for many (d,p) reactions of practical interest for which relatively consistent spectroscopic factors have been obtained over a range of subcoulomb energies and/or with a variety of acceptable optical-model parameters [10,15-20]. Neglecting the uncertainty in the bound state neutron wave function which affects reactions both above and below the Coulomb barrier [19], spectroscopic factors reliable to approximately 10% have been reported for Coulomb stripping compared to approximately 30% above the Coulomb barrier [14,15,16].

Some of the heavier isotopes of tin were chosen for the present experiment because the ground state Q value of the (d,p) reaction to odd tin isotopes decreases with increasing mass. A lower Q value for the reaction to a given state means the outgoing proton is at a lower energy and the bound state neutron wave function falls off more slowly with radius thus enabling more accurate calculations and yielding higher cross sections.

In comparison with the Coulomb barrier of approximately 9 MeV in tin, the lowest proton energy of interest was approximately 4 MeV. The highest proton energy of interest was approximately 10 MeV from the (d,p) reaction to the ground state of ^{117}Sn at 5.35 MeV bombarding energy. The zero orbital angular momentum transfer in this case favors a smaller interaction radius for this reaction, thus making it the most sensitive to optical-model parameters and compound nucleus effects. The effect of various optical-model parameters on the calculated differential cross section for the ground state and first excited state of ^{117}Sn was tested. Excitation functions were measured at one angle for the first three states in ^{117}Sn from 4.35 to 5.35 MeV to check for the smooth variation with energy expected of pure stripping reactions. As a final reliability check and to obtain accurate averaged results, spectroscopic factors were extracted from angular distributions for several states from all three reactions at several incident deuteron energies.

The major uncertainty remaining in the spectroscopic factors is due to our lack of knowledge of how to treat the bound state neutron wave function. We have followed the usual separation energy prescription for determining the potential well depth. We have tried to obtain the best possible potential well parameters for use with that prescription, and have assessed the effects of those parameters on the spectroscopic factors.

The calculated DWBA cross section for Coulomb stripping is dependent only on the tail of the bound state neutron wave function, and only the normalization of the tail is uncertain. A reduced width which

is proportional to the spectroscopic factor times the square of the bound state neutron wave function at some large radius R_o is independent of the uncertainties in the wave function [10,11]. To test another method of calculating bound state wave functions one must merely calculate the value of the new wave function at R_o to obtain spectroscopic factors from our reported reduced widths.

Experimental procedures including methods of data analysis to obtain energy calibrations and cross sections are discussed in Chapter II. In Chapter III, experimental results including excitation energies, angular distributions and excitation functions are presented. The angular distributions at these bombarding energies are not very sensitive to orbital angular momentum transfer ℓ_n and are certainly not sensitive to total angular momentum transfer j. Our cross sections and excitation energies are compared in Chapter III with results of other experiments to establish the ℓ_n and j value assignments of states we have observed.

Explanation of the DWBA calculations is included in Chapter IV. The determination of important parameters in the calculations is explained and the sensitivity of spectroscopic factors and reduced widths to various parameters is discussed. The extracted values of the spectroscopic factors and reduced widths are presented.

In Chapter V, the spectroscopic factors are compared with other experimental values and with the predictions of pairing theory for the low-lying states. A summary and conclusions are presented in Chapter VI.

CHAPTER II

EXPERIMENTAL PROCEDURES

Experimental Arrangement

The experiments described in this dissertation were carried out in the Van de Graaff Laboratory of the University of Arizona. Deuteron beams up to 5.55 MeV were available from the High Voltage Engineering Corporation Model CN Van de Graaff. A new beam line was established with control slits and viewing quartz approximately 3.1 meters from the axis of rotation of the 90° bending magnet. The scattering chamber was installed with the target position 66 cm from the control slits. The control slits and scattering chamber were within the focal range of the Van de Graaff and 90° bending magnet system.

The beam energy was selected in the 90° bending magnet. The magnetic field was monitored with a Varian FH-20 Hall-effect gaussmeter, whose probe was firmly attached between the pole faces of the bending magnet. The beam energy was calibrated for this beam line to 3 keV precision using the 1881-keV threshold in the $^{7}Li(p,n)^{7}Be$ reaction. On a separate occasion, the beam energy was calibrated at 4806 keV to 5 keV precision using a resonance in proton elastic scattering on ^{12}C [21]. The two measurements were consistent to 1 keV using the non-relativistic formula for a charged particle in a magnetic field,

$$E = (B^2Z^2)/MK \ . \qquad (1)$$

The constant, K, was determined to be 405.64 $(\text{gauss})^2/(\text{AMU-MeV})$ using a proton mass of 1 AMU. Using an integer mass for the deuteron as was done gives a 5-keV error at 5-MeV incident deuteron energy. A recent measurement of the $^7\text{Li}(p,n)^8\text{Be}$ threshold by D. L. Barker and L. C. McIntyre [22] showed a change in the constant K of 0.2% over a one-year period. They also determined that with protons at 1881 keV, the beam energy changes only 4 keV for each cm change in the vertical position of the control slits.

The scattering chamber was developed from an existing chamber and stand. The chamber and stand were built by A. S. Goodman for a different type of experiment.

Drawings of the scattering chamber viewed from the top and from the side are presented in Figs. 1 and 2, respectively. A given letter labels the same parts in both drawings. Detectors can be mounted within 30° of each other, and positioned from 170° to 0° from the beam direction on either side of the beam, cables permitting. The detector angle is set from outside by manually turning the small 10-cm gear which drives the 23-cm gear-scattering table. When set at integer angles, the scattering table position may be read directly through the glass viewing port to ± 0.1°. The positioning of a detector relative to the beam direction was checked by measuring elastic scattering between 21° and 25° on either side of the beam. The detector angle at that time was found to be accurate to ± 0.1°.

The collimating apertures used throughout these experiments for the movable detectors were 0.475 cm in diameter. These safely defined a

Fig. 1. Top view of the 44-cm scattering chamber.

A cross section through the horizontal plane of the beam line is shown. Major parts below the beam line are included. Parts are identified as follows:

A. Stainless steel chamber
B. Port for 12-pin electrical feedthrough
C. Ten-cm gear on shaft to outside
D. Tantalum Faraday cup
E. Tantalum electron suppressor ring
F. Twenty-three-cm aluminum gear-scattering table
G. Target and holder
H. Teflon insulators, supports, and bearings
I. Tantalum-surfaced backscatter shield
J. Detector angle indicator
K. Aluminum arm with dovetail track
L. Detector collimating apertures
M. Silicon surface-barrier detector
N. Brass detector mount
O. Cooling line
P. Vacuum port
Q. Tantalum anti-scattering apertures
R. Carbon beam-defining aperture
S. Tantalum beam-defining aperture
T. Removable beam collimator assembly
U. Stray beam shield
V. Monitor detector aperture
W. Monitor detector and mount
X. Microdot detector cable feedthrough
Y. Stainless steel detector coolant feedthrough
Z. Tantalum anti-reaction aperture
a. Insulators

Parts C, F, H, J, K, O, P are below the horizontal plane of the beam line.

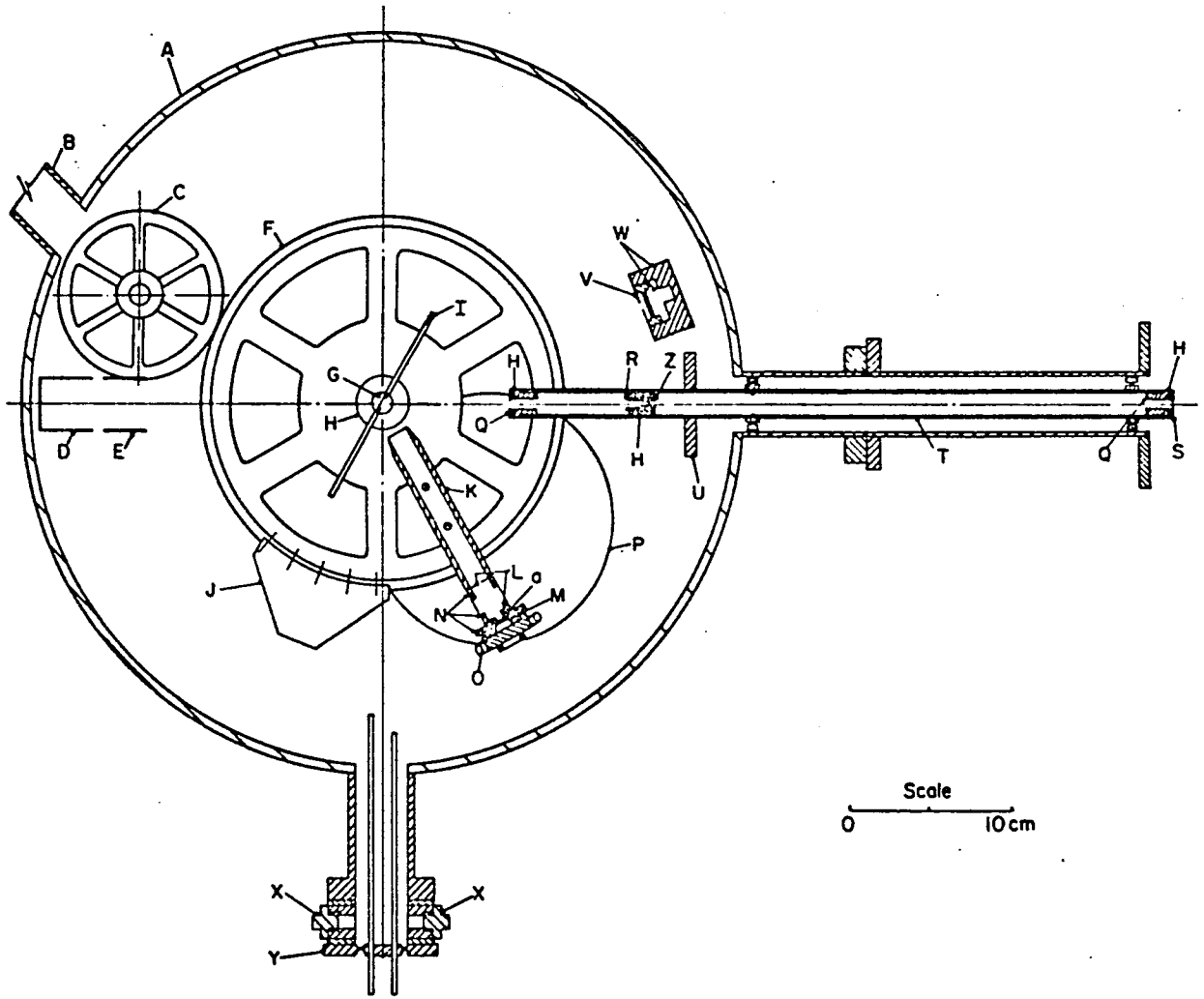

Fig. 1. Top view of the 44-cm scattering chamber.

Fig. 2. Cross section drawing of the 44-cm scattering chamber.

The parts are identified as follows:

A. Stainless steel chamber
D. Tantalum Faraday cup
E. Tantalum electron suppressor ring
F. Aluminum gear-scattering table
G. Three-position target holder
H. Teflon insulators, supports and bearings
I. Tantalum-surfaced backscatter shield
K. Aluminum arm with dovetail track
L. Detector collimating apertures
M. Silicon surface-barrier detector
N. Detector mounts, brass
P. Small arc of 15-cm vacuum port
Q. Tantalum anti-scattering aperture
R. Carbon beam-defining aperture
T. Removable beam collimator assembly
U. Stray beam shield
Z. Tantalum anti-reaction aperture
a. Insulators
b. Electron suppression magnets
c. Removable stainless steel top
d. Target angle dial
e. Target position scale
f. Glass viewing port

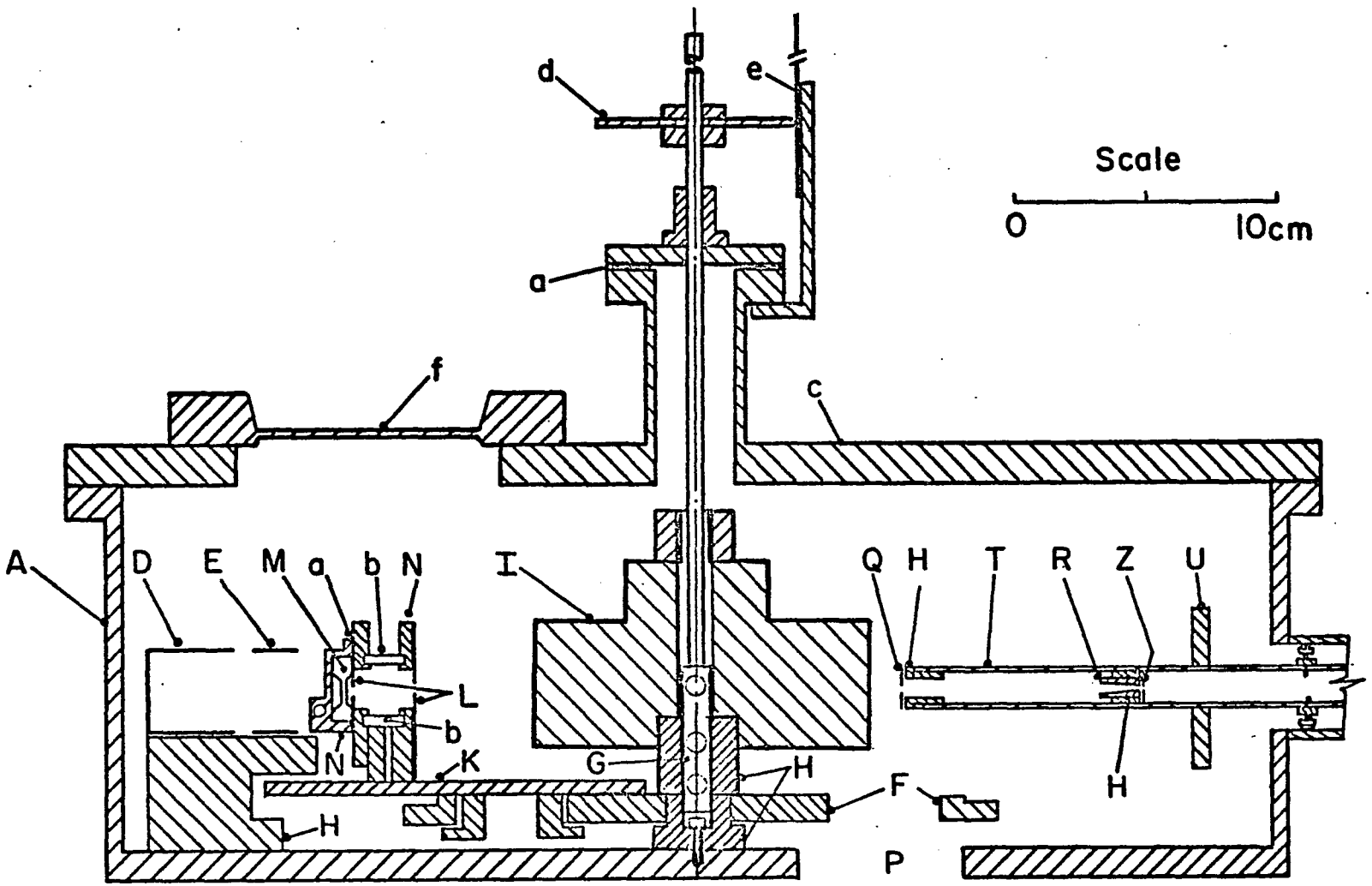

Fig. 2. Cross section drawing of the 44 cm scattering chamber.

large sensitive area on the smallest detectors used, 25 mm^2. The detector collimators were separated by 2.2 cm. The back collimator was 13.2 cm from the target. In this geometry the movable detectors subtended a solid angle about the target of 1.02 millisteradians. The solid angle on three such detector assemblies was shown to be the same within the 1.4% statistics obtained when an alpha particle source was placed in the target position. The fixed monitor detector was covered with a 0.32 cm diameter aperture, 17.6 cm from the target. The aperture was centered at a scattering angle of 160.5°. Thus the monitor detector subtended a solid angle of 0.264 millisteradians. Although several detectors were often mounted on the scattering table, only one detector was used in a given run because the available routing to the pulse-height analyzer memory was possibly too slow, and all 1024 channels of the memory were usually needed for one detector. Also, at any given time, one detector would prove far superior in resolution.

The target angle could be determined to ± 0.5° and the target height to ± 0.04 cm. Target angles were set in a reflection geometry for scattering angles greater than 100° and in a transmission geometry for scattering angles of 100° or less. The target angle was determined in the following manner. Uniform targets are assumed. If the differential energy loss for the incident deuterons is R times greater than that for the outgoing protons of interest, then the minimum proton energy resolution loss due to target thickness is obtained in the case of reflection geometry by minimizing R sec φ_d + sec φ_p, where φ_d and φ_p are the angles less than 90° between the normal to the target and the direction of the deuterons and protons respectively. In the transmission

geometry the best proton resolution is obtained if R sec φ_d = sec φ_p. A value of 2 was used for R which is appropriate for approximately 4.8 MeV deuterons and 7 MeV protons.

The beam collimator assembly was constructed from a 40.4 cm length of 1.6 cm O.D. stainless steel pipe. The whole assembly could be removed from inside the chamber. The current on any beam-defining aperture as well as the current on the target or Faraday cup, could be read in the control room. The detector ground was insulated from the chamber.

The beam-defining apertures used were 0.24 cm in diameter. The front one was made of tantalum and was placed 41.2 cm from the target. The back beam-defining aperture was 15.7 cm from the target. It was made of carbon to minimize elastic scattering, and was covered by a tantalum aperture of slightly larger diameter to reduce neutron production. Two tantalum anti-scattering apertures 0.32 cm in diameter were used. The back aperture was placed 8.3 cm in front of the target, and the front one was fixed 1.7 cm behind the front beam-defining collimator. Although this collimation could allow a ± 0.5° uncertainty in the beam direction and a 0.46 cm diameter beam spot on the target, such large deviations were never realized in practice. During alignment, the beam cross section was about as large as the collimators and the chamber was aligned to minimize the current on both collimators and give a circular beam spot on a quartz crystal in one of the target positions. Proper collimation is, of course, quite important in obtaining high resolution and being able to obtain accurate elastic cross sections and cross sections for peaks below the elastic peak.

Provisions were made for cooling the detectors. Twenty-pound blocks of dry ice could be placed in several inches of ethyl alcohol in an insulated chest. The alcohol was pumped with a standard sump pump used for evaporative coolers. The alcohol was pumped through copper tubing in each brass detector mount. Tygon or vinyl plastic tubing was used outside the chamber and tygon tubing was used for a flexible connection inside the chamber. The tygon outgassed rapidly at room temperature but did not affect the vacuum appreciably when cooled. When the chamber was fully loaded, detectors cooled, and the detector cables had outgassed for ten hours, the chamber pressure was on the order of 4×10^{-7} mm of mercury. The detectors could be warmed rapidly by attaching a second pump in room temperature alcohol to the chamber feedthroughs. Warm water up to body temperature was used for the final warming.

The movable detectors, as opposed to the fixed monitor detector, were always used in the half of the chamber which had the detector lead feedthroughs and the detector cooling line feedthroughs. Having both the cooling and the detector leads coming in the same port necessitated warming of the Microdot detector lead feedthroughs with a flow of warm air to prevent condensation. The tygon cooling lines also were too inflexible when cooled to dry ice temperatures to be able to flex enough for a detector rotation in the small space available. Imperial Eastman "Polyflo" maintains its flexibility at low temperatures. Also, standard vacuum tight fittings exist for that tubing. However, even at room temperature Polyflo is probably not flexible enough to replace the tygon in

the chamber in the present configuration. This less than ideal configuration was necessitated by the geometry of the chamber which we were not free to modify appreciably. A better configuration is to have the cooling lines and the detector leads come through the center of the bottom of the chamber, such that the feedthroughs rotate with the scattering table. This would allow shorter lines inside the chamber with less chance of their getting fouled. The cooling lines on the outside could be arranged to rotate while cold. At present the gate valve flange on the pump-out port covers the center of the bottom of the chamber.

Clearly it would also be better to have a long extension port for the Faraday cup. The tantalum-surfaced backscatter shield, labeled I in Figs. 1 and 2, was required to insure that the detectors at backward angles could not receive particles backscattered from the internal Faraday cup. When the target holder is raised, the backscatter shield rotates with the target holder, so the shield can be placed at any desired angle.

Electron suppression magnets were placed in the brass detector mounts. The 290 gauss field between the magnets is enough to deflect 20-keV electrons incident normal to the detectors so that the electrons will not reach the plane of the back detector collimator. The front fringing field should prevent low-energy electrons from making a tight spiral right into the detector. A 0.5-MeV proton is deflected by the suppression magnets only 30 μm at the back detector collimator. Spectra were never taken without the electron suppression magnets. The necessity of using them for high resolution spectra is well established [23].

Electronics and Detectors

Silicon surface-barrier detectors with a maximum depletion depth of 1000 μm were used in the experiments described in this dissertation. Two Ortec detectors of 200 mm^2-area performed well cooled and uncooled throughout the experiments, but at best had only 50-keV resolution. One was always used for the monitor detector. Most spectra were taken with a 25 mm^2-area detector from Princeton Gamma-Tech Inc. or its identical replacement. After being cooled and warmed up several times, both of the 25 mm^2 detectors suffered microplasma breakdown at less than 1/4-full bias at room temperature. The second detector clearly showed some recovery ability over a one-month time sitting at atmospheric pressure.

A block diagram of the usual electronics configuration is shown in Fig. 3. The detector signals were amplified by charge-sensitive Ortec 109 preamplifiers. The pulses were further amplified and shaped for maximum energy resolution with Ortec 410 amplifiers. The resolution of this basic amplifier system was determined with equivalent 8-MeV pulses from a precision pulser, using typical shaping including single differentiation and integration of 0.5 μsec time constant. With no detector, the system resolution was 7 keV FWHM. With the best detector, uncooled, 12-keV resolution was obtained with the pulser. The resolution under running conditions was limited by the thickness and non-uniformity of the targets to 23 keV FWHM.

A single channel analyzer was used to place a window on the Monitor detector peak produced by deuterons elastically scattered from the tin. The resulting logic signals were scaled. Care was taken to center the window on the elastics in the same manner for all runs.

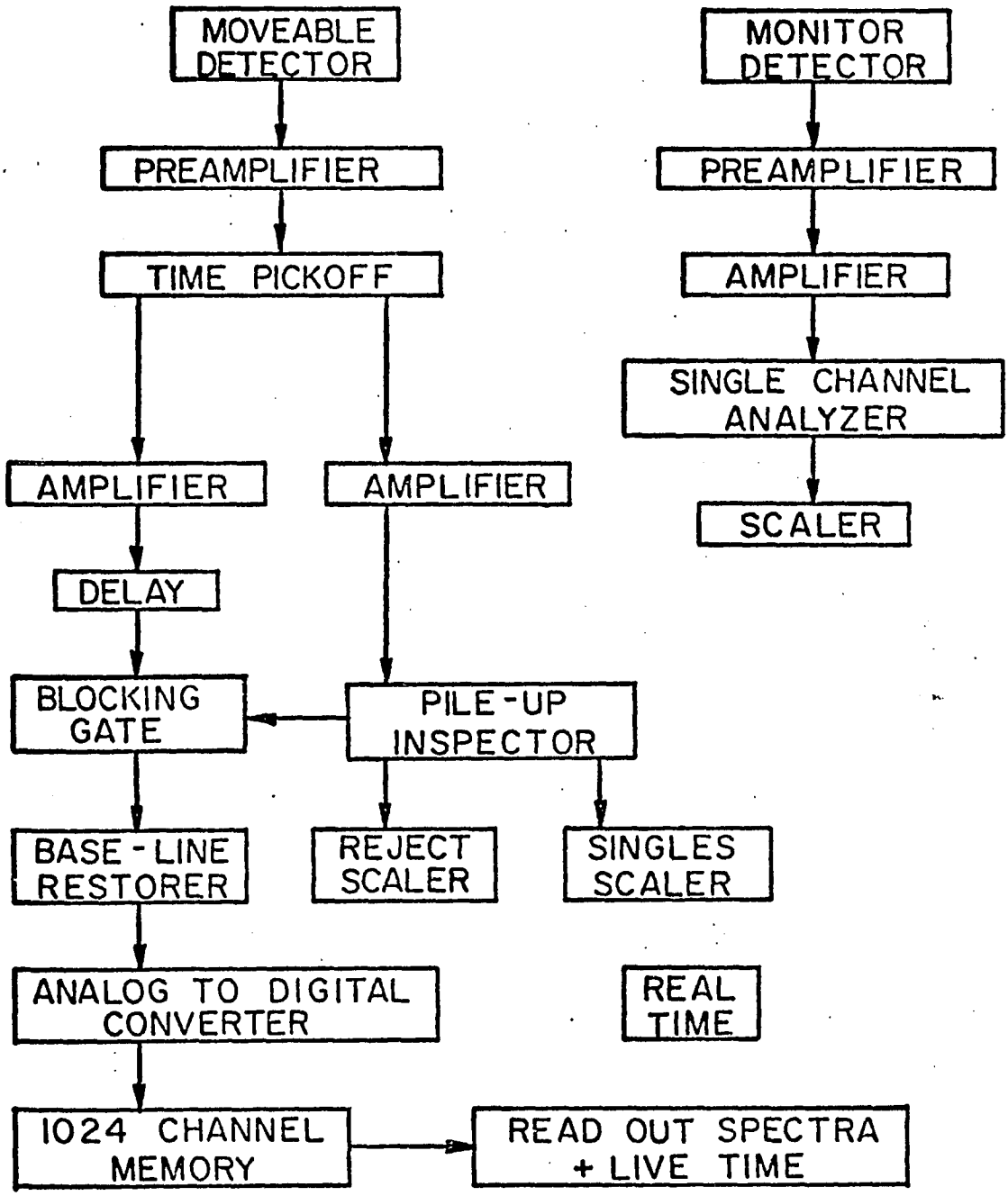

Fig. 3. Block diagram of the electronics arrangement.

Pulse pile-up within the resolving time of the multichannel analyzer was a clear problem in the present applications with an elastic count rate often 10^5 times higher than the reactions of interest. The fast time derivation of the Ortec 260 Time Pickoff produces fast logic signals for pulses including those much closer together than the resolving time of the multichannel analyzer. After slight amplification, the logic signals drove an Ortec 404A Pile-up Inspector. Pulses within a certain inspect interval triggered a blocking pulse of twice the duration of the inspect interval. For the duration of a blocking pulse applied to a d.c.-coupled Canberra Industries 1451 Linear Gate in its anti-coincidence mode, no linear signal is allowed to pass through the gate. The linear signals were suitably delayed such that two pulses within the usual 8-microsecond inspect interval of the pile-up inspector were blocked completely at the gate. The number of pulses rejected by the pile-up inspector were counted, as were the number allowed to pass. These numbers gave the system dead time in each run due to pile-up inspection.

An Ortec 438 Baseline Restorer and direct access to the ADC improved resolution considerably. The multichannel pulse-height analyzer consisted of a 161F 4096-channel ADC and 180M 1024-channel memory unit of the Nuclear Data Corporation. The analyzer live time was compared with a real time clock to obtain analyzer dead time. The analyzer live time was based on an internal clock subject to the same dead time as analyzed signals. The resulting dead time was then accurate, assuming a steady count rate.

Target Preparation

The three isotopes of tin used as targets were obtained from Oak Ridge National Laboratory in the form of metal powder. The most effective method developed for producing thin self-supporting targets with a small amount of material involved evaporating the metal in a high vacuum from a vertical tantalum tube approximately 0.28 cm in diameter. A tube 9 cm long was cut 3/4 of the way through, 2 1/2 cm from the top, and bent over 90° to allow the tin vapor to escape straight up. The bottom 2 1/2 cm was bent 90° the other direction. Near the bottom of the vertical section the tube was flattened and welded shut. The two ends were clamped to copper electrodes for resistive heating of the tube.

Tin was deposited on soaped glass microscope slides approximately 2.6 cm above the mouth of the tube. Target-size squares of tin were floated off in water. Surface tension of the water was reduced with photo-flo and the foils were lifted off with target holders. During evaporation, the tin did not stick to the soap, or even to 10 $\mu g/cm^2$ carbon foils, nearly as well as to clean glass. Approximately 10 targets, 0.8 cm in diameter of thickness from 200-400 $\mu g/cm^2$, were produced in one evaporation of 35 mg of ^{124}Sn. A few targets of ^{122}Sn were similarly obtained, ranging from 200-450 $\mu g/cm^2$. Targets of ^{116}Sn ranging from approximately 180-300 $\mu g/cm^2$ were evaporated with a tantalum tube. An earlier set of ^{116}Sn targets 500-800 $\mu g/cm^2$ thick were evaporated from a carbon crucible with an electron gun.

An analysis of the amount of ^{28}Si and other contaminants, present in the targets and in the material before evaporation, indicated

that the amount of these contaminants evaporated onto the targets can be reduced greatly by heating the material only enough to slowly evaporate the tin. This procedure was followed with ^{124}Sn targets. The temperature of the tantalum tube was raised at the end of the evaporation of the ^{116}Sn and ^{122}Sn targets. On these targets, the surface receiving the final evaporation had a dull grey to bluish cast indicating contamination.

Data Collection Procedures

At the beginning of a series of runs, the chamber was aligned as previously described in the discussion of the beam collimation assembly. Minimum slit scattering was essential for clean spectra; however, the beam could not be too well focused without endangering the target. A beam of 320 nA melted a hole in a ^{124}Sn target. Also, to obtain reasonable count rates the current on target had to be reduced to a level that could only be obtained by stopping much of the beam with the control slits and front collimator. It proved essential to have the beam focus in front of the target rather than after it. Under typical running conditions with 200 nA registered in the Faraday cup, the front and back collimators registered 25 and 10 nA respectively.

Run times were varied considerably to obtain reasonably consistent statistics. Ninety minutes was usual at 5.55 MeV and backward angles. This yielded better than 1000 microcoulombs of integrated beam current at 250 nA with 1.5% total dead time. Runs of seven hours with 8% dead time were common at lower energies and forward angles.

After each run, the spectra plus the pulse-height analyzer live time were listed, punched on paper tape, and plotted on a linear scale. Integrated beam current taken with an Elcor Model A309A integrator was recorded along with the run real time, and the number of pulses passed and rejected by the pile-up inspector.

Data Analysis

To facilitate reduction of the data on the University of Arizona's CDC 6400 computer, the spectra on paper tape were converted to punched cards using a tape-to-card converter or the fortran program TTC of R. L. Hershberger. Semi-log plots of the spectra on translucent paper were produced using the CALCOMP plotting routine SMLPLT. These could be overlaid to identify levels by size and kinematic shift.

The number of counts in peaks and their positions were determined several ways. Multiplets were often unfolded with the program Gaussian-II [24]. It fits up to ten peaks with symmetric or skewed Gaussians along with a quadratic or exponential background. The counts in many peaks and the error were determined by hand in the same manner as will now be described for the program ACK.

The position and total counts of most of the peaks were determined with the computer code ACK. This program requires as input the position and height of a background point on each side of each peak in a single run. A linear background is assumed. For each peak, the number of counts, A, the number of background counts below the peak, B, and the centroid are determined. The error calculated for A is $(A+2B)^{\frac{1}{2}}$. The number of counts in each peak of a given run and the error in that

number is normalized to give relative or absolute cross sections. Masses, ground state Q values, and known or estimated excitation energies for all the levels being studied plus possible contaminant levels can be included in the program input. Where suitable, an actual peak in the spectrum can be associated with a given level. Kinematics are calculated to yield center-of-mass scattering angle and outgoing particle energy for each level. To give the expected channel, x_{calc}, for each level, the outgoing particle energy is used with linear energy calibration parameters which are part of the program input. Where a peak has been associated with a level, the centroid of the peak, x, minus the expected position for the level, x_{calc}, is given.

To obtain an accurate, nonlinear energy calibration, the ACK output, $x-x_{calc}$, was plotted against the outgoing particle energy for each identified peak. An example of such an energy calibration procedure is demonstrated in Fig. 4 for the $^{122}Sn(d,p)^{123}Sn$ reaction at 160° with 5.15-MeV incident deuterons. As in all such plots, a smooth calibration curve, dashed curve in Fig. 4, could be drawn through the unobscured contaminant peaks from deuterons on ^{12}C, ^{16}O, and ^{28}Si. The excitation energies of these contaminant levels [25] and the ground state Q values [26] are well known. A second curve, the solid curve in Fig. 4, is drawn equidistant from the first, dashed, curve and passing through the ground state of the tin nucleus being studied. The deviation of the point for an excited state in the tin from the final curve gives the difference between the state's assumed excitation energy and the observed excitation energy. The amount the second curve had to be

Fig. 4. Energy calibration curve for a charged-particle spectrum.

Deuterons of 5.15 MeV were incident on ^{122}Sn and products were viewed at 160°. The deviation, $x-x_{calc}$, from a linear energy calibration with 10.09 keV/ch is plotted against outgoing particle energy, E_{out}, for each peak. Numbers above the points are excitation energies used with the linear energy calibration to obtain the expected position of the peak, x_{calc}, and the outgoing particle energy. The dashed curve is a fit to the contaminant. The solid curve is equidistant from the dashed curve and passes through the ^{123}Sn ground state doublet.

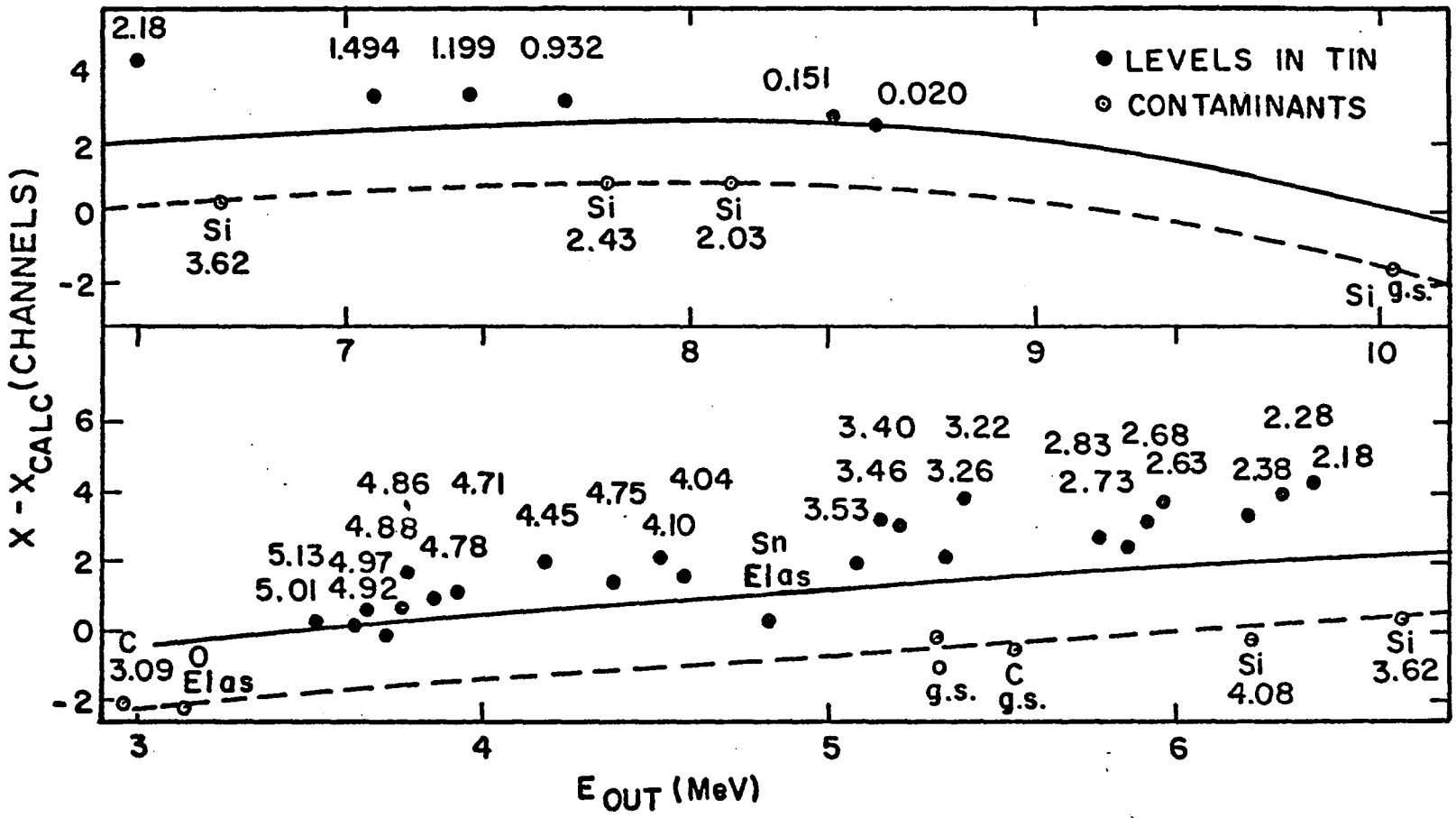

Fig. 4. Energy calibration curve for a charged-particle spectrum.

shifted is related to the error in the assumed Q value for the reaction leading to the ground state of the nucleus being studied. However, a correction must be made because most of the contaminants are on the downstream surface of the target, the last side evaporated. This is indicated by calibration plots at more forward angles in which the contaminant curve moves up relative to the tin (d,p) and elastic peaks.

A fortran program, Q, was written to do the above calibration procedure numerically. Program Q uses the output of ACK. A least squares fit of any chosen calibration peaks in a spectrum is made to a polynomial of up to tenth order to obtain an accurate energy calibration. The new Q value and excitation energy of each peak in the spectrum is then calculated. Agreement within a few keV is obtained between the numerical and graphical methods. The experimental results reported in this dissertation were obtained with the graphical method.

Normalization of Cross Sections

The absolute cross sections for the (d,p) reaction were obtained by assuming that for each energy studied the deuteron elastic scattering cross section on tin at 160° is accurately calculated with the DWBA program DWUCK using parameter set A as described in Chapter IV. Let $(d\sigma/d\Omega)(d,p)$ represent the measured laboratory differential cross section for some level at a given energy and scattering angle, and let $(d\sigma_E/d\Omega)(160°)$ represent the elastic cross section calculated with DWUCK for that energy at 160° and converted to the laboratory frame. Then,

$$\frac{d\sigma}{d\Omega}(d,p) = \frac{d\sigma_E}{d\Omega}(160°)\, R_\Omega\, \frac{N(d,p)}{M_E}, \qquad (2)$$

where M_E is the number of counts in the elastic peak in the monitor detector set at 160°, and N(d,p) is the number of counts observed in the movable detector for the peak whose cross section is being measured. The effective ratio of the solid angle of the monitor detector to that of the movable detector is represented by R_Ω.

The term effective solid angle ratio is used because the window on the elastics in the monitor spectra was necessarily wide to insure the elastic peak was not being attenuated by the single channel analyzer thresholds. Also, no background was subtracted from the monitor elastics. R_Ω was determined by comparing the number of elastic counts in the movable detector to the monitor yield for eleven runs using various energies and targets and with both detectors at 160°. Care was taken to determine the number of elastic counts in the movable detector in the same manner in which the smaller peaks from the (d,p) reaction would be handled. Uniform criteria for determining the number of elastic counts were used which were consistent to less than 3%, but an absolute error of 6% is assigned to R_Ω.

The DWBA calculations of the elastic cross section, $(d\sigma_E/d\Omega)(160°)$, were verified in two ways. First, the shape of the calculated and experimental elastic scattering angular distributions were compared. The angular distribution of calculated and experimental elastic scattering relative to Rutherford scattering is shown in Fig. 5 for 5.55-MeV deuterons on ^{124}Sn and for 4.55-MeV deuterons on ^{116}Sn. All the differential cross sections are given for the center-of-mass frame. The solid curves connect results calculated with the program DWUCK using

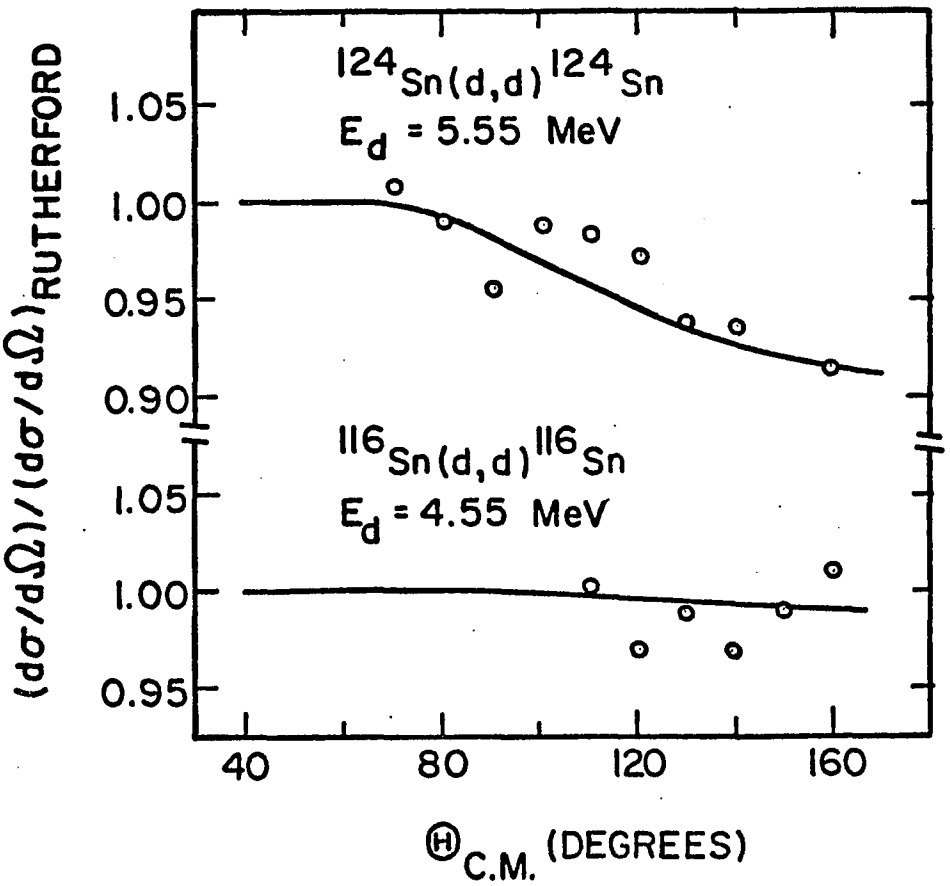

Fig. 5. Deuteron elastic scattering angular distributions.

The ratio of the experimental differential cross section in the center-of-mass frame to the Rutherford differential cross section is shown for deuterons elastically scattered from ^{124}Sn at 5.55 MeV and ^{116}Sn at 4.55 MeV. The solid curves connect results calculated with the program DWUCK using parameter set A as described in Chapter IV.

parameter set A. Deuteron parameter sets A and B discussed in Chapter IV as well as two other quite different deuteron parameter sets yielded elastic scattering consistent to 1% at all angles for 5.35-MeV deuterons incident on ^{116}Sn. Absolute normalization of the experimental points is determined by the theoretical curves. The agreement of the shape of the theoretical curves with the data justifies our use of the theoretical cross sections at 160° for normalization, since the elastic scattering at these energies and this target Z is known to be Rutherford at forward angles [10,16,27]. The experimental points are obtained from the same runs as the (d,p) angular distributions reported in the next chapter for the same targets and incident energies. These relatively smooth elastic angular distributions then serve to verify the accuracy of the shape of our (d,p) angular distributions.

A second test shows that our use of $(d\sigma_E/d\Omega)(160°)$ at all energies is equivalent to trusting the elastic scattering calculation only at 4.55 MeV where the deviation from Rutherford scattering is less than 1%. In seven runs taken under similar conditions on a ^{124}Sn target at 5.55, 5.15, and 4.55 MeV, the monitor elastic yield, integrated beam current, and calculated elastic cross section at the appropriate energy were used to give a number proportional to the target thickness for each run. The standard deviation of these numbers was ± 1.3% of the mean.

The above tests imply our use of the DWBA calculated elastic scattering at 160° for normalization contributes only about a 2% error to the (d,p) cross sections. The total normalization error for the (d,p) cross sections is estimated to be 7%.

CHAPTER III

EXPERIMENTAL RESULTS

The experimental results will be presented separately for each of the three reactions studied, $^{116}Sn(d,p)^{117}Sn$, $^{122}Sn(d,p)^{123}Sn$, and $^{124}Sn(d,p)^{125}Sn$. Results included in this chapter for all three reactions are:

1. The ground state Q values and the excitation energy of observed levels,

2. The angular distribution of the differential cross section for the population of certain states of interest at several incident deuteron energies.

The angular distribution of the differential cross section is tabulated for all resolved levels in ^{117}Sn and ^{125}Sn from the reactions at E_d = 5.35 MeV for ^{117}Sn and E_d = 5.55 MeV for ^{125}Sn. Cross sections at 160° are presented for all observed levels in ^{123}Sn. Excitation functions at incident deuteron energies from 4.35 to 5.35 MeV are presented for the first three levels in ^{117}Sn. Because angular distributions at subcoulomb energies are not very sensitive to orbital angular momentum transfer, and because our statistics are poor for weaker levels, comparisons are made with other experiments to help determine the orbital and total angular momentum of the observed states in all three nuclei studied. Discussion of spectroscopic factors is deferred to the following chapter on reaction theory and analysis.

The $^{116}Sn(d,p)^{117}Sn$ Reaction

Discussion of the Spectra

A typical charged particle spectrum resulting from incident deuterons at 5.35 MeV on a target enriched to 95.7% in ^{116}Sn is shown in Fig. 6. The target thickness is approximately 200 $\mu g/cm^2$. At this backward scattering angle of 160°, the peaks for (d,p) reactions on tin are higher relative to low-mass contaminants and elastic deuterons than at more forward angles. The deuteron elastic scattering peak is in channel 363. The elastics are not shown in this figure but are included in Figs. 12 and 15 for the other nuclei. The broad bump labeled pile-up of elastics is at twice the energy of deuterons scattered elastically from the ^{116}Sn. The reduction of the width of the pile-up from several MeV to around 250 keV was discussed in the previous section on electronics. At 50°, with a beam current much reduced from that allowable at backward angles, this pile-up peak is 18 times higher than the ^{117}Sn ground state peak. The kinematic shift of the pile-up peak to the region of the first three states in ^{117}Sn discouraged measurement of angular distributions for this nucleus at incident deuteron energies greater than 4.55 MeV and less than 5.15 MeV.

Ground State Q Value

The ground state Q value was determined for this reaction to be 4720 ± 8 keV. It was obtained from six energy calibration curves similar to the sample in Fig. 4 which is discussed in the previous chapter. This Q value measurement is in good agreement with the accepted value of

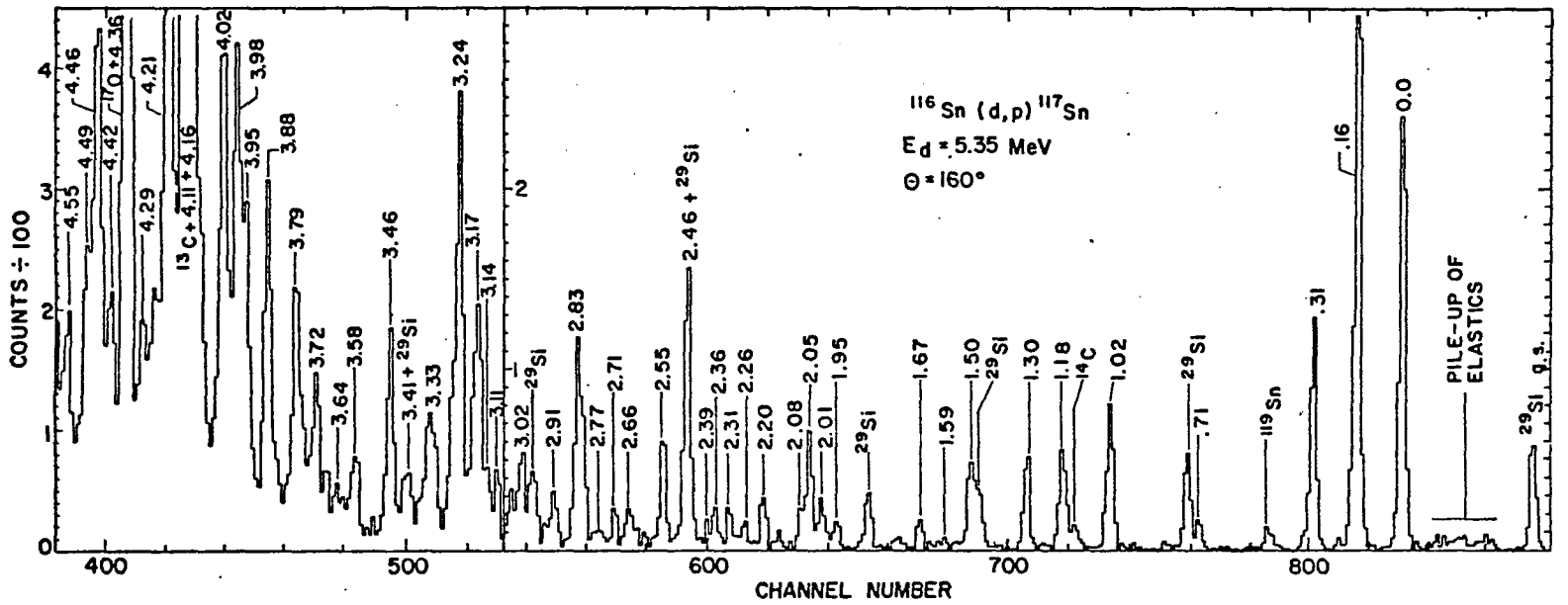

Fig. 6. Proton spectrum from the ^{116}Sn(d,p)^{117}Sn reaction at E_d = 5.35 MeV and θ = 160°.

4717 ± 5 keV of Ref.[26]and serves to help establish the less-well-known Q values for the (d,p) reaction to ^{123}Sn and ^{125}Sn.

Excitation Energies and
Possible ℓ_n and J Values

The measured excitation energies of states in ^{117}Sn are listed in Table 1. As with the other two nuclei studied only those levels are reported which were observed at different scattering angles and incident energies to separate them from light mass contaminants. The isotopic abundance of contaminant isotopes of tin were known for the targets. The expected positions of peaks from strong levels in the other isotopes of tin were followed carefully during the analysis. The excitation energies were determined from four energy calibration curves similar to Fig. 4. The energies are self-consistent to approximately ± 5 keV. They have an rms deviation of less than 9 keV from the energies of the levels up to 2.83 MeV determined in each of several recent γ-decay studies [13,28,29]. The energies of the levels around 4.55-MeV excitation have an absolute accuracy of better than 15 keV.

Also included in Table 1 are ℓ_n and J value assignments for states in ^{117}Sn based primarily on other experiments. Most of the assignments are from Ref. 8 based on their (d,p) angular distributions and the ratio test with their (d,t) cross sections at two angles. Assignments from other references are footnoted. Several small levels are identified with levels observed in the (p,d) reaction at 30 MeV [12], but it is of course not certain that the two experiments are exciting the same states. Uncertain assignments are enclosed in parentheses.

Table 1. Energy levels in ^{117}Sn.[a]

E_x (MeV)[b]	ℓ_n, $2\cdot J$[c]	E_x (MeV)[b]	ℓ_n, $2\cdot J$[c]	E_x (MeV)[b]	ℓ_n, $2\cdot J$[c]
0.000	s1	2.36		3.637	(p3)
0.157	d3	2.39	(s1)[f]	3.716	
0.313	h11	2.461	(f7)	3.785	(f7)
0.705	g7	2.545	(f7)	3.875	
1.015	d5,(3)[d]	2.656	(d)[f]	3.95	
1.178	d5	2.707		3.98	
1.302	(f7)	2.770	(d3)[e]	4.02	
1.499	d(5,3)	2.827	(p3)	4.11	
1.589		2.909		4.16	
1.668	(d5)	3.024		4.21	
1.948	(p+f,3+5)	3.113	(d3)[e]	4.29	
2.007	(p)[e]	3.14		4.36	
2.046	(f7)	3.172		4.42	
2.076	(s1)[e]	3.235	(f7)	4.46	
2.146	(d3)[e]	3.325	(p3)	4.49	
2.203		3.414		4.55	
2.256		3.464	(p3)		
2.31	(d5)	3.580			

[a]Excitation energies determined in the ^{116}Sn(d,p)^{117}Sn reaction are listed with probable orbital and total angular momentum assignments.

[b]Absolute uncertainties are less than 10 keV and 15 keV for energies listed with 1- and 10-keV precision respectively.

[c]All but the footnoted assignments are the same as in Ref.[8]. Assignments in parentheses are uncertain.

[d]See Ref. [28].

[e]See Ref. [12].

[f]See Ref. [30].

Several recent works have included level diagrams reviewing experimental observations on the low-lying states of ^{117}Sn [9,28,29]. The total angular momentum assignments for the first six states as well as the limits for the 1.499-MeV level have been verified in Ref. [28] on the basis of log-ft values and relative photon intensities from ^{117}Sb decay and in some cases by ^{117}In decay. In that work the 1.015-MeV level is clearly a doublet with a J=5/2 state at 1.020 MeV. It is unclear whether the lower member of the doublet is populated in the (d,p), (d,t), and (p,d) experiments. Refs. [8] and [12] report a $d_{\frac{5}{2}}$ assignment for the 1.015-MeV level. If the 1.015-MeV peak were a doublet composed of two levels of equal strength and separated by 15 keV, its width would be noticeably large in the present spectra. A typical peak adjacent to the 1.015-MeV peak was fitted best with a Gaussian of 21.5 ± 1.9-keV FWHM. That peak was then added to an identical peak 15 keV away. The resulting peak was fitted best with a Gaussian of 31.2 ± 0.9-keV FWHM. Fits to the 1.015-MeV peak at two angles did not show a significant increase in width over adjacent states.

The 1.499- and 1.589-MeV levels were tentatively assigned $d_{\frac{5}{2}}$ configurations in Ref. [8], as were all the ℓ_n=2 states with high excitation energies. The $d_{\frac{3}{2}}$ states were generally expected at much lower energies. Some $d_{\frac{3}{2}}$ strength for the 1.499-MeV level was reported in Ref. [12]. Gamma branching indicated J=5/2 or 3/2 for both the 1.499- and 1.589-MeV levels. In Ref. [12], $d_{\frac{3}{2}}$ assignments were made to high excited states on the basis of their angular distributions. However, they found no clear indication for either J assignment for the 1.499-MeV level.

The 1.589-MeV level is more weakly populated relative to the other ℓ_n=2 states in our experiment at 5.35 MeV than at 15 MeV [8]. A much larger value of ℓ_n could give that difference, but the spin assignment of 5/2 or 3/2 makes a large ℓ_n unlikely. The 1.589-MeV level may actually be the ℓ_n=1 or 5 state reported by Ref.[12] at 1.58 MeV. It should be noted, however, that the energy calibration in Ref.[12] appears about 30 keV high in this region.

The levels at 2.007, 2.076, 2.146, 2.770, and 3.113 MeV are previously unobserved in the (d,p) reaction, but may correspond to the levels observed with approximately the same energies in the pick-up reactions of Ref.[12]. In that paper they were assigned the configurations listed in Table 1 (footnote e). The 2.39- and 2.656-MeV levels may be respectively the ℓ_n=0 and ℓ_n=2 level observed at those excitation energies in Ref.[30]. The energy calibration in that paper seems to be within 10 keV of ours.

A level was observed in Ref.[12] at 2.83 MeV with the same $d_{\frac{3}{2}}$ assignment and the same strength as their 2.77-MeV level. That suggests there is some $d_{\frac{3}{2}}$ component in our 2.827-MeV level. However, as can be seen from our cross sections in Table 2, which will be discussed later, the 2.827-MeV level is populated ten times more strongly than the 2.770 in our experiment at 5.35 MeV. The remainder of the 2.827-MeV level is then probably $f_{\frac{7}{2}}$ or $p_{\frac{3}{2}}$ from the unfilled N=82 to 126 shell. Such states would of course not be excited in simple pick-up reactions, while they dominate (d,p) spectra at excitation energies above 2.5 MeV. There seems to be some confusion on the relative identity of the 2.92- and

2.83-MeV levels in Ref.[8]. In their sample (d,p) spectrum, the 2.92-MeV peak is about six times smaller than the 3.83-MeV peak in agreement with our results. In their Table III, the 2.83 peak is treated as a small, unidentified state, and the 2.92 is listed with a large cross section and the assignment shown in their Fig. 5. The angular distributions in that energy range do not fluctuate that much. The 2.83 probably had the large $p_{\frac{3}{2}}$ yield assigned to their 2.92-MeV level.

In ^{117}Sn, the $d_{\frac{5}{2}}$ orbit is almost completely filled while the $d_{\frac{3}{2}}$ is less than half full. The ratio of pick-up to stripping cross sections should then be larger for reactions to the $d_{\frac{5}{2}}$ than the $d_{\frac{3}{2}}$ states. This ratio test has been applied in previous work on the odd tin isotopes. Cavanagh et al. [12] compared their (p,d) cross sections with the (d,p) cross sections of Ref.[8] for all the ℓ_n=2 states common to both experiments in the odd tin isotopes from A=113 to 123. Cavanagh et al. found good agreement in J assignments between their angular distribution method and the ratio test. This included many weakly-populated levels.

Clearly, the ratio test could be misleading for levels, particularly weak ones, which have a complex configuration. Caution is recommended in applying the ratio test to weak levels [3].

A comparison of our (d,p) cross sections with those from the (p,d) reaction of Ref.[12] appear useful for identification of our levels as well as assignment of spins since we have observed levels new to the (d,p) reaction possibly corresponding to ℓ_n=2 states of Ref.[12]. One should keep in mind the fact that cross sections for a given type of

level should increase more rapidly with excitation energy for our reactions below the Coulomb barrier than for the pick-up reaction at 30 MeV.

For the $d_{\frac{3}{2}}$ states, the 0.157-MeV level, and the much smaller 2.146, 2.770, and 3.113, the ratio $(\sigma_{max}(p,d))/(\sigma(160°)(d,p))$ is 60, 70, 40, and 20, respectively. For the predominantly $d_{\frac{5}{2}}$ 1.015 and the $d_{\frac{5}{2}}$ 1.178, the same cross section ratio is 440 and 300 respectively. This large (p,d)/(d,p) cross section ratio for the 1.015 implies the $d_{\frac{3}{2}}$ 1.005 level is not strongly excited in the (d,p) reaction. The cross section ratio for the $d_{\frac{5}{2}}$ or $d_{\frac{3}{2}}$ 1.499-MeV level is 60, favoring the $d_{\frac{3}{2}}$ assignment. If the 1.499-MeV level were pure $d_{\frac{3}{2}}$ it would have an unexpectedly large (d,p) spectroscopic factor. Little can be deduced from the intermediate value of 130 for the ratio for the 1.668. The 1.668 was assigned J=5/2 in Ref.[12], based on its angular distribution. It is assumed this state is the 1.71-MeV level of Ref.[12] and the 1.670 of Ref.[29]. Based on its (p,d) angular distribution [12], the 1.47 was given a $d_{\frac{3}{2}}$ assignment. Its absence in the (d,p) spectra along with its (p,d) cross section suggests a $d_{\frac{5}{2}}$ configuration. From angular correlations, a spin of 5/2 was assigned to the corresponding 1.446-MeV level in Ref.[31].

In the comparison of the 15-MeV (d,p) yields of Ref.[8] with the (p,d) yields of Ref.[12], approximately the same relative cross section ratios as those we have just given are obtained for all the above-mentioned ℓ_n=2 states from the 0.157 through the 1.668. Approximately the same relative ratios are obtained for the same states up through the 1.499 in comparing the (d,p) cross-sections of Ref.[8] with their own (d,t) data reported in the same paper.

The 2.203-MeV level is new and rather strongly populated. The 2.38-MeV level of Ref.[8] is a doublet. The 3.14 of Ref.[32] is a triplet including the 3.113 already discussed. Other new levels are those at 3.414-, 3.580-, 3.716-, 3.95-, and 4.02-MeV excitation, as well as all but two or three of those from 4.11 through 4.55 MeV. Some association of the 4.11- to 4.55-MeV levels can be made with broad groups seen in the early work of Ref.[32], if it is assumed their energy calibration was high by up to 150 keV. There is no evidence that we have observed the possible $23/2^+$ state reported at 3.683 MeV in Ref.[33].

Angular Distributions of Differential Cross Sections

The measured cross sections from 70° to 160° for the (d,p) reaction at E_d = 5.35 MeV to all observed states in ^{117}Sn are listed in Table 2. Cross sections and errors are in μb/sr. The cross sections and errors were obtained with the computer code ACK described in Chapter II. Therefore, with the exceptions noted shortly, errors listed are based on the statistical error in determining the number of counts in a peak with a given background. The 7% absolute normalization error is not included, nor is the error in separating adjacent levels. The separation error is quite high on close states at high excitation energy such as the 3.95-3.98-MeV doublet. In the 160° spectrum, the 1.948- to 2.076-MeV quartet was fitted simultaneously with four Gaussians using the computer code Gaussian II [24]. The errors for those states are based on that fit. The cross sections for the 3.113- to 3.735-MeV quartet were checked with the Gaussian-fit program at 160° and 100°. A vertical line in the table connects states which were not separated

Table 2. Experimentally-measured cross sections of levels excited in the reaction $^{116}Sn(d,p)^{117}Sn$ at 5.35 MeV.[a]

Excitation Energy (MeV)	Laboratory Angles							
	160°	150°	140°	120°	100°	90°	80°	70°
0.00	63 ± 3	57 ± 3	61 ± 2	56 ± 3	63 ± 3	73 ± 3	68 ± 3	45 ± 3
0.16	86 ± 3	93 ± 4	93 ± 3	103 ± 4	87 ± 3	83 ± 3		60 ± 3
0.31	33 ± 2	32 ± 3	29 ± 2	27 ± 2	22 ± 2		14.4 ± 1.3	5.4 ± 0.9
0.71	3.7 ± 0.7			4.2 ± 0.9	2.9 ± 0.7	4.3 ± 1.0	2.2 ± 0.6	1.5 ± 0.6
1.02	22 ± 2	17 ± 2	22.1 ± 1.5	24 ± 2	21 ± 2		17.2 ± 1.5	16.1 ± 1.5
1.18	17.1 ± 1.4	15 ± 2	14.8 ± 1.2	14.8 ± 1.5	12.5 ± 1.4	12.5 ± 1.5	8.8 ± 1.0	10.5 ± 1.3
1.30	13.4 ± 1.3	16 ± 2	12.4 ± 1.0		13.5 ± 1.5	9.6 ± 1.3		
1.50		9.1 ± 1.5	13.5 ± 1.0	13.6 ± 1.5		10.0 ± 1.3	7.7 ± 1.0	8.2 ± 1.1
1.59	0.7 ± 0.5	0.9 ± 0.8	1.6 ± 0.5		1.7 ± 0.6	0.9 ± 0.6		1.1 ± 0.6
1.67	3.6 ± 0.7	2.9 ± 0.9	4.3 ± 0.8		2.0 ± 0.7		1.9 ± 0.7	2.5 ± 0.7
1.95	3.6 ± 0.6	2.2 ± 1.1	3.3 ± 0.7	3.4 ± 0.9	1.6 ± 0.6	2.1 ± 0.8		
2.01	6.6 ± 0.8	4.7 ± 1.4		3.3 ± 1.1	3.7 ± 0.8			
2.05	14.3 ± 1.3	16 ± 2	19.4 ± 1.5	17 ± 2	14 ± 2		14.4 ± 1.5	4.4 ± 1.1
2.08	5.0 ± 0.8							
2.15	1.9 ± 0.5	1.7 ± 0.7		1.4 ± 0.6			1.7 ± 0.6	
2.20	7.1 ± 0.9	5.9 ± 1.4	5.1 ± 0.8	3.9 ± 0.9	4.2 ± 0.9		4.6 ± 0.9	
2.26	2.6 ± 0.8	2.2 ± 1.1	2.2 ± 0.8		2.3 ± 0.9			
2.31	4.6 ± 0.9	1.7 ± 1.0	3.4 ± 0.8		3.2 ± 0.9			
2.36	4.3 ± 1.0				2.6 ± 0.8			

Table 2 (continued). Experimentally-measured cross sections of levels excited in the reaction $^{116}Sn(d,p)^{117}Sn$ at 5.35 MeV.[a]

Excitation Energy (MeV)	Laboratory Angles							
	160°	150°	140°	120°	100°	90°	80°	70°
2.39	1.5 ± 0.6	5 ± 2			2.1 ± 0.8			
2.46		27 ± 3	26 ± 2	27 ± 2	21 ± 2	16 ± 2		7.1 ± 1.1
2.55	14.5 ± 1.5	12 ± 2	11.6 ± 1.1	9.6 ± 1.5	7.7 ± 1.1		5.2 ± 1.0	4.4 ± 0.9
2.66	4.5 ± 1.0	8 ± 2	6.8 ± 0.9	5.7 ± 1.0		4.5 ± 1.0	5.0 ± 1.0	
2.71	3.9 ± 0.8	5.3 ± 1.5	4.3 ± 0.9	4.1 ± 1.0	4.2 ± 0.9	3.5 ± 1.1	3.5 ± 0.9	2.2 ± 1.1
2.77		4.4 ± 1.5			2.1 ± 0.7	1.8 ± 0.9		
2.83	38 ± 2	34 ± 3	34 ± 2		25 ± 2	21 ± 2	21 ± 2	
2.91	8.0 ± 1.1	6 ± 2			4.3 ± 0.9	5.9 ± 1.3		
3.02	13 ± 2	16 ± 3	15.4 ± 1.5	11 ± 2	6.0 ± 1.4			4.0 ± 1.3
3.11	9.6 ± 1.5	10 ± 2			4 ± 2			
3.14	6 ± 3				2.7 ± 1.5			
3.17	68 ± 4	53 ± 4	46 ± 3	42 ± 3	35 ± 3		24 ± 2	12 ± 2
3.24	110 ± 4	97 ± 5	90 ± 3	86 ± 5	60 ± 4		29 ± 3	
3.33	43 ± 3	33 ± 4		24 ± 3		15 ± 3	12 ± 2	
3.41				4.0 ± 1.1				
3.46	45 ± 3	37 ± 4	37 ± 2	34 ± 3	37 ± 3	32 ± 3		
3.58	20 ± 2	12 ± 3	12 ± 2	13 ± 2	11 ± 2	7 ± 2		
3.64	5 ± 2	6 ± 2	5 ± 2		7 ± 2			
3.72	28 ± 3	22 ± 4	26 ± 2		19 ± 3			

Table 2 (continued). Experimentally-measured cross sections of levels excited in the reaction $^{116}Sn(d,p)^{117}Sn$ at 5.35 MeV.[a]

Excitation Energy (MeV)	Laboratory Angles							
	160°	150°	140°	120°	100°	90°	80°	70°
3.79	69 ± 4	58 ± 5	56 ± 3			26 ± 4		16 ± 2
3.88	79 ± 4	70 ± 5	62 ± 3	72 ± 4	39 ± 4		30 ± 3	16 ± 2
3.95	138 ± 5				33 ± 4			
3.98		80 ± 6			50 ± 4			11 ± 3
4.02	108 ± 5	65 ± 6			66 ± 4		48 ± 3	26 ± 3
4.11			20 ± 4		30 ± 3		22 ± 3	10 ± 3
4.16		87 ± 6		75 ± 6	60 ± 5	66 ± 5	55 ± 4	30 ± 4
4.21	204 ± 6	174 ± 8		173 ± 6	192 ± 7	120 ± 5	85 ± 4	
4.29					30 ± 4			
4.36			16 ± 3	24 ± 4	33 ± 4	18 ± 3		
4.42	25 ± 4	22 ± 4			13 ± 3			
4.46	123 ± 5	111 ± 7	157 ± 5		62 ± 5			
4.49		23 ± 4			16 ± 3			
4.55	21 ± 3							

[a]Errors are just statistical except where noted in the text.

at a given angle. The cross section is then given for the whole group of unresolved states.

A few of the angular distributions of cross sections listed in Table 2 are plotted in Figs. 7 and 8. The smooth curves indicate theoretical cross sections normalized to the data. The calculation of the theoretical cross sections with the computer code DWUCK and the resulting spectroscopic factors are discussed in the next chapter. Note the relative cross sections between states have been changed in Figs. 7 and 8 for display purposes. Fig. 7 includes some of the larger proton groups assigned $f_{\frac{7}{2}}$ configurations [8]. The states with low Q values tend to have an angular distribution more peaked in the backward direction as one would expect. The levels at 1.302- and 3.785-MeV excitation energy have Q values of 3.418 and 0.935 MeV respectively. The fit to the 2.55-MeV level is almost flat enough to suggest it has a lower orbital angular momentum transfer than $\ell_n=3$, but it is not as flat as an $\ell_n=1$ angular distribution. Fig. 8 shows angular distributions for a few $\ell_n=2$ states and the $g_{\frac{7}{2}}$, 0.705-MeV state and the $h_{\frac{11}{2}}$, 0.313-MeV state.

The angular distribution at incident deuteron energies of 5.35, 5.15, and 4.55 MeV is plotted for the transition to the ground state and the 0.157-MeV level in Figs. 9 and 10 respectively. At the higher incident energies one can easily identify the orbital angular momentum of the $\ell_n=0$ ground state and the $\ell_n=2$ 0.157-MeV, first excited state by the shape of the angular distributions. Separation of similar ℓ_n values by angular distribution shapes is generally possible at those energies only with the high-Q-value states or with very good statistics. The 4.55-MeV

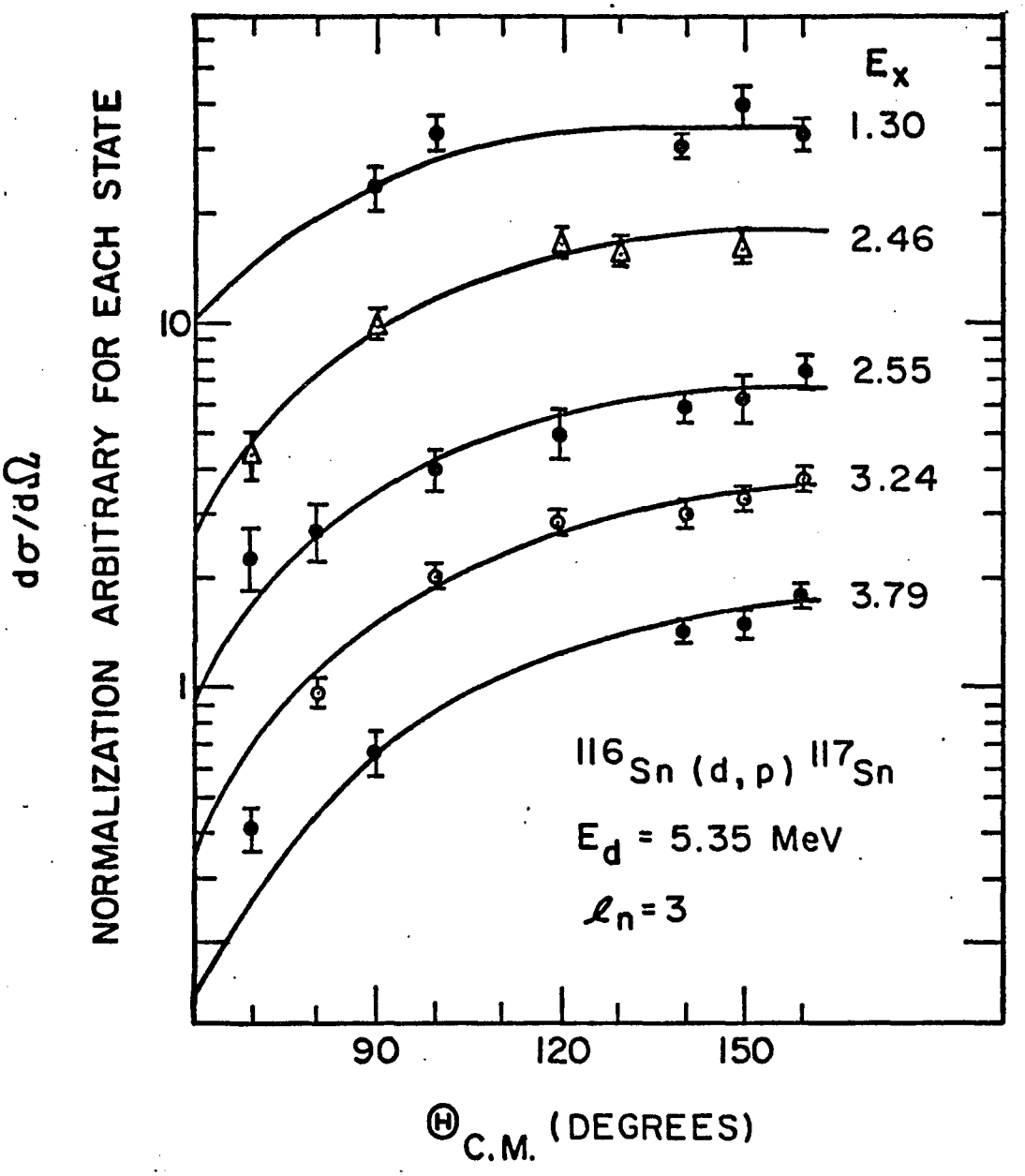

Fig. 7. Angular distribution for several ℓ_n=3 states in ^{117}Sn. Relative differential cross sections with different normalization for each state, are given for the ^{116}Sn(d,p)^{117}Sn reaction at E_d = 5.35 MeV. The smooth curves are from DWBA calculations with parameter set A and are normalized to the experimental points.

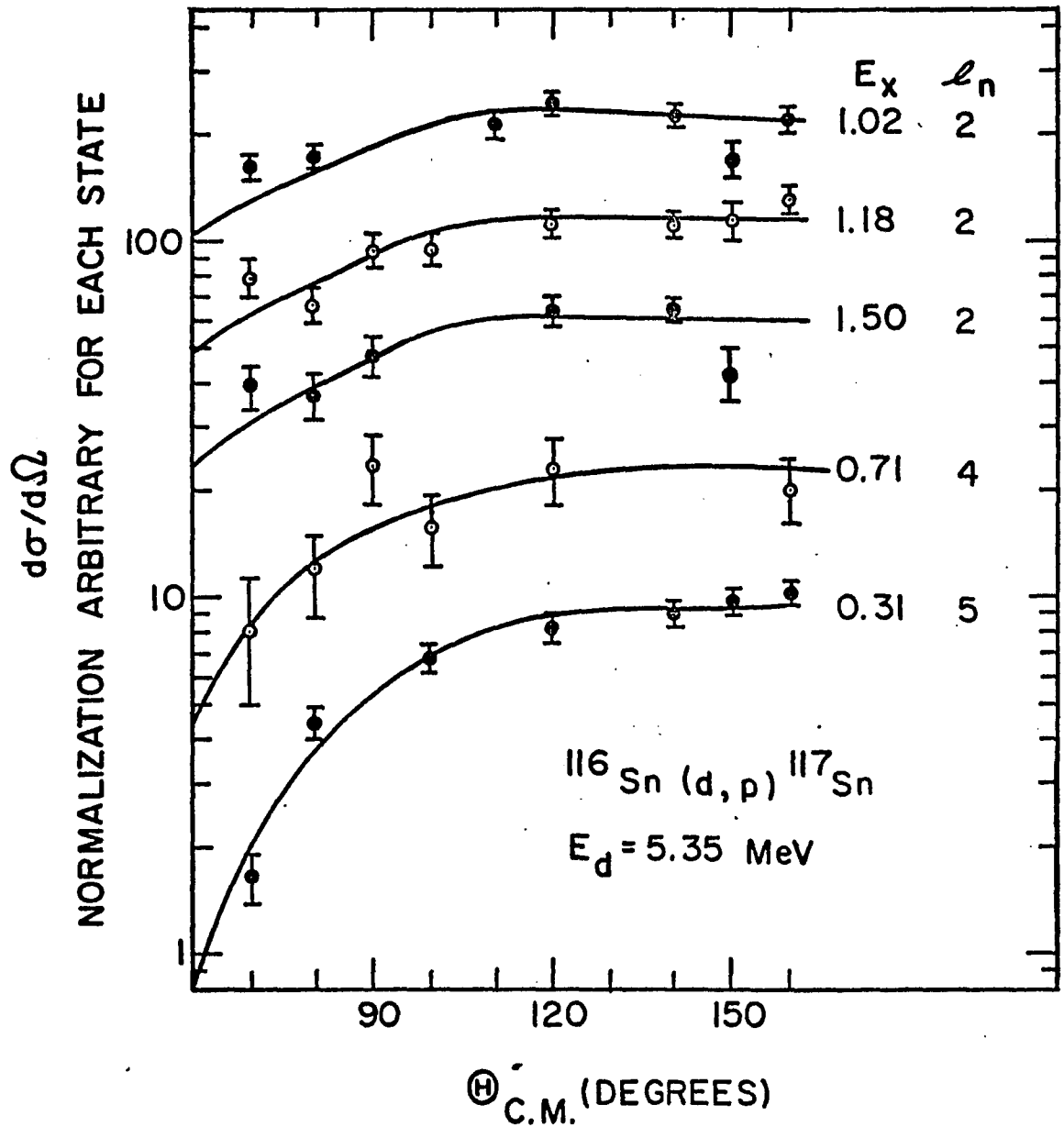

Fig. 8. Angular distribution for several states in ^{117}Sn.

Relative differential cross sections with different normalization for each state, are given for the ^{116}Sn(d,p)^{117}Sn reaction at E_d = 5.35 MeV. The smooth curves are from DWBA calculations with parameter set A and are normalized to the experimental points.

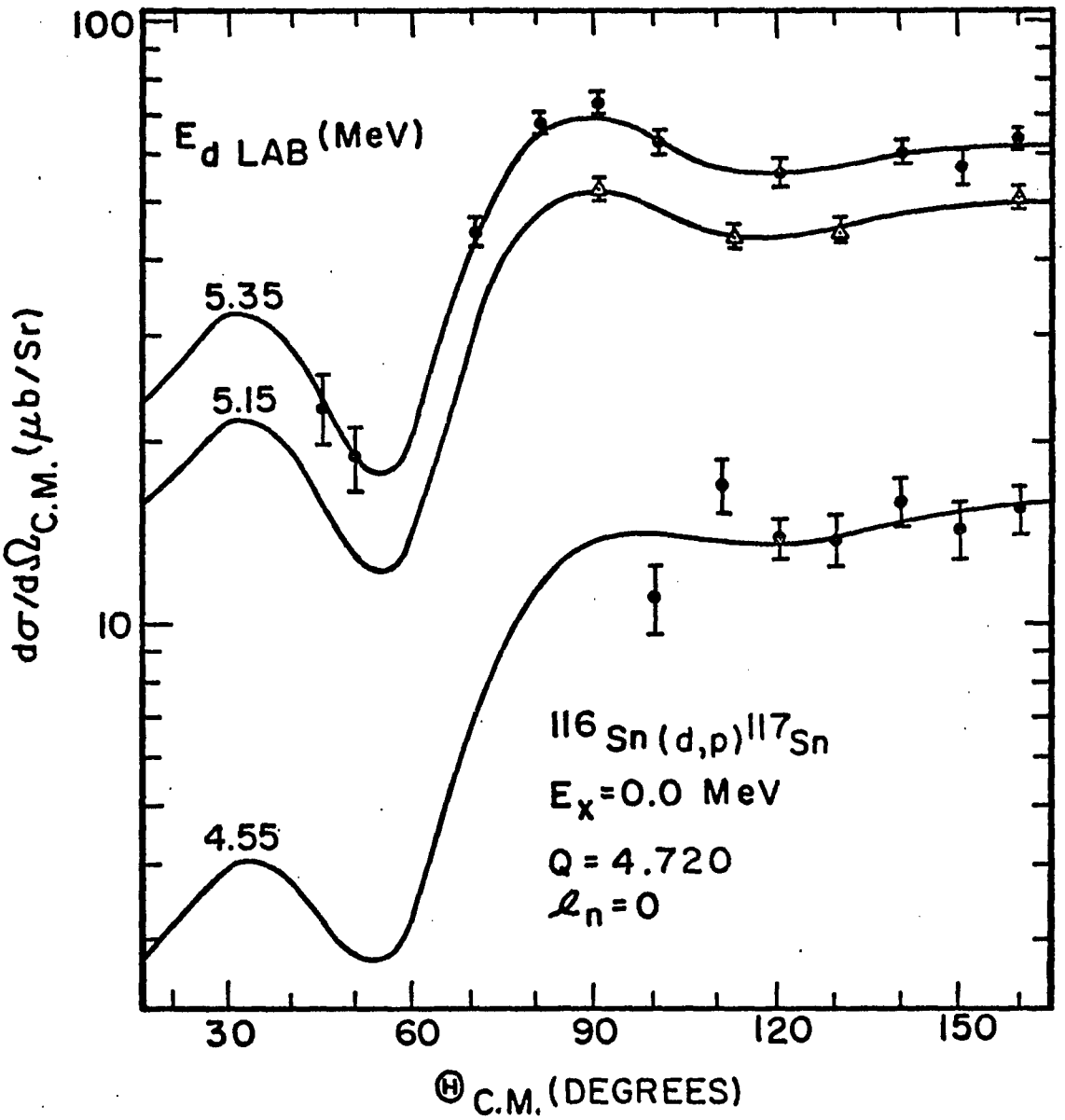

Fig. 9. Angular distribution for the ground state of ^{117}Sn.

The differential cross section is given for the ^{116}Sn(d,p)^{117}Sn reaction leading to the ground state of ^{117}Sn at E_d = 5.35, 5.15, and 4.55 MeV. The solid curves are from DWBA calculations with potential set A and are normalized to the experimental points.

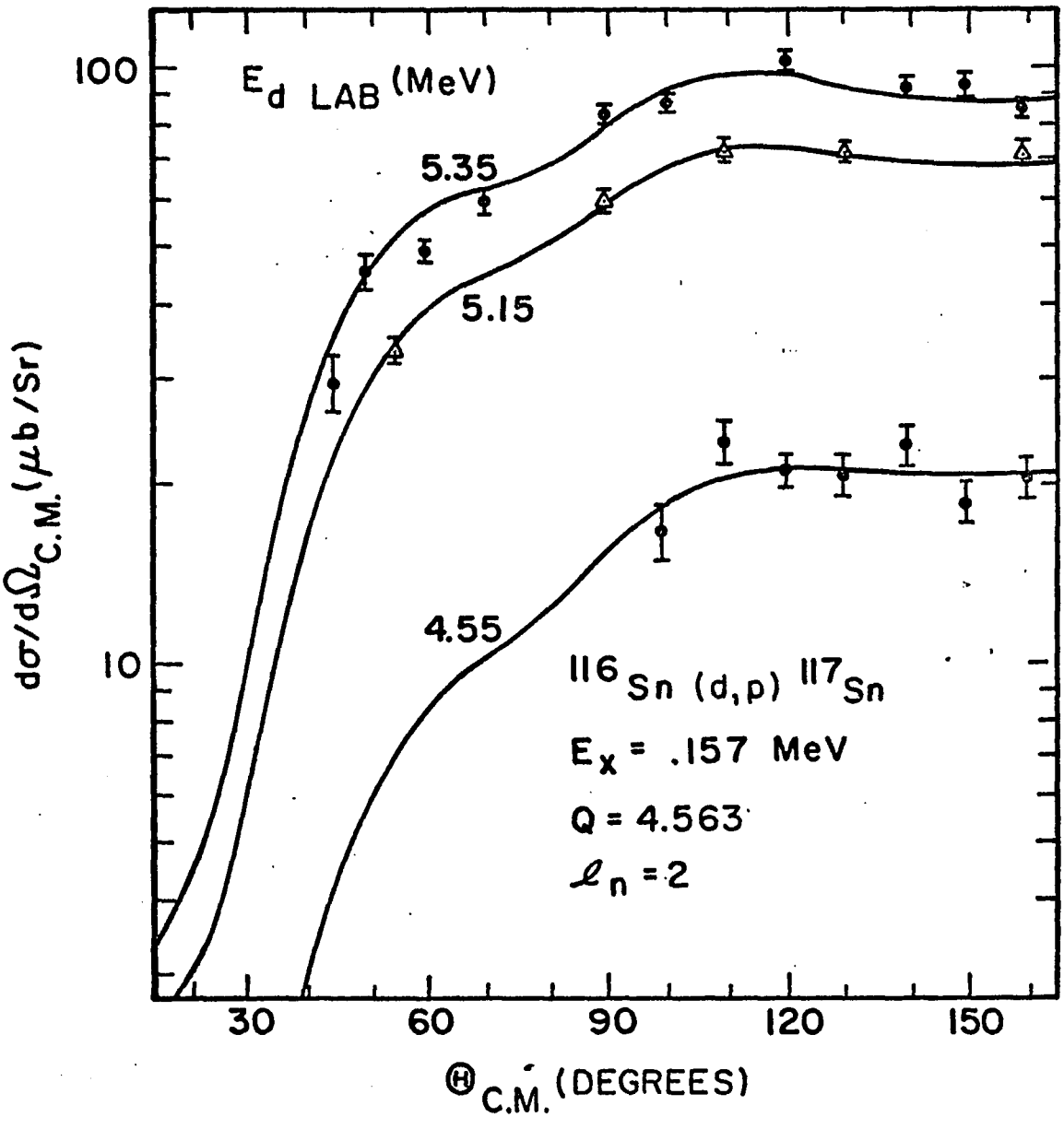

Fig. 10. Angular distribution for the first excited state in ^{117}Sn. The differential cross section is given for the ^{116}Sn(d,p)^{117}Sn reaction leading to the first excited state of ^{117}Sn at E_d = 5.35, 5.15, and 4.55 MeV. The solid curves are from DWBA calculations with potential set A and are normalized to the experimental points.

angular distributions for ^{117}Sn were the only angular distributions taken before pile-up inspection and thinner targets were introduced. Several points were taken later which verified the normalization of the 4.55-MeV set of angular distributions.

Excitation Functions for the First Three States in ^{117}Sn

Relative yields for the population of the first three states in ^{117}Sn via the ^{116}Sn(d,p)^{117}Sn reaction were measured at 160° for deuteron energies from 4.35 MeV to 5.35 MeV at 100-keV intervals. These excitation functions are plotted as points in Fig. 11. Representative statistical errors are shown for the points at 4.35 and 5.25 MeV. Theoretical cross sections at 4.55, 5.15, and 5.35 MeV are plotted as open circles normalized to the experimental points at 5.35 MeV. The theoretical cross sections were calculated using the computer code DWUCK. The calculations are discussed in the next chapter. The experimental yields were normalized against elastic scattering in the monitor detector positioned at 160°. The elastic scattering was assumed to be Rutherford. This is correct at the lowest energies, but overestimates the elastic scattering by about 6% at 5.35 MeV. The calculated points were corrected to show this same bias, i.e., each theoretical (d,p) cross section was multiplied by the optical-model elastic cross section of DWUCK, and divided by the Rutherford cross section.

The main information to be obtained from the excitation functions is that they are relatively smooth and have approximately the same slope as the DWBA stripping calculations. Pure stripping cross sections

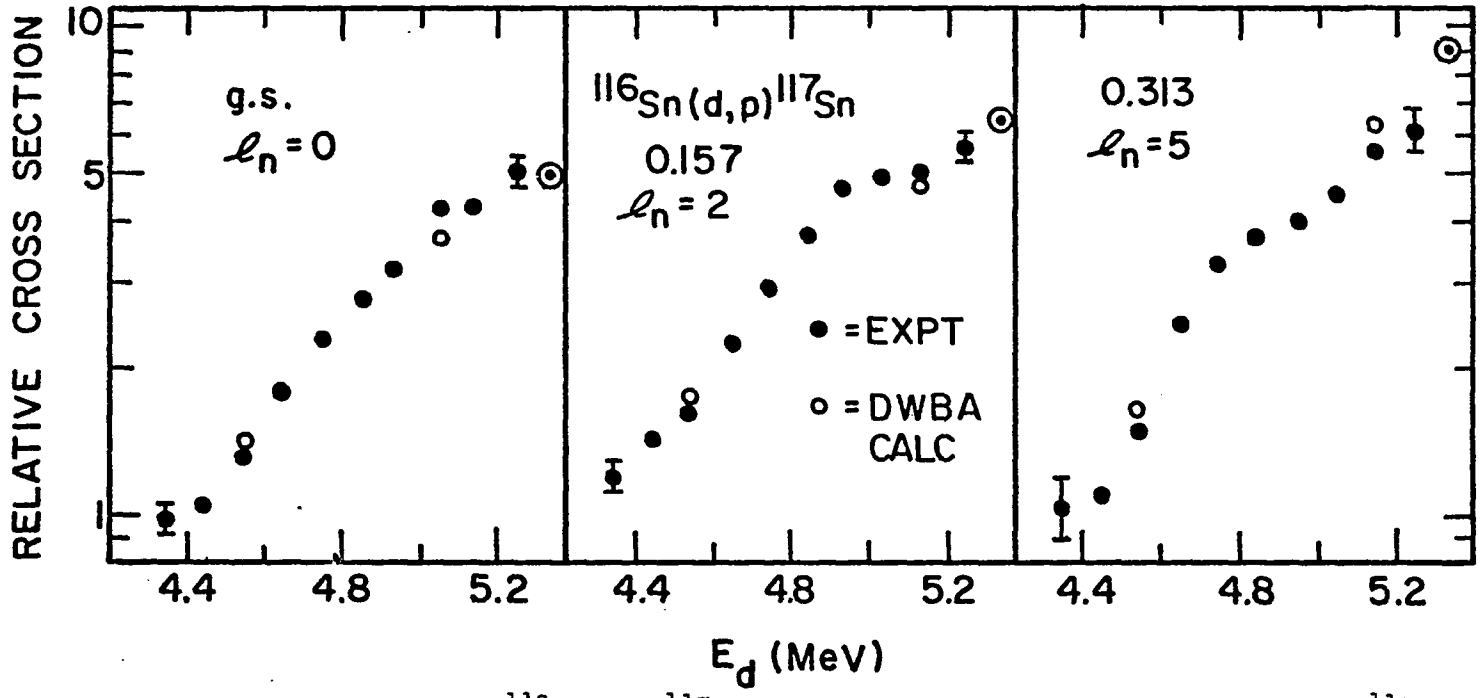

Fig. 11. Excitation functions for the $^{116}Sn(d,p)^{117}Sn$ reaction to the first three states in ^{117}Sn. Relative cross sections at 160° are shown for E_d = 4.35 to 5.35 MeV. The open circles are from DWBA calculations with potential sets A and are normalized to the experimental solid points at 5.35 MeV.

should change smoothly with energy, whereas compound-nucleus contributions can make excitation functions quite bumpy at some angles. One does not expect to have much compound-nucleus formation at these low energies, and the decay of the compound nucleus to the (d,p) channel should be minimal as we are high above the threshold for neutron emission from the compound nucleus. Torti and Graetzer [18] used a Hauser-Feshbach calculation to estimate the compound-nucleus contribution to the $^{87}Rb(d,p)^{88}Rb$ reaction at deuteron energies near the Coulomb barrier. The maximum calculated contribution to the (d,p) differential cross section was less than 5%. Of all the single-particle states studied in any of the three nuclei, the ℓ_n=0 ground state and ℓ_n=2 0.157-MeV level of ^{117}Sn might show the largest deviations from pure subcoulomb stripping behavior because of their low ℓ_n values and high Q values.

It is not clear whether the waviness is real in the excitation functions of the 0.157- and 0.313-MeV levels. The excitation functions were taken with a thick target and relatively poor detector yielding 60-keV resolution. They were also taken before pile-up inspection was added to the electronics system. The peak of the pile-up at twice the energy of the elastic deuterons is moving through the three states studied toward states of higher excitation energy as the incident deuteron energy is decreased. The small pile-up peak could have affected the excitation function slightly although counting rates were kept low to minimize this effect. The ground state should have been clear of the pile-up at energies below 4.95 MeV and the 0.313-MeV level should have been clear at energies less than 4.65 MeV.

The $^{122}Sn(d,p)^{123}Sn$ Reaction

Discussion of the Spectra

The sample charged-particle spectrum in Fig. 12 shows the levels observed in ^{123}Sn from the reaction $^{122}Sn(d,p)^{123}Sn$. The incident deuteron energy was 5.15 MeV, and the scattering angle 150°. The targets were approximately 300 $\mu g/cm^2$ and were enriched to 92.3% in ^{122}Sn. The amount of unidentified contaminants of approximate atomic mass 50 was greater for the ^{122}Sn targets than for those of ^{116}Sn and ^{124}Sn. Due to target thickness or non-uniformity, the resolution was not quite as good as in the best cases for the ^{116}Sn and ^{124}Sn. These factors coupled with a lower maximum deuteron energy for ^{122}Sn probably prevented identification of as many weakly-populated states in ^{123}Sn as were evident in ^{117}Sn and ^{125}Sn. However, seven new levels were found in the region of 4.7- to 5.2-MeV excitation energy. Angular distributions were extracted for the first two excited states, from the reaction at 5.15, 4.75, and 4.55 MeV incident deuteron energy. The data did not seem to warrant the extraction of angular distributions for all the excited states, so only the cross section at 160° from the reaction at E_d = 5.15 MeV is given for all observed levels.

Ground State Q Value

The Q value for the reaction $^{122}Sn(d,p)^{123}Sn$ to the ground state of ^{123}Sn was determined to be 3716 ± 11 keV, intermediate between the often-accepted values of 3707 ± 11 keV [26], and 3726 ± 12 keV [34]. The present determination was based on energy calibration curves for the

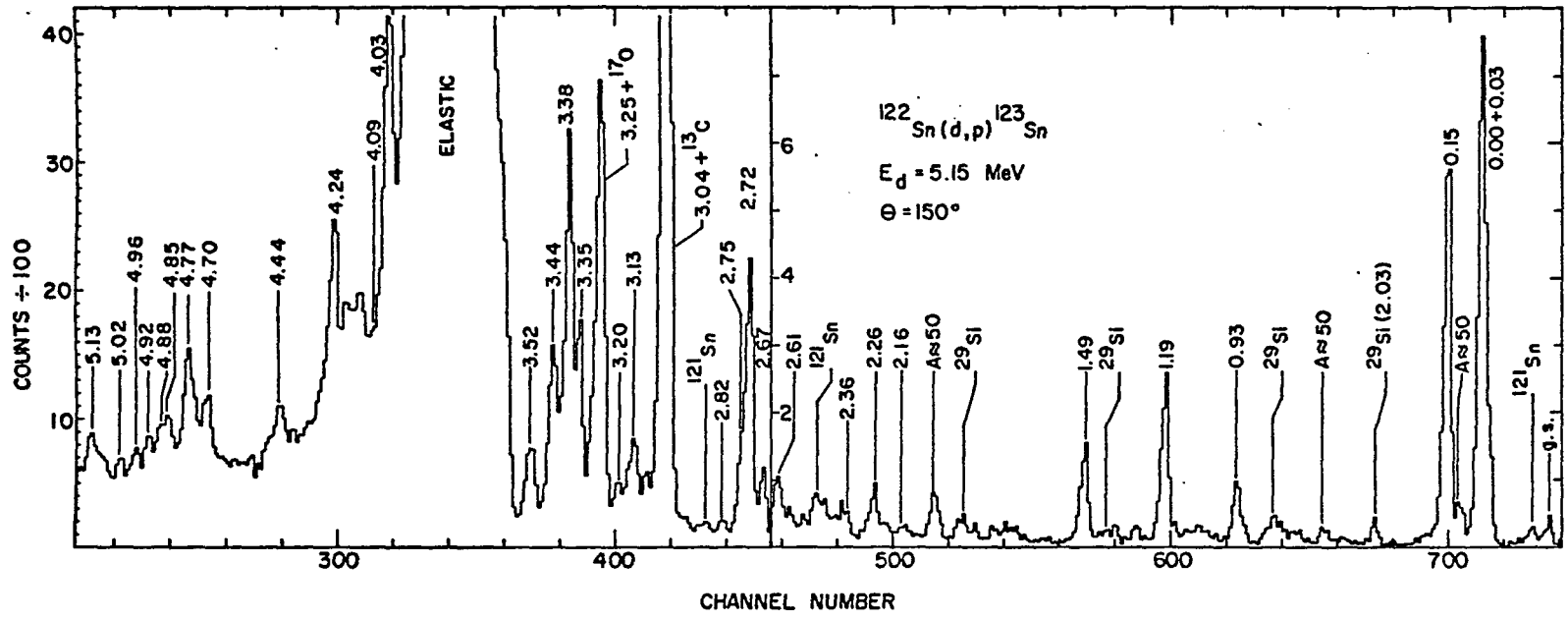

Fig. 12. Proton spectrum from the ^{122}Sn(d,p)^{123}Sn reaction at E_d = 5.15 MeV and θ = 150°.

runs at 5.15-MeV incident deuteron energy at 160° and 90°. This Q value is accurate to ± 7% relative to the ground state Q values for the $^{116}Sn(d,p)^{117}Sn$ and $^{124}Sn(d,p)^{125}Sn$ reactions.

Observed States in ^{123}Sn and Comparison to Previous Studies

The energy levels of ^{123}Sn have been studied via several reactions; some of the studies covered ^{117}Sn which we have already discussed. Schneid, Prakash, and Cohen [8], in their major work on available tin isotopes, obtained spectroscopic factors and assigned ℓ_n and J^π values to many states in ^{123}Sn. These assignments were based on angular distributions from the (d,p) reaction at 15 MeV, and some (d,t) data at 15 MeV. Nealy and Sheline [34] resolved the ground state and first excited state in ^{123}Sn and ^{125}Sn, as well as many new states above 2.5-MeV excitation. They looked at only three angles in the (d,p) reaction at approximately 12 MeV, and reported no cross sections. In their study of odd tin isotopes from A=111 to 123, Cavanagh et al. [12] used the (p,d) reaction at 30 MeV. They determined orbital and total angular momentum of a large number of states in the N=50 to 82 shell. The (p,d) reaction did not excite states from the N=82 to 126 shell. That shell should be completely unfilled in the ground states of the even tin isotopes, and the (p,d) reaction to odd tin isotopes must pick neutrons from those even ground states. Boyd and Arking [35] and Arking et al. [36] have assigned spins and parities to states in isotopes of antimony which are the isobaric analogs of states in ^{121}Sn, ^{123}Sn, and ^{125}Sn. The analysis was made from cross section and polarization measurements of protons

scattered elastically from even isotopes of tin. Many new states in ^{113}Sn and ^{123}Sn have reportedly been observed by Borello et al. [37], but we have not obtained those results. They are as yet unpublished.

The excitation energies of states in ^{123}Sn, as measured in the present experiment, are listed in Table 3. These excitation energies were determined from two energy calibration curves similar to the one in Fig. 4, and from comparison with many other runs. All excitation energies should be accurate to less than 15 keV. The excitation energies of levels above 1 MeV are uniformly about 10 keV less than those reported in Ref. [34].

There is a noticeable widening of the high energy side of the proton peak for the ground state plus the 0.025-MeV state doublet. The widening is due to the weakly populated ground state. The ground state and first excited state peak in the 5.15-MeV runs at six angles were fitted by two Gaussians. The only restriction on the parameters of the fit was that the widths, although variable, had to be the same for both Gaussians. The mean separation of the two Gaussians for the six runs was found to be 25 ± 3 keV. The ground state was an average 12 ± 6% of the total peak area. This gives little error to the spectroscopic factor for the 0.025-MeV level.

Differential cross sections for the population of states in ^{123}Sn in the reaction ^{122}Sn(d,p)^{123}Sn at E_d = 5.15 MeV and a scattering angle of 160° are listed in Table 3. These cross sections and errors in μb/sr, were extracted in the same manner as the cross sections listed in Table 2. Errors are statistical, not including the absolute normalization error of 7%. The peak separation errors are not included except

Table 3. Energy levels in ^{123}Sn.[a]

E_x (MeV)[b]	dσ/dΩ (160°) μb/sr	ℓ_n,2·J[c]	E_x (MeV)[b]	dσ/dΩ (160°) μb/sr	ℓ_n,2·J[c]
0.000	11 ± 8	h11	3.252	50 ± 4	(d3[d],p3[e])
0.025	94 ± 8	d3	3.345	61 ± 17	
0.150	73 ± 2	s1	3.383	363 ± 7	p3[e,f]
0.926	9.9 ± 1.1		3.443	91 ± 4	
1.191	32 ± 2	d5,(+g7[d])	3.522	77 ± 4	(p3)
1.485	17.1 ± 1.3	d5	4.033	121 ± 8	p3[e,f]
2.157	1.5 ± 0.6	(p3,d5)	4.087	127 ± 7	
2.260	7.5 ± 1.0	(p3,d3[d])	4.242	87 ± 8	(p3)[e]
2.362	2.0 ± 0.8		4.436	56 ± 6	
2.612	5.2 ± 1.3	(s1)[d]	4.702	63 ± 5	
2.667	55 ± 8		4.773	137 ± 7	
2.716	257 ± 18	(f)7[-e]	4.845	29 ± 4	
2.746	80 ± 13		4.875	37 ± 5	
2.820	18 ± 2	(f7)	4.923	22 ± 4	
3.040	16 ± 4	(f7)	4.964	16 ± 4	
3.130	46 ± 11	f7[e,f]	5.019	12 ± 4	
3.196	15 ± 3		5.127	37 ± 5	

[a] Listed are excitation energies and the differential cross sections at 160° for levels observed in the ^{122}Sn(d,p)^{123}Sn reaction at 5.15 MeV. Also given are the probable orbital and total angular momentum assignments.

[b] Absolute uncertainties are less than 15 keV.

[c] All but the footnoted assignments are the same as in Ref. [8]. Assignments in parentheses are uncertain.

[d] See Ref. [12].

[e] See Refs. [35] and [36].

[f] See Ref. [8].

for the unresolved ground state and 0.025, and the triplet including the 2.667- to 2.746-MeV levels. The triplet was fitted simultaneously with three Gaussians yielding the listed cross sections and errors and their relative excitation energies. The ground state and 0.025 cross sections and errors were obtained from the Gaussian fits described in the previous paragraph. The differential cross section at 160° is indicative of the relative production of a state at this low incident energy since the angular distributions are almost flat for all states at the most backward angles.

The orbital and total angular momentum assignments in Table 3 are based on the best possible identification of the observed states in ^{123}Sn with those in the previously-mentioned references for which ℓ_n and J values were deduced. The assignments are those of Schneid et al. [8] unless otherwise noted by footnote. Uncertain assignments are listed in parentheses. The first three states are well known and contain most of the strength for the $h_{11/2}$, $d_{3/2}$, and $s_{1/2}$ orbits in order of increasing excitation energy. The main $d_{5/2}$ strength is split between the 1.191- and 1.485-MeV levels. Some $g_{7/2}$ component was also apparent for the 1.191 in the pickup reaction of Ref.[12]. In Ref.[34], two peaks in the region of the 1.191-MeV level were reported with a separation of 40 keV.

The configuration of the 0.926-MeV level and the possibly analogous 0.936 in ^{125}Sn has been a question for some time. Schneid et al. [8] note the structureless angular distribution and the weak production of the 0.926 and the 0.936 in the (d,t) reaction relative to the (d,p) reaction. They contend these are not single-particle states in ^{123}Sn

and ^{125}Sn. The 0.926 was indeed only weakly excited in the (p,d) reaction of Ref.[12] in which it was given a $d_{\frac{5}{2}}$ assignment. In the present (d,p) reactions around 5 MeV, the 0.926 of ^{123}Sn and 0.936 of ^{125}Sn were produced with approximately the same yield as the other states relative to the (d,p) cross sections at 15 MeV [8]. The ratio of stripping to pick-up yields for the two states are more consistent with a $d_{\frac{3}{2}}$ than a $d_{\frac{5}{2}}$ assignment. The 0.936 of ^{125}Sn has been shown to have a spin of 3/2 or 1/2 [13].

Our failure to observe any levels between 1.5- and 2.1-MeV excitation is more indicative of the background and statistics in our spectra than the nature of the states that have already been reported there.

All the levels in ^{123}Sn reported here up through the 4.436 have been observed in previous (d,p) reactions, except for the 2.612. It is probably the $s_{\frac{1}{2}}$ state observed in the (p,d) reaction at 2.62-MeV excitation [12]. The $7/2^-$ resonance corresponding to the 2.716-MeV level which was studied in Refs.[35] and [36] probably includes the 2.746- and possibly the 2.667-MeV levels. The six levels above 4.8 MeV have not been previously reported.

Angular Distributions of Differential Cross Sections

Angular distributions were extracted for the production of the first two excited states in ^{123}Sn via the ^{122}Sn(d,p)^{123}Sn reaction at E_d = 5.15, 4.75, and 4.55 MeV. The angular distributions for the 0.150-MeV $s_{\frac{1}{2}}$ level are shown in Fig. 13, and those for the 0.025-MeV $d_{\frac{3}{2}}$ level are shown in Fig. 14. These angular distributions are still indicative

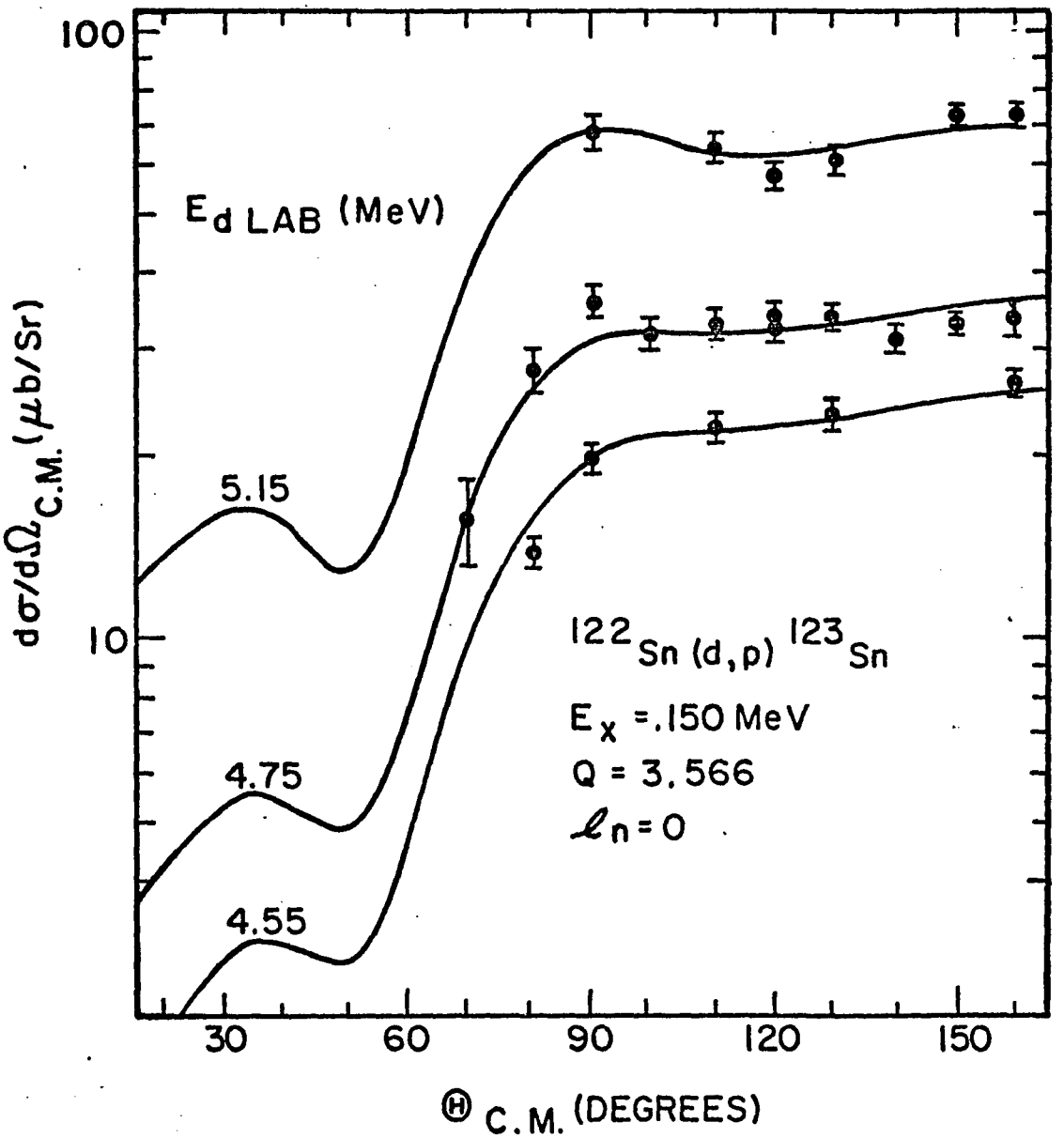

Fig. 13. Angular distribution for the second excited state in ^{123}Sn. The differential cross section is given for the ^{122}Sn(d,p)^{123}Sn reaction leading to the second excited state of ^{123}Sn at E_d = 5.15, 4.75, and 4.55 MeV. The solid curves are from DWBA calculations with potential set A and are normalized to the experimental points.

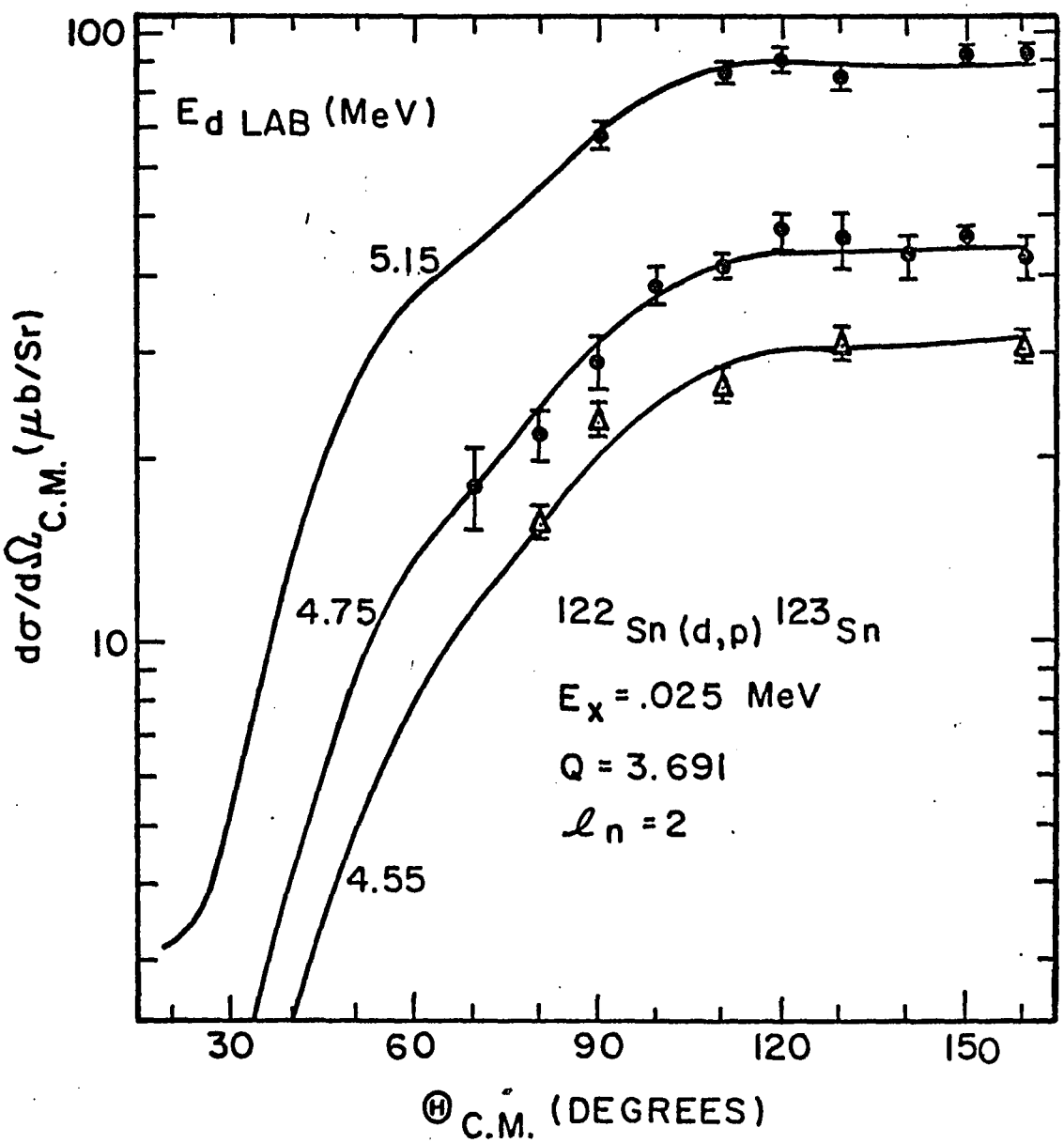

Fig. 14. Angular distribution for the first excited state in ^{123}Sn. The differential cross section is given for the ^{122}Sn(d,p)^{123}Sn reaction leading to the first excited state of ^{123}Sn at E_d = 5.15, 4.75, and 4.55 MeV. The solid curves are from DWBA calculations with potential set A and are normalized to the experimental points.

of the orbital angular momentum transfer, ℓ_n. The smooth curves connect theoretical cross sections normalized to the data. The theory and its results will be discussed in the next chapter.

The separation of the ground state and 0.025-MeV state by fitting with two Gaussians was discussed in the previous section on the excitation energies of states in ^{123}Sn. As we said before, the ground state was found to be an average of 12 ± 6% of the total peak area in the runs at 5.15 MeV. The peak separation was found to be consistent both between runs and with a previous high resolution determination [34]. Due to the large fitting errors, the extracted cross sections for the ground state did not show an angular distribution characteristic of an ℓ_n=5 transition. For that reason, the 0.025-MeV level angular distribution at E_d = 5.15 MeV was normalized by subtracting 12% from the doublet cross section at each angle. The angular distributions at E_d = 4.75 and 4.55 MeV were corrected for the ground state by subtracting 11%. This is in contrast to the similar case in ^{125}Sn, where slightly better resolution and less contaminants yielded a good angular distribution for the small ℓ_n=5 ground state with 27 keV separation from the first excited state.

The ^{124}Sn(d,p)^{125}Sn Reaction

Discussion of the Spectra

A typical charged-particle spectrum from the reaction ^{124}Sn(d,p)^{125}Sn is shown in Fig. 15. The number over a peak is the excitation energy of the resulting level in ^{125}Sn. The incident deuteron

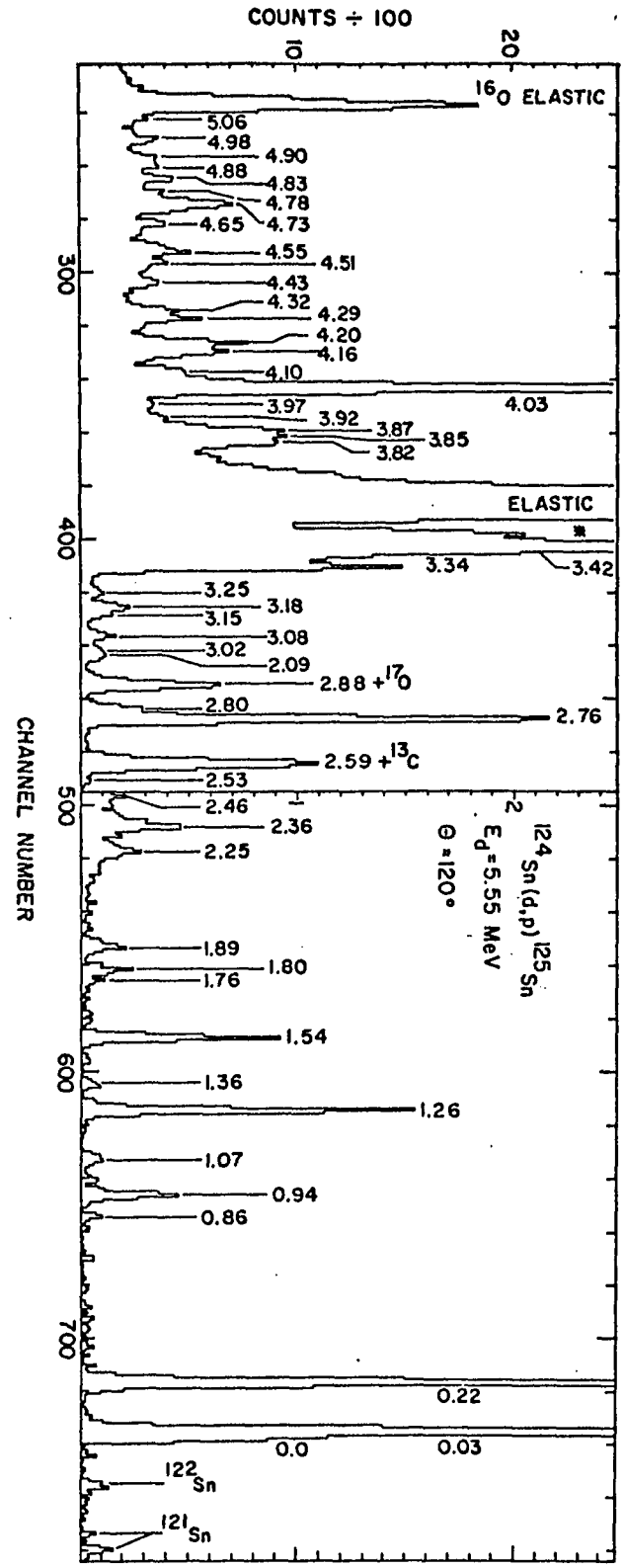

Fig. 15. Proton spectrum from the $^{124}Sn(d,p)^{125}Sn$ reaction at E_d = 5.55 MeV and θ = 120°.

energy was 5.55 MeV for this run and the scattering angle was 120°. The targets had an isotopic purity of 94.7% ^{124}Sn. Other contaminants than ^{16}O and ^{12}C were almost undetectable in the 5.55-MeV runs. The targets were self-supporting and approximately 270 $\mu g/cm^2$ thick.

The small peak marked with an asterisk to the right of the main elastic peak was an electronic effect which we will call elastic spillover. It was approximately proportional in size to the ^{124}Sn(d,d)^{124}Sn elastic peak and maintained a set separation from the elastics. The elastic spillover prevented reliable measurement of the cross section for the 3.416-MeV level. The spillover was also evident in the reactions on ^{116}Sn and ^{122}Sn, but it was unresolved from the elastic peak in those spectra except in the runs of 5.35-MeV deuterons incident on ^{116}Sn.

The ground state of ^{125}Sn is unresolved from the 0.027-MeV first excited state. The ground state is evident as a slight hump on the ground-state plus 0.027-MeV-state doublet.

Ground State Q Value

The ground state Q value for the reaction ^{124}Sn(d,p)^{125}Sn was determined to be 3515 ± 11 keV. The usually quoted values are 3543 ± 13 keV [26] or 3506 ± 12 keV [34]. The present value was determined from two energy calibration curves for runs at 160° and 90°, with E_d = 5.15 MeV. Calibrations were also made for the immediately preceding or succeeding runs which were at the same energy and angle, but used the ^{116}Sn and ^{122}Sn targets.

Excitation Energies and Possible ℓ_n and J Values

The states of ^{125}Sn have been studied in all but one of the references described in the section of this chapter titled "Observed States in ^{123}Sn and Comparison to Previous Studies". The unavailability of ^{126}Sn as a target rules out single-neutron pick-up reactions to ^{125}Sn. A study of the states in ^{125}Sn below 1.6-MeV excitation via the (d,p) reaction at 5.1 and 12.0 MeV has recently been completed [19]. In that work, spectroscopic factors are extracted for 7 of the first 9 states in ^{125}Sn, and two new orbital angular momentum values are obtained.

The measured excitation energies of states in ^{125}Sn are listed in Table 4. They were obtained from several energy calibration curves of the type demonstrated in Fig. 4. Uncertainties are less than 10 keV for excitation energies listed with 1-keV precision and less than 15 keV for those listed with 10-keV precision. The listed excitation energies usually agree with those of Ref. [34] to less than 5 keV.

The orbital and total angular momentum of the states observed in ^{125}Sn are listed in Table 4. In discussing the identity of some observed states we rely on their yield. Cross sections are listed in Table 5, and are discussed in the next section. The assignments for the ground state, first, second, sixth, and eighth excited states in ^{125}Sn are well known [8,13,19,34-36]. The 0.859-MeV level is new. We have no information on its possible identity. The 0.936-MeV level was discussed in conjunction with the 0.926-MeV level of ^{123}Sn. It does not show a characteristic single-particle angular distribution [8,19], but its angular distribution at 12 MeV was fitted best [19] by an ℓ_n=2 DWBA

Table 4. Energy levels in ^{125}Sn.[a]

E_x (MeV)[b]	ℓ_n, $2\cdot J$[c]	E_x (MeV)[b]	ℓ_n, $2\cdot J$[c]	E_x (MeV)[b]	ℓ_n, $2\cdot J$[c]
0.000	h11	2.800		4.16	
0.028	d3	2.883		4.20	(f7)
0.217	s1	2.99		4.29	
0.859		3.02		4.32	
0.936	(d3)[e,f]	3.080	(p3)	4.43	
1.069	? 1,3[+f]	3.15		4.51	
1.261	d5	3.18	(f7)	4.55	
1.364	(g7)[e]	3.247		4.65	
1.540	d5	3.344	(f7,p3[d])	4.73	
1.756		3.416	p3	4.78	
1.803		3.82		4.83	(f7)
1.892		3.85	(f7,p1[d])	4.88	
2.254	s1	3.87		4.90	
2.355	(p3)	3.92		4.98	
2.46		3.97		5.06	
2.589	(f7)	4.03	(p3,1[d])		
2.760	(f)7[-d]	4.10			

[a]Excitation energies determined in the ^{124}Sn(d,p)^{125}Sn reaction are listed with probable orbital and total angular momentum assignments.

[b]Uncertainties are less than 10 keV for energies listed with 1-keV precision and less than 15 keV for those listed with 10-keV precision.

[c]All but the footnoted assignments are the same as in Ref.[8]. Assignments in parentheses are uncertain.

[d]See Refs.[35] and [36].

[e]See Ref.[19].

[f]See Ref.[13].

calculation. The spin and parity of both the 0.936- and 1.069-MeV levels have been shown to be $1/2^+$ or $3/2^+$ [13]. The 1.756- and 1.803-MeV levels form a previously unresolved doublet.

All the assignments in Ref.[8] to levels above 2.3-MeV excitation are to the $f_{\frac{7}{2}}$ and $p_{\frac{3}{2}}$ orbits. The spins were assigned on the basis of the simple shell model. Isobaric analogs to five of these states have been assigned $7/2^-$, $3/2^-$, and $1/2^-$ spins [35,36], not always in agreement with the tentative choices in Ref.[8]. The assignment by Boyd and Arking [35] of $J = 1/2^-$ to the analog of the strong ℓ_n=1 level at 4.03 MeV is somewhat unexpected from the simple shell model. The 3/2 spin assignment in Table VII of Ref.[8] for the ℓ_n=3 state at 4.20 MeV was probably meant to be 7/2. Twelve of the levels we have observed above 3.95-MeV excitation are new.

Angular Distributions of
Differential Cross Sections

Tabulated in Table 5 is the angular distribution of the differential cross section in the $^{124}Sn(d,p)^{125}Sn$ reaction to each state or group of states resolved at E_d = 5.55 MeV. Errors are statistical with the same limitations described for the ^{117}Sn cross sections in Table 2, i.e., the absolute normalization error of 7% is not included nor is the error in separating adjacent levels with a few exceptions. The doublet comprised of the 2.760- and 2.800-MeV levels was fitted with two Gaussians in four runs at angles from 160° to 90°. The relative intensity of the two levels was approximately the same in those four runs. The relative intensity was taken to be the same at all angles. The errors

Table 5. Experimentally-measured cross sections of levels excited in the reaction $^{124}Sn(d,p)^{125}Sn$ at 5.55 MeV.[a]

Excitation Energy (MeV)	Laboratory Angles							
	160°	140°	130°	120°	100°	90°	80°	70°
0.00[b]	26 ± 4	31 ± 4	22 ± 4	24 ± 5	16 ± 3	13 ± 2	9 ± 2	6.5 ± 1.4
0.03	143 ± 6	145 ± 6	144 ± 6	144 ± 7	127 ± 6	121 ± 5	98 ± 4	79 ± 3
0.22	112 ± 5	105 ± 4	104 ± 5	102 ± 5	106 ± 5	111 ± 4	103 ± 4	82 ± 3
0.86	2.1 ± 0.6	4.1 ± 0.8	2.1 ± 0.5	0.6 ± 0.3	1.8 ± 0.5	1.8 ± 0.6		
0.94	13.1 ± 1.5	13.8 ± 1.5	11.4 ± 1.2	15.1 ± 1.3	14.4 ± 1.3	8.7 ± 1.3	7.2 ± 1.2	
1.07	2.4 ± 0.7	2.5 ± 0.7	2.4 ± 0.6	4.1 ± 0.7	3.2 ± 0.6	3.9 ± 0.8		
1.26	47 ± 3	48 ± 3	50 ± 2	43 ± 2	39 ± 2	36 ± 2	29 ± 2	
1.36	2.9 ± 0.7	3.5 ± 0.8	2.5 ± 0.6	2.4 ± 0.6	2.6 ± 0.6			
1.54	29 ± 2	33 ± 2	31 ± 2	26 ± 2	27 ± 2	21 ± 2	18 ± 2	
1.76	2.2 ± 0.7	2.3 ± 0.6	1.3 ± 0.4	1.7 ± 0.6	2.1 ± 0.6			
1.80	6.1 ± 1.1	5.6 ± 0.9	5.5 ± 0.8	6.8 ± 0.5	4.7 ± 0.8			
1.89	5.9 ± 1.1	6.5 ± 1.1	4.1 ± 0.7	7.6 ± 1.1	4.0 ± 0.8			
2.25	7.9 ± 1.4	7.6 ± 1.4	13.1 ± 1.4	9 ± 2				
2.36	16 ± 2	14 ± 2	10.7 ± 1.3	17 ± 2	16 ± 2			
2.46	2.8 ± 0.7	2.6 ± 1.1		2.9 ± 0.8	3.2 ± 1.3			
2.59	13 ± 2	14 ± 2	15 ± 2					
2.76	954 ± 38	857 ± 35		723 ± 28	532 ± 21	425 ± 17	281 ± 12	
2.80	106 ± 15	96 ± 14		80 ± 12	59 ± 8	47 ± 6	32 ± 4	
2.88	56 ± 3		47 ± 3		32 ± 2	31 ± 3	17 ± 2	

Table 5 (continued). Experimentally-measured cross sections of levels excited in the reaction $^{124}Sn(d,p)^{125}Sn$ at 5.55 MeV.[a]

Excitation Energy (MeV)	Laboratory Angles							
	160°	140°	130°	120°	100°	90°	80°	70°
2.99		15 ± 3			15 ± 2	15 ± 2		
3.02		27 ± 3		48 ± 3	17 ± 2	18 ± 2	27 ± 3	
3.08			59 ± 3	44 ± 3	58 ± 3	37 ± 3	25 ± 3	
3.15								
3.18		100 ± 4	107 ± 4	95 ± 4	82 ± 4	53 ± 4		
3.25		28 ± 3	30 ± 3	25 ± 3	7 ± 3	11 ± 3		
3.34	432 ± 9	483 ± 8						
3.42								
3.82	184 ± 9							
3.85								
3.87	276 ± 9	560 ± 15	691 ± 15	428 ± 14	415 ± 15	242 ± 12	221 ± 21	
3.92	18 ± 4				9 ± 4			
3.97			22 ± 5	8 ± 3	20 ± 6			
4.03	1509 ± 46	1632 ± 18	1368 ± 15	1279 ± 15	1016 ± 28	853 ± 18	647 ± 18	419 ± 17
4.10	130 ± 19				71 ± 16			
4.16	175 ± 8	216 ± 19	156 ± 6	167 ± 7	122 ± 11	78 ± 7		
4.20	219 ± 9	181 ± 7	181 ± 7	164 ± 7	157 ± 7	93 ± 7	115 ± 11	
4.29	275 ± 10	190 ± 9	173 ± 8	106 ± 6	170 ± 9	72 ± 8	104 ± 13	
4.32				73 ± 6		28 ± 5		

Table 5 (continued). Experimentally-measured cross sections of levels excited in the reaction $^{124}Sn(d,p)^{125}Sn$ at 5.55 MeV.[a]

Excitation Energy (MeV)	Laboratory Angles							
	160°	140°	130°	120°	100°	90°	80°	70°
4.43	61 ± 7	64 ± 7	83 ± 6	64 ± 6	79 ± 6	47 ± 7		
4.51	62 ± 7	56 ± 7	68 ± 5	66 ± 6	76 ± 6	31 ± 7		
4.55	118 ± 7	105 ± 7	135 ± 6	118 ± 7	100 ± 6	69 ± 8		
4.65		57 ± 6	82 ± 6	45 ± 5	47 ± 4			
4.73	333 ± 11	296 ± 11	325 ± 9	291 ± 9	230 ± 9			
4.78								
4.83	88 ± 7	75 ± 7	90 ± 6	78 ± 6				
4.88	25 ± 5	22 ± 4		51 ± 5				
4.90	48 ± 5	44 ± 6	97 ± 7	37 ± 5				
4.98	80 ± 6	72 ± 7	76 ± 6	58 ± 6	57 ± 7			
5.06	66 ± 7	66 ± 7						

[a] Cross sections and errors are given for the laboratory frame in μb/sr. Errors are just statistical except where noted in the text.

[b] The ground state cross section may be more uncertain than indicated. See text.

for the 2.760- and 2.800-MeV levels are based on the fitting errors. Gaussian fits and errors are given for the 4.03- and 4.10-MeV doublet at 160° and 100°.

As with the ^{123}Sn spectra, Gaussians of equal width were fitted to the first three states in ^{125}Sn to separate the unresolved ground state and first excited state doublet. Reasonable values of Chi squared were obtained for these fits while attempted fits of three Gaussians to two single peaks in the same spectra failed to converge. In fits to the eight runs at E_d = 5.55 MeV and at angles from 160° through 70°, the r.m.s. separation of the ground state and first excited state was found to be 28 ± 2 keV. The cross sections and errors listed in Table 5 and plotted in Figs. 16, 17, and 18 for the ground state and first two excited states are from those Gaussian fits. The ground state cross section varies from only 8% of the first excited state cross section at 70° to 21% at 140°. As can be seen in Fig. 16, the angular distribution of the ground state cross section is a good fit to the smooth curve representing the DWBA ℓ_n=5 calculation. This would seem to be unlikely unless we were actually measuring the ground state cross section. However, this cross section cannot be viewed as absolutely certain.

Other angular distributions from Table 5 are shown in Fig. 16 along with fitted DWBA curves. They include the $d_{\frac{5}{2}}$ states at 1.261 and 1.540 MeV and the states at 0.936 and 1.364 MeV with probable assignments of $d_{\frac{3}{2}}$ and $g_{\frac{7}{2}}$ respectively.

Angular distributions and fitted DWBA curves for incident energies of 5.55, 5.15, 4.75, and 4.55 MeV are shown in Figs 17 and 18 for the $d_{\frac{3}{2}}$ first excited state and $s_{\frac{1}{2}}$ second excited state respectively.

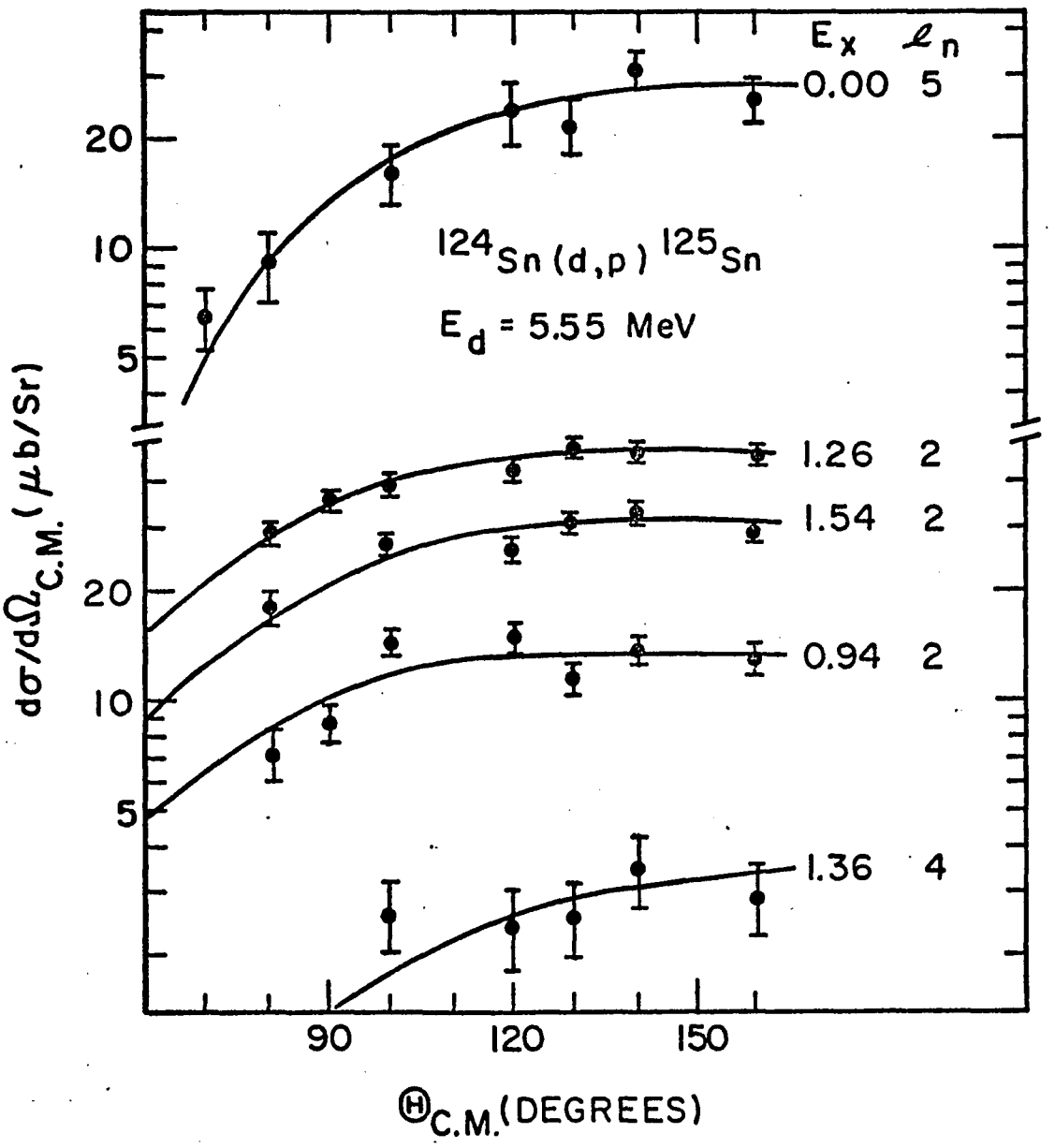

Fig. 16. Angular distribution for several states in ^{125}Sn.

The differential cross section is given for the ^{124}Sn(d,p)^{125}Sn reaction leading to several states in ^{125}Sn at E_d = 5.55 MeV. The solid curves are from DWBA calculations with potential set A and are normalized to the experimental points.

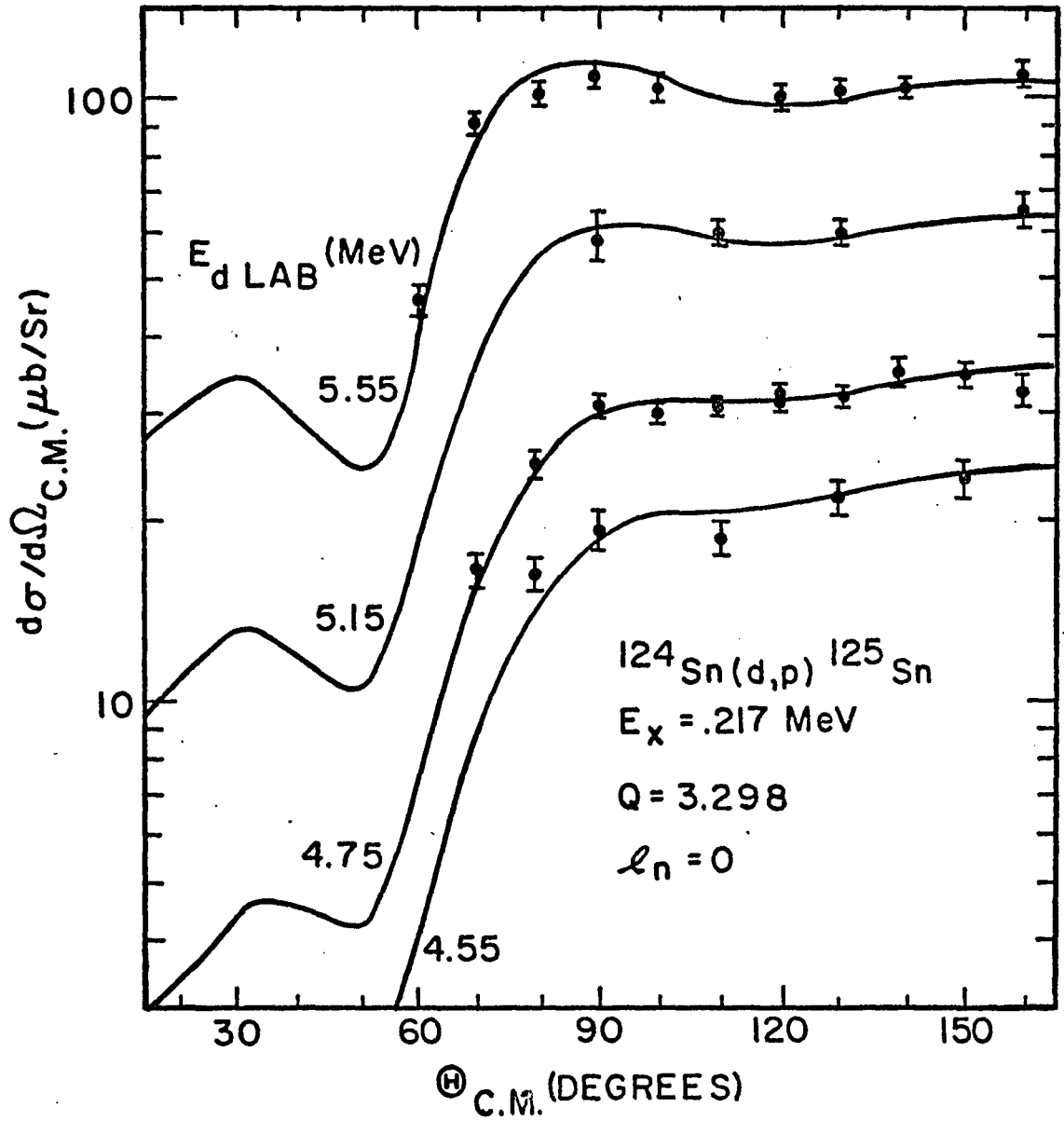

Fig. 17. Angular distribution for the second excited state in ^{125}Sn. The differential cross section is given for the ^{124}Sn(d,p)^{125}Sn reaction leading to the second excited state of ^{125}Sn at E_d = 5.55, 5.15, 4.75, and 4.55 MeV. The solid curves are from DWBA calculations with potential set A and are normalized to the experimental points.

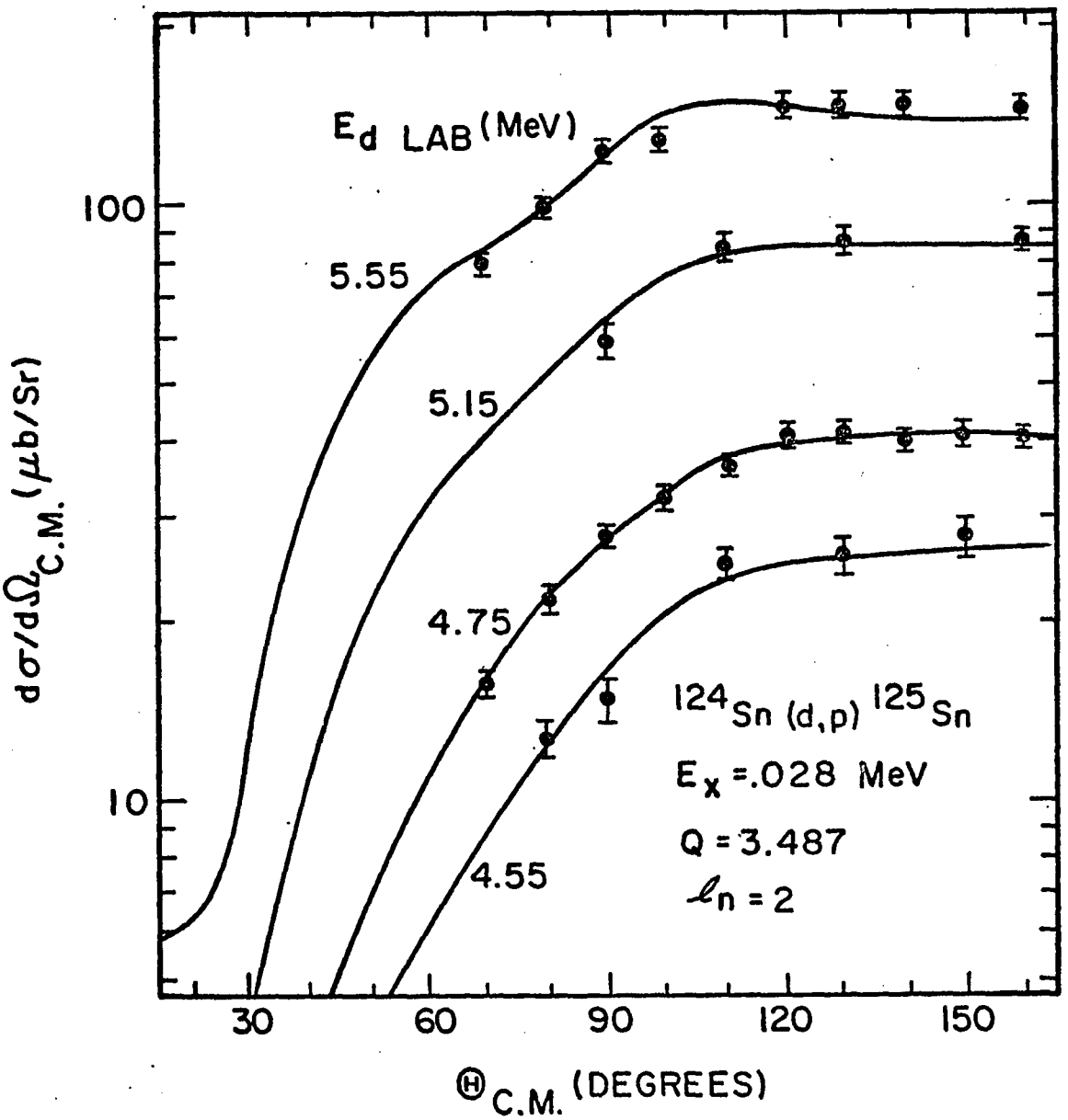

Fig. 18. Angular distribution for the first excited state in ^{125}Sn. The differential cross section is given for the ^{124}Sn(d,p)^{125}Sn reaction leading to the first excited state of ^{125}Sn at E_d = 5.55, 5.15, 4.75, and 4.55 MeV. The solid curves are from DWBA calculations with potential set A and are normalized to the experimental points.

The separation of the ground state and first excited state peaks in the E_d = 5.55-MeV runs was just discussed. Gaussian fits were made in the same manner in the spectra at 5.15 and 4.55 MeV. In all but the E_d = 4.75-MeV angular distributions, fitted cross sections and errors are plotted in Figs. 17 and 18 for the first and second excited states respectively. A dispersion of 20 keV per channel used in the 4.75-MeV spectra made fitting impractical. In the E_d = 5.15-MeV spectra the average fitted ground state cross section was 11 ± 4% of the total ground state and first excited state cross section. At 4.55 MeV the average ratio was 12 ± 4%. The ground state to first excited state yield ratio did not change in a strong, systematic way with angle at 4.55 and 5.15 MeV, so the 0.26-MeV first excited state cross section at 4.75 MeV was taken to be 88% of the doublet cross section. The errors shown for the E_d = 4.75-MeV angular distributions are the usual statistical errors.

Fig. 19 shows the angular distribution at 5.55, 4.75, and 4.55 MeV for the ℓ_n=1 state at 4.03-MeV excitation energy. With a Q value of -0.51 the 4.03-MeV level has angular distributions strongly peaked in the backward direction as is characteristic of pure Coulomb stripping. The first two excited states have somewhat more detailed angular distributions similar to the corresponding low-lying ℓ_n=0 and ℓ_n=2 states in ^{117}Sn and ^{123}Sn.

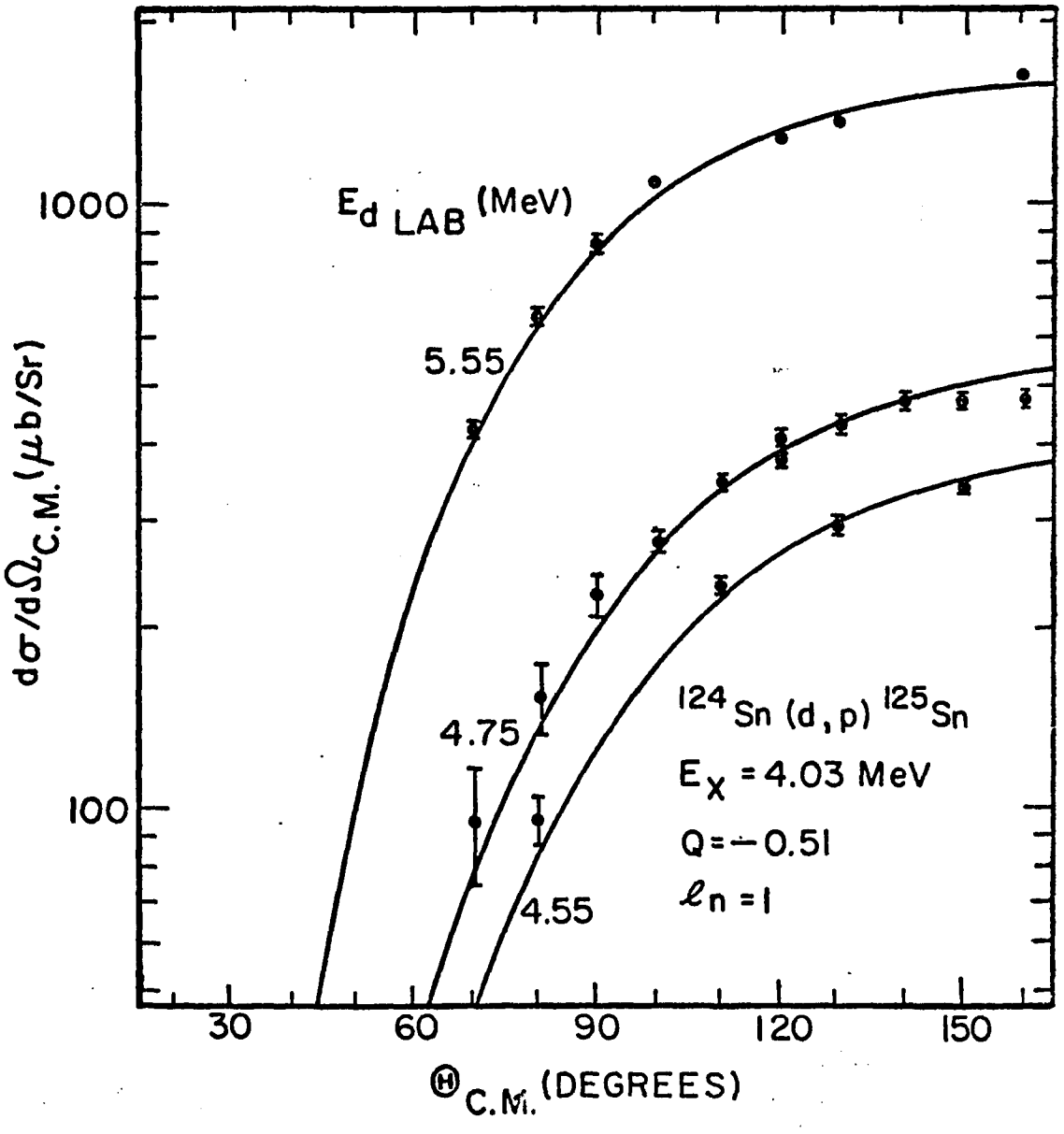

Fig. 19. Angular distribution for the 4.03-MeV level in ^{125}Sn. The differential cross section is given for the ^{124}Sn(d,p)^{125}Sn reaction leading to the 4.03-MeV level of ^{125}Sn at E_d = 5.55, 4.75, and 4.55 MeV. The solid curves are from DWBA calculations with potential set A and are normalized to the experimental points.

CHAPTER IV

DWBA ANALYSIS

Description of the DWBA Calculations

The DWBA calculations of differential cross sections reported in this work were performed with the computer code DWUCK, version of 26 October 1967, written and supplied by P. D. Kunz, in a private communication [38].

In the present description we will rely heavily on Kunz' "Algebra used by DWUCK" [39] and "Instructions for use of DWUCK" [40]. The calculations are performed in the zero-range approximation. The option is included for calculating the local energy approximation for finite range effects and non-local potentials. Spin-orbit forces may be included in the entrance and exit channels as well as in the bound state for the transferred particle(s).

The Transition Amplitude

The transition amplitude assumed for the reaction A(a,b)B is of the form

$$T = J \int d\underset{\sim}{r}_{bB} \int d\underset{\sim}{r}_{aA}\, \chi_b^{(-)*}(\underset{\sim}{k}_b, \underset{\sim}{r}_b)\, \langle bB|V|aA\rangle\, \chi_a^{+}(\underset{\sim}{k}_a, \underset{\sim}{r}_a)\ , \qquad (3)$$

where χ_b^- is the distorted wave of particle b with momentum $\underset{\sim}{k}_b$ and separation $\underset{\sim}{r}_b$ relative to the residual nucleus B. Similarly, χ_a^+ is the

distorted wave for particle a with coordinates relative to the target nucleus A. The calculation of the distorted waves will be described later. J is the Jacobian of the transformation to the relative coordinates. The matrix element $\langle bB|V|aA\rangle$ signifies integration over all internal coordinates of the colliding pairs, (b,B) and (a,A). When projectile a is a deuteron and projectile b is a proton, the interaction potential is usually approximated by the proton-neutron interaction V_{np} which is independent of the coordinates of the target nucleus, A, and the residual nucleus, B. Thus the matrix element may be separated into two parts [16],

$$\langle bB|V|aA\rangle \simeq \langle B|A\rangle \langle b|V_{np}|a\rangle . \tag{4}$$

In practice, the matrix element is expanded in a series of terms, each of which corresponds to the target nucleus receiving a particle and a transfer of total angular momentum j with orbital and spin angular momentum ℓ and s respectively. If the projectiles a and b have spins s_a and s_b respectively, and nuclei A and B have spins J_A and J_B, then [41,p. 82]

$$\underset{\sim}{j} = \underset{\sim}{J_B} - \underset{\sim}{J_A} , \quad \underset{\sim}{s} = \underset{\sim}{s_a} - \underset{\sim}{s_b} ; \text{ and } \underset{\sim}{\ell} = \underset{\sim}{j} - \underset{\sim}{s} \tag{5}$$

When only the S-state contribution of the deuteron is treated, as is the case in DWUCK, the matrix element vanishes for the (d,p) reaction except when $s = 1/2$ [41,p. 162]. The parity of the transition in a zero-range calculation is given by $(-1)^{\ell}$, a condition called "natural parity".

Written out completely, the matrix element $\langle bB|V|aA\rangle$ becomes for (d,p) stripping [39]

$$\langle J_B M_B s_b m_b | V_{np} | J_A M_A s_a m_a \rangle = \sum_{\ell j} \left[\sqrt{S_{\ell j}}\, D(\underset{\sim}{r}_{nb}) u_{\ell j}(r_{nA}) (-i)^{\ell}\, Y_{\ell m}^{*}(\hat{r}_{nA}) \right.$$

$$\left. \langle \ell s\, m\ \mu - m | j \mu \rangle\ \langle s_b s m_b m_b - m_a | s_a m_a \rangle\ \langle J_A j M_A M_B - M_A | J_B M_B \rangle \right] , \qquad (6)$$

where $u_{\ell j}(r_{nA})$ arises from the overlap integral $\langle B|A\rangle$, of the residual and target nucleus wave functions. $u_{\ell j}(r_{nA})$ may be regarded as the radial wave function of the captured neutron normalized by

$$\int u_{\ell j}^{2}(r_{nA}) r^2 dr = 1. \qquad (7)$$

The product, $\sqrt{S_{\ell j}}\, D(\underset{\sim}{r}_{nb})$ is a measure of the strength of the interaction, $\langle p|V_{np}|d\rangle$. The spectroscopic factor $S_{\ell j}$ will be explained shortly. In the zero range approximation,

$$D(\underset{\sim}{r}_{nb}) = D_o\, \delta(\underset{\sim}{r}_n - \underset{\sim}{r}_b) . \qquad (8)$$

A value of approximately 1.5×10^4 $MeV^2\text{-}F^3$ is standard for D_o^2. A value of 1.53×10^4 $MeV^2\text{-}F^3$ was used, based on derivations in [39] and [40] in which a Hulthèn wave function was used for the deuteron.

If one wants to express the reaction for definite isospin transfer, t, then the summation in (6) must be over t as well as ℓ and j and the isospin vector addition coefficient C must be added inside the summation [41,p.82]. One then may quote $C^2 S_{\ell j}$ which is independent of the

actual and assumed isospin transfer. But this does not concern us in neutron stripping reactions where t is always 1/2 and $C^2 = 1$.

The Differential Cross Section

The differential cross section for the reaction A(a,b)B is given in terms of the transition amplitude by [39]

$$\frac{d\sigma}{d\Omega} = \frac{\mu_a \mu_b}{(2\pi\hbar^2)^2} \frac{k_b}{k_a} \frac{1}{2J_A+1} \frac{1}{2s_a+1} \sum_{M_A M_B M_a M_b} |T|^2 , \qquad (9)$$

where μ_i and k_i are the reduced mass and relative momentum in channel i.

The cross section actually calculated by DWUCK does not include the spectroscopic factor and certain other terms. The differential cross section for (d,p) stripping to a single-particle state in terms of the differential cross section calculated by DWUCK, $\sigma_{DW}^{\ell j}$ is given in Ref.[39], in fm^2/sr by

$$\frac{d\sigma^{\ell j}}{d\Omega} = \frac{2J_B+1}{2J_A+1} S_{\ell j} \frac{D_o^2}{10^4} \frac{\sigma_{DW}^{\ell j}}{2j+1} \frac{2s+1}{2} . \qquad (10)$$

For even-even target nuclei, $J_A = 0$ and $j = J_B$ yielding simply

$$\frac{d\sigma^{\ell j}}{d\Omega} = 1.53 \, S_{\ell j} \, \sigma_{DW}^{\ell j} . \qquad (11)$$

The cross section calculated by DWUCK is related to the usual single-particle cross section of the program Julie, for single nucleon transfer, by

$$\sigma_{Julie}^{\ell j} = \frac{D_o^2}{10^4} \frac{\sigma_{DW}^{\ell j}}{2j+1} . \qquad (12)$$

The Spectroscopic Factor

The spectroscopic factor, $S_{\ell j}$, is determined experimentally as the normalization factor in matching the angular distribution of the theoretical differential cross section for the full single-particle strength, $1.53\ \sigma_{DW}^{\ell j}$, to the angular distribution of the experimental differential cross section, $d\sigma^{\ell j}/d\Omega$. For simplicity, we will drop the "ℓj" identification. S is varied to minimize the chi squared

$$\sum_i \left\{ \frac{1}{\delta_i^2} \left[\frac{d\sigma(\theta_i)}{d\Omega} - 1.53S\ \sigma_{DW}(\theta_i) \right]^2 \right\} , \qquad (13)$$

where δ_i is the error in the experimental cross section at angle θ_i. In practice this least squares fit was approximated by overlaying semi-logarithmic plots of the theoretical and experimental angular distributions to obtain the fits shown in the figures of angular distributions in the previous chapter.

The spectroscopic factor for (d,p) stripping, $S_{\ell j}$, can be understood in terms of the shell model as the square of the projection of the wave function of the residual nucleus, Ψ_B, onto the vector-coupled product of the target nucleus wave function, Ψ_A, and a single-particle state, $\Psi_{\ell j}$. If we consider the case where nuclei A and B consist respectively of n-1 and n equivalent active or valence neutrons plus inert spin zero cores [41,p. 290],

$$\sqrt{S_{\ell j}} = \sqrt{n} \left\langle \left\{ \Psi_{\ell j}, \Psi^a_{J_A} \right\}_{J_B M_B} \middle| \Psi^a_{J_B M_B} \right\rangle . \qquad (14)$$

the superscript a indicates wave functions for only the active neutrons.

When a maximum number of the active neutrons are paired to spin zero in the target and residual nucleus,

$$S_{\ell j} = 1 - \frac{n-1}{2j+1} \tag{15}$$

for pickup from odd nuclei or stripping to odd nuclei; and

$$S_{\ell j} = n \tag{16}$$

for pickup from even nuclei, or stripping to even nuclei. We have taken n to be the number of valence neutrons in the heavier of the two nuclei.

The Reduced Width

As we will see later, the major uncertainty in the distorted wave theoretical cross section is in the calculation of the radial part of the bound state neutron wave function, $u_{\ell j}(r_{nA})$. If the incident and outgoing particles are well below the Coulomb barrier, the stripping occurs predominantly far outside the nucleus. Outside the nucleus the neutron wave function is known to be proportional to a spherical Hankel function [16];

$$u_n(r) = N h_\ell^{(1)}(ikr), \quad \text{for} \quad r > R_N. \tag{17}$$

Here

$$k = \frac{1}{\hbar}\sqrt{2\mu_{An}\,|B_n|}\ , \tag{18}$$

where B_n is the neutron binding energy or, in experimental terms, the separation energy, and μ_{An} is the reduced mass. The constant of

proportionality, N, is determined by the overall normalization of the radial wave function, Eq. (7), and is therefore dependent on the neutron well parameters. However, for stripping outside the nucleus the calculated cross section is proportional to N^2, and the quantity σ_{DW}/N^2 is independent of the neutron well model and choice of parameters.

Two quantities, the reduced width factor [10,11] and, more recently, the reduced normalization [16] have been introduced to represent spectroscopic information while taking advantage of the relatively model-independent calculation of σ_{DW}/N^2 for Coulomb stripping. We use the former for convenience.

Noting again that at some radius, R_o, well outside the nucleus, $u_n(R_o)$ is proportional to N, we define the single-particle reduced width as [10,11]

$$\gamma_o = \frac{\hbar^2 R_o u_n^2(R_o)}{2\mu_{An}} \quad , \tag{19}$$

where μ_{An} is the reduced mass. The reduced width $\gamma_{\ell j}$ is defined by

$$\gamma_{\ell j} = S_{\ell j}\, \gamma_o \, . \tag{20}$$

Its independence of the normalization of the neutron wave function is apparent in the following equation analogous to Eq. (11),

$$\left(\frac{d\sigma}{d\Omega}\right)_{expt} = 1.53\, \gamma_{\ell j}\, \frac{\sigma_{DW}}{\gamma_o} \quad . \tag{21}$$

To be certain that the shape of the asymptotic tail of the neutron wave function was unaffected by the matching to the inner wave function, a radius R_o = 11 fm was chosen for calculation of the reduced widths. This compares with an average 6.2 fm for $r_o A^{\frac{1}{3}}$, the neutron well radius for the tin isotopes studied. As we will see later, the reduced width with this R_o is quite independent of our neutron well parameters including the correction for non-local potentials.

This relatively model-independent experimental quantity, γ, is only valuable for comparison with nuclear-structure calculations if a trustworthy value of $u_n(R_o)$ is available to convert γ to a spectroscopic factor. Most structure calculations use neutron wave functions which are not matched to a proper asymptotic tail and are therefore useless in producing a theoretical value for the reduced width at the large radius R_o chosen to be in the region of the asymptotic tail. The main use of the reduced width, or just publication of $u_n(R_o)$ for each level, should then be the elimination of the need for full DWBA calculations just for comparison of experimental measurements and for study of the behavior of spectroscopic factors, using certain new ways of calculating neutron wave functions.

The Distorted Waves

The distorted waves X_a^+ and X_b^- are well represented outside the nucleus by Coulomb partial waves with nuclear phase shifts obtained from elastic scattering [11]. For incident and outgoing particle energies well below the Coulomb barrier, the distorted waves contribute to the

overlap integral contained in Eq. (3), only in the region outside the nucleus. The distorted waves calculated with optical-model potentials obtained from elastic scattering should therefore be accurate for Coulomb stripping. At particle energies far below the Coulomb barrier there are major ambiguities in the nuclear optical-model parameters obtained from elastic scattering analysis. As is evident in Fig. 5, our featureless elastic deuteron angular distributions, which vary only slightly from Rutherford scattering, do not contain enough information to determine the many optical-model parameters unambiguously. However, this is mainly a reflection of the insensitivity of the distorted waves to the nuclear distorting potentials. Parameters extrapolated from higher-energy analysis should serve quite well.

The fairly standard form for the optical model potential is [40]

$$V(r) = V_c(r) + V_R f(x_R) + iV_I \frac{df(x_I)}{dx_I} - \frac{V_{SOR}}{r} \frac{df(x_{SO})}{dr} \underline{\ell} \cdot \underline{s} . \qquad (22)$$

In the above equation, V_c is the potential between a point projectile of charge z and a uniformly-charged nucleus of charge Z and radius $A^{\frac{1}{3}}$. For the nuclear potentials, the real central well shape is of the volume Woods-Saxon form,

$$f(x_i) = (1 + e^{x_i})^{-1} , \qquad (23)$$

where

$$x_i = \frac{r - r_i A^{\frac{1}{3}}}{a_i} \qquad (24)$$

and r_i and a_i are the well radius parameter and diffuseness, respectively, for a well of type i. In DWUCK, the atomic number A of the target nucleus is taken from the input M_T, the target mass in AMU, so the radius of a potential well, $r_i A^{\frac{1}{3}}$, is given as $r_i M_T^{\frac{1}{3}}$. The masses therefore have to be given precisely. The depth of the real volume well and that of the imaginary surface derivative well are given by V_R and V_I, respectively. Compared with the parameters V_S and W_D used by Perey [42], $V_R = -V_S$ and $V_I = 4W_D$. The real spin-orbit potential is of the Thomas form. The spin-orbit parameter is related to the usual spin-orbit term, V_{SO}, by

$$V_{SOR} = 2 \lambda_\pi^2 V_{SO} \approx 4V_{SO} \quad , \tag{25}$$

where λ_π is the reduced pion Compton wavelength. The negative sign of the spin-orbit term in Eq. (22) contradicts Ref.[40], but is compatible with the program DWUCK and with the use of a negative V_{SOR} in the examples in Ref.[40].

The Neutron Radial Wave Function

In the usual DWBA calculation, the summation over ℓ and j in Eq. (6) is replaced by a single term of a given ℓ and j. The neutron bound state radial wave function $u_{\ell j}$ is calculated in a potential well, usually Woods Saxon. The well depth is varied to give the proper separation energy for the neutron so the internal wave function can be matched to the proper asymptotic tail of the form in Eq. (17). This is the conventional separation energy, SE, prescription. Such a procedure would be

correct for stripping to a pure single-particle state. Significant variations of this procedure [43-47] allow for configuration mixing of different shell model states, but the calculations are at present too cumbersome to apply to nuclei as complex as the tin isotopes. Results of such calculations on various nuclei indicate differences in cross section from the SE procedure as high as 20-50% [45-47].

A variation of the usual prescription was suggested by Pinkston and Satchler [44] for vibrational nuclei. They propose keeping the well depth constant for all states and adjusting the neutron radius parameter to obtain the correct separation energy for each state. As they indicate, this can require large changes in well radius which have rather large effects on the spectroscopic factors. In principle, however, there is no reason for varying the neutron radius by large amounts, rather than the well depth. For our reported results, the standard well depth variation was used. Our reduced widths make further testing of this Pinkston and Satchler approach quite simple.

In the present calculation, the neutron wave function is calculated in a potential well of the same form as Eq. (22), with fixed geometry and with V_I=0 and V_{SOR} replaced by $V_R \cdot$(VSOR/45.2), where VSOR is the input variable for a second spin-orbit option in DWUCK. Since V_R is close to 45 MeV, $V_{SOR} \simeq$ VSOR. The previous warning to choose the target mass properly because of its relation to the radius of the potentials is particularly important in the neutron wave function calculations because of the dependence of the cross section on the potential radius.

Corrections to Local,
Zero-Range Calculations

The finite range correction for the n-p potential and the correction for non-locality in the distorting potential for each wave function including the bound state neutron wave function are calculated by DWUCK in the local energy approximation (LEA) [48;41,pp. 113,215] Each correction introduces into the integrand of the transition amplitude the factor given below which is dependent on the various potentials used.

The finite range correction is given by [40]

$$\omega(r) = \left[1 + \frac{2}{\hbar^2} \frac{m_p m_n}{m_d} R^2 (V_d(r) - V_p(r) - V_n(r) - \epsilon\right]^{-\frac{1}{2}}, \qquad (26)$$

where V_i is the optical potential for particle i, ϵ is the binding energy of the deuteron, and R is the finite range correction parameter. The non-local correction factor for particle i is [40]

$$\omega_i(r) = \left[1 - \frac{\beta^2}{4} \frac{2m_i}{\hbar^2} V_i(r)\right]^{-\frac{1}{2}}, \qquad (27)$$

where β is the non-local range parameter. The non-local correction for the deuteron and proton and the finite range correction were included in all the quoted calculations, although the effect was quite small.

The non-local correction for the bound state neutron potentials, however, has a marked effect on the cross section; since the non-local correction decreases the wave function in the nuclear interior, it thereby increases the normalization of the asymptotic tail in the region where stripping occurs. The non-local correction for the bound state

potentials is not included in our main results, although the effects of the correction are studied carefully. Ulrici and Hering [49] have shown that the LEA is in good agreement with a more complete treatment of non-local effects in the bound state wave function. There had been earlier indications that the LEA had an incorrect effect on the tail of the bound state wave function [50].

DWUCK does not include provisions for calculating the effects of electric polarization of the deuteron by the Coulomb potential of the target. Calculations have shown the effect on differential cross sections is rather small [11,16,51]. The effect varies appreciably with large changes in incident energy and Q value but varies only slightly with orbital angular momentum transfer. For Coulomb (d,p) stripping to the first two states in ^{139}Ba, Rapaport and Kerman [16] obtain approximately a 6% increase in the calculated cross section from the electric polarization of the deuteron. The effect on all our reported cross sections is probably less than 10%, and the effect is probably almost uniform for the low-lying states in all three nuclei studied.

DWBA Parameters Used and Their Effects

Deuteron and Proton Parameters

As we discussed in the previous section on the deuteron and proton distorted waves, unique optical-model parameters are not obtainable from elastic scattering angular distributions of particles well below the Coulomb barrier. This is clearly the situation for deuterons incident on tin at the energies we have employed, and is true for some of

the lower-energy protons of interest to us, as low as 4 MeV for the 4.03-MeV level in ^{125}Sn. However, when the elastic scattering angular distributions become insensitive to the potential parameters, so should the stripping angular distributions and cross sections. Parameters extrapolated from higher energies should then suffice. In fact, the often-used procedure of adjusting optical-model parameters for fitting stripping angular distributions can lead to more consistent results than are obtained with "proper" optical-model parameters [15]. We have tried various deuteron and proton parameters from higher energy elastic-scattering analysis, and checked the effects of the parameters on the DWBA stripping calculations.

Several sets of potential parameters for potentials of the form in Eq. (22) were tried and varied to obtain the best fit to the angular distribution of the (d,p) reaction at 5.35 MeV, leading to the ℓ_n=0 ground state of ^{117}Sn. This angular distribution should have the greatest dependence on the optical parameters.

The proton parameters of Perey [42] and the deuteron parameters of Perey and Perey set a [52] gave the best fits. They are listed as parameter set A in Table 6. These sets are from average fits over a wide range of nuclei and energies, and include a term in $Z/A^{\frac{1}{3}}$, a nuclear symmetry term, and an energy dependence in the real and imaginary well depth. The linear energy dependence in the real central well of $\Delta V_R/\Delta E$ = + 0.55 for protons and + 0.51 for deuterons was included in the present calculations for the different states in all three reactions. These are rather small changes, but slight improvement in fits to

Table 6. Potential parameters.[a]

Particle	Set	V_R (MeV)	r_R (F)	a_R (F)	V_I (MeV)	r_I (F)	a_I (F)	r_c (F)	V_{SOR} (MeV)
Deuteron	A	-73.[b]	1.15	0.87	64.	1.37	0.70	1.15	0.0
	B^+	-109.	1.15	0.81	64.	1.34	0.68	1.15	0.0
Proton	A	-55.8[b]	1.25	0.65	60.	1.25	0.47	1.25	-30.0
	D'	-51.0	1.25	0.747	60.	1.352	0.53	1.25	-30.0
									VSOR
Neutron	A_1	c	1.25	0.65					25
	A_2	c	1.27	0.65					25

[a]Parameter set A was used for quoted results, with neutron set A_1 used for the $^{116}Sn(d,p)^{117}Sn$ reaction, and set A_2 was used for the $^{122}Sn(d,p)^{123}Sn$ and $^{124}Sn(d,p)^{125}Sn$ reactions.

[b]Adjusted for particle energy.

[c]The neutron real well depth is adjusted to obtain the proper binding energy.

angular distributions from the $^{90}Zr(d,p)^{91}Zr$ reaction over a wide range of subcoulomb energies was observed [27] with inclusion of a similar energy dependence for the deuterons. The other variables in the real and imaginary well depth were kept constant for all of the final calculations.

The geometrical parameters r_R and a_R of the real volume potential well were used for the spin-orbit well. The proton spin-orbit potential had only a 1% effect on the differential cross sections, and was dropped in some of the later calculations to save computer time.

Deuteron set B^+, listed in Table 6, was obtained from set b of Ref. [52], but V_R is increased 22% as suggested by an analysis of the energy dependence of deuteron elastic scattering parameters for ^{114}Cd [53]. The larger V_R is more in accord with the present preference for deuteron potentials approximately twice those for protons. Proton set D' is from analysis of proton elastic scattering on ^{116}Sn at 9.8 MeV [54], except the value of V_I has been increased from 43 to 60 MeV. Proton energies from the population of the ground state of ^{117}Sn were as high as 10 MeV in our experiments.

Angular distributions calculated with the parameter sets listed in Table 6 are compared with experiment in Fig. 20 for the (d,p) reaction at 5.35 MeV, leading to the first two states in ^{117}Sn. As is typical for reasonable sets of optical-model parameters, the spectroscopic factors resulting from these sets vary by less than 12%, and relative spectroscopic factors between states vary a smaller amount. Similar tests, concentrating on the real well depths for the deuteron and proton showed a variation of less than 5% in the spectroscopic

Fig. 20. Sensitivity of angular distributions to deuteron and proton potentials.

Calculated angular distributions are compared with experiment for the (d,p) reaction at 5.35 MeV leading to the first two states in ^{117}Sn. Deuteron sets A and B^{+}, and proton sets A and D' are used to show the effects of various parameters on the shape and magnitude of the angular distributions. Nuclear potentials are zero for the curve labeled Coulomb.

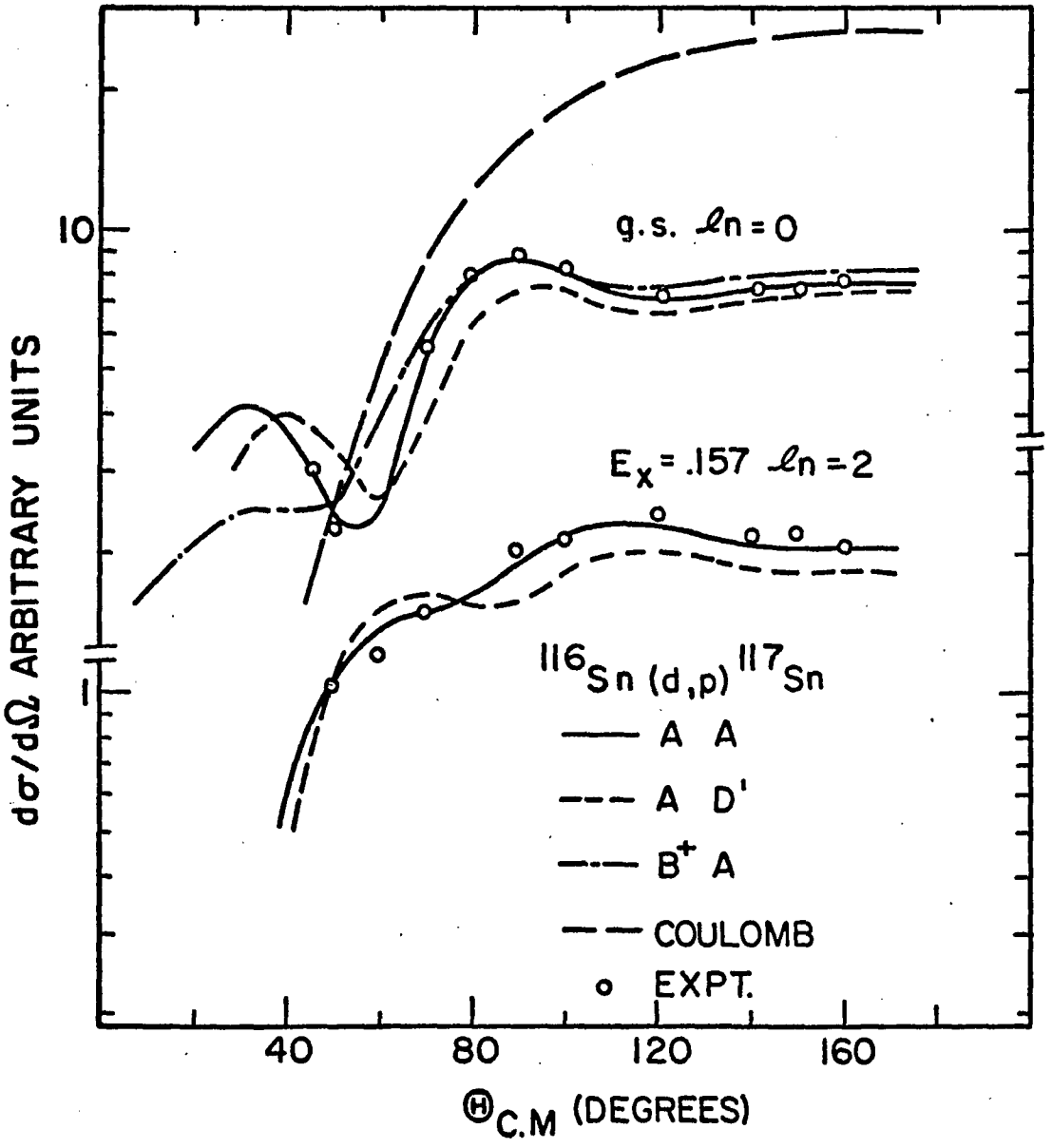

Fig. 20. Sensitivity of angular distributions to deuteron and proton potentials.

factor for the 0.217-MeV level in the $^{124}Sn(d,p)^{125}Sn$ reaction at 5.1 MeV [19]. At higher energies the variation is often much larger, using parameter sets that fit the elastic scattering data equally well [15,55].

Reduction of the proton imaginary potential increases the oscillatory behavior of the angular distributions. A 30% decrease in V_{Ip} can cause a 60% increase in the calculated height of the peak at 35° in the ^{117}Sn ground state angular distribution. The changes at angles greater than 70°, however, are around 10%. Variation of the proton imaginary potential with isotope as indicated by the nuclear symmetry term, $\Delta V_I = 180\ \Delta[(N-z)/A]$, of the Perey analysis [42] would increase V_{Ip} from 60 MeV for ^{117}Sn to 65 MeV for ^{125}Sn. Such a change has a negligible effect on the shape and magnitude of calculated angular distributions and was not included for the reported calculations.

The dashed curve in Fig. 20 labeled Coulomb shows the ground state angular distribution with all nuclear potentials set to zero. With increasing orbital angular momentum transfer and decreasing Q value, the regular optical-model angular distributions approach the pure Coulomb values. For the angular distribution shown in Fig. 19 for the 4.03-MeV level in ^{125}Sn, the calculations with and without nuclear potentials at $E_d = 4.75$ MeV differ by less than 4% at any angle greater than 40°.

The finite range correction, Eq. (26), was included in the reported calculations. A value of 0.621 [40] for the finite range correction parameter R was used causing a typical increase of approximately 4% in the calculated cross sections. The value of the non-local range parameter β in Eq. (27) was set at 0.85 for the proton and 0.54 for the deuteron [40]. The combined non-local correction for these two

particles resulted in a decrease in the calculated cross section of less than 1% at angles greater than 60°.

Choice of Neutron Well Geometry

Clearly the greatest uncertainty in the calculated cross sections arises from the uncertainty in the neutron potential parameters, in particular the Woods-Saxon well geometry, which is taken to be the same for both the central and spin-orbit potentials. The more critical well parameter, the radius r_n, is usually varied, and the diffuseness, a_n, kept constant at some value. Happily for those making comparisons, a_n is becoming somewhat standard in Coulomb-stripping analysis at 0.65 fm, the value we have chosen. Keeping the diffuseness constant is somewhat justified by the success of the reformulated optical potential [56], which has shown that variation of only one parameter, the volume integral of the potential well, is needed to fit elastic scattering data as well as the standard optical model does.

As will be discussed later, varying the neutron radius parameter has an effect on the spectroscopic factor of a state which depends primarily on the principal quantum number of the state [15]. In (d,p) stripping reactions on doubly-closed shell nuclei, one should be able to determine the neutron radius parameter and have a consistency check by requiring that spectroscopic factors be near unity for the major low-lying states, and not change systematically with the principal quantum number of those states. In two separate experiments [15,17] on the $^{208}Pb(d,p)^{209}Pb$ reaction at subcoulomb energies, this method has yielded

a value for heavy nuclei of r_n = 1.23 fm with a_n = 0.65 fm. The value of r_n would have been somewhat smaller if correction had been made for non-locality in the bound state potential.

The real well radius parameter of 1.25 fm and diffuseness of 0.65 fm used in the Perey set of proton parameters are close to the figures just mentioned for lead. They are also the values used by Schneid et al. [8] in their comprehensive analysis of spectroscopic factors in the tin isotopes, and are consistent to approximately ± 2% with the parameters obtained recently from proton elastic scattering on the higher A even tin isotopes at many incident energies [35,36,57].

The values r_n = 1.25 fm and a_n = 0.65 fm were therefore adopted for most of the present calculations. However, measurements of the difference in rms matter radii of the even tin isotopes show a radius dependence of greater than $A^{\frac{1}{3}}$. This indicates r_n should be larger for ^{124}Sn than ^{116}Sn.

In a study of polarization and cross section angular distributions for protons elastically scattered from isotopes of tin, standard optical-model analysis was used by Boyd et al. [57] to determine the nuclear matter rms radius for ^{120}Sn. Differences in the elastic scattering data were then used to obtain relative rms matter radii for ^{116}Sn, ^{118}Sn, and ^{124}Sn to ± 0.01 fm.

In the reformulated optical model [56], the mean square radius of a real central optical-model potential well $\langle r_{RC}^2 \rangle$ may be obtained from the rms radius of nuclear matter $\langle r_M^2 \rangle$ by

$$\langle r_{RC}^2 \rangle = \langle r_M^2 \rangle + \langle r_{2B}^2 \rangle , \qquad (28)$$

where $\langle r_{2B}^2 \rangle$ is the rms radius of the spin and isospin independent part of the two-nucleon interaction. A value of 4.3 fm^2 was used in Ref.[57] for $\langle r_{2B}^2 \rangle$, and we therefore use it to obtain $\langle r_{RC}^2 \rangle$ for ^{116}Sn and ^{124}Sn.

The mean square radius of a Woods-Saxon well can be related to the radius parameter and diffuseness by [56]

$$\langle r_{RC}^2 \rangle = \frac{3}{5} r_n^2 A^{\frac{2}{3}} + 7\pi^2 a_n^2 . \qquad (29)$$

Using a value of a_n = 0.65 fm, we obtain from the rms matter radii of Ref.[57], an r_n of 1.220 fm for ^{116}Sn and 1.243 fm for ^{124}Sn. From the quoted errors for the $\langle r_M^2 \rangle^{\frac{1}{2}}$, assuming a_n is a known constant, the absolute uncertainties in r_n are 0.03 fm and the relative uncertainties are 0.003 fm. Using the average $\langle r_M^2 \rangle^{\frac{1}{2}}$ from three separate experiments quoted in Ref.[57], one obtains values for r_n of 1.233 fm for ^{116}Sn and 1.251 fm for ^{124}Sn.

A difference in r_n of about 0.02 fm between ^{116}Sn and ^{124}Sn seems to be clearly indicated. This is a non-negligible difference for obtaining relative spectroscopic factors between these two isotopes. As can be seen from Table 8 to be discussed shortly, a decrease of 0.02 fm in r_n increases the spectroscopic factors from about 7% for the $3s_{\frac{1}{2}}$ states to about 13% for the $1h_{\frac{11}{2}}$ states. For comparison of our more extensive DWBA calculations for the (d,p) reaction on ^{116}Sn with those of Ref.[8], the value of r_n = 1.25 fm was maintained for ^{116}Sn while a value of r_n = 1.27 fm was adopted for ^{122}Sn and ^{124}Sn. Based on all the recent proton elastic scattering information [35,36,54,57], 0.03 fm is a

reasonable estimate for the absolute uncertainty in r_n for the fixed diffuseness.

Effects of Variations in the Neutron Potential

As we have mentioned several times, the major limit on the accuracy of extracted spectroscopic factors lies in the uncertainty in the bound state neutron potentials. The resulting uncertainty is not just in the absolute spectroscopic factors, but in the relative values for different states of the same nucleus.

The variation of spectroscopic factors with important neutron potential parameters is summarized in Table 7 for several states in ^{117}Sn and ^{126}Sn. Spectroscopic factors are given for two or three different values of the neutron radius parameter r_n. In the first case shown in Table 7, calculations were done with a local potential with no spin-orbit interaction. For the states in ^{117}Sn, results are given also for calculations with a spin-orbit interaction using VSOR=25 MeV, and for calculations with the same spin-orbit interaction and a correction for non-local potentials using $\beta = 0.8$. The spectroscopic factor for each state calculated with $r_n = 1.25$ fm, VSOR = 25 MeV, and $\beta = 0$ is taken as a standard. Listed in parentheses beside spectroscopic factors calculated with different parameters is the percent deviation from the standard value.

The neutron spin-orbit potential obviously has a different effect for states depending on their orbital and total angular momentum. As the figures for ^{117}Sn in Table 7 indicate, removing the spin-orbit

Table 7. Effects of the neutron potential parameters.[a]

Corrections		$^{116}Sn(d,p)^{117}Sn$ Q g.s. = 4.720			E_d = 5.35 MeV			
		$3s_{\frac{1}{2}}$ E_x = 0.0			$2d_{\frac{3}{2}}$ E_x = 0.16		$1h_{\frac{11}{2}}$ E_x = 0.31	
VSOR	β	r_n = 1.19	r_n = 1.25		r_n = 1.25		r_n = 1.19	r_n = 1.25
0	0	0.65(27)	0.51(0)		0.67(-12)		1.54(105)	0.97(29)
25	0	0.65(27)	0.51(*)		0.76(*)		1.17(56)	0.75(*)
25	0.8	0.54(6)	0.42(-18)		0.62(-18)		0.90(20)	0.58(-23)
		$^{124}Sn(d,p)^{125}Sn$ Q g.s. = 3.515			E_d = 5.55 MeV			
		$3s_{\frac{1}{2}}$ E_x = 0.22			$2d_{\frac{3}{2}}$ E_x = 0.03		$3p_{\frac{3}{2}}$ E_x = 4.03	
		r_n = 1.19	r_n = 1.25	r_n = 1.29	r_n = 1.19	r_n = 1.25	r_n = 1.19	r_n = 1.25
0	0	0.326(24)	0.263(*)	0.228(-13)	0.55(31)	0.42(*)	0.31(15)	0.27(*)

[a]Spectroscopic factors are given as a function of the neutron bound state radius parameter, inclusion of a bound state spin-orbit potential of VSOR=25 MeV, and inclusion of the non-local correction to the bound state potentials (β = 0.8). The well diffuseness is fixed at a_n = 0.65 fm, and r_n is in fm. Listed in parentheses is the percent deviation of a spectroscopic factor from the one with an asterisk.

potential increases the spectroscopic factor for the $h_{\frac{11}{2}}$, 0.31-MeV state by 29% while decreasing the spectroscopic factor for the $d_{\frac{3}{2}}$, 0.16-MeV state by 12%. The effect is a 7% increase for the 0.16-MeV state treated as a $d_{\frac{5}{2}}$ state and a 5% increase for the $d_{\frac{5}{2}}$ state at 2.31 MeV. This is indicative of a slight dependence of the spin-orbit effect on Q value or, equivalently, neutron binding energy.

The need for a bound state spin-orbit potential is well established and its strength can be determined reasonably well by proton elastic scattering. For a given geometry and central potential, the spin-orbit potential should be able to reproduce the splitting between two good single-particle states with $j = \ell + 1/2$ and $j = \ell - 1/2$.

Our value of VSOR = 25 MeV corresponds to a usual spin-orbit potential, V_{so}, varying from 5.7 to 6.7 MeV, depending on the central well depth. This is in the lower range of spin-orbit strengths determined from elastic scattering. Values of V_{so} commonly range as high as 8 MeV. Refs. [8] and [19], with which we will compare our spectroscopic factors, used V_{so} = 7.5 MeV and VSOR = 20 MeV, respectively.

The variation of spectroscopic factors with the neutron well radius is approximately linear over the small range of radii we have considered. In Ref. [16], the dependence is shown to be exponential for ℓ_n=1 transitions in the $^{40}Ca(d,p)^{41}Ca$ reaction over a range of r_n = 1.0 to 1.5 fm. In a rather complete study [15] of the effects of varying the neutron potential well geometry for the $^{208}Pb(d,p)^{209}Pb$ reaction, Jeans et al. [15] observed that the main difference from state to state in the effect of varying r_n was due to the number of nodes in the neutron wave function, i.e., the principal quantum number, n, minus one and

to a lesser extent to the differences in the binding energy of each state. These observations seem to be verified by our analysis.

As Table 7 indicates, the increase in spectroscopic factor as the neutron well radius is changed from 1.25 to 1.19 fm is 24% and 31%, respectively for the $3s_{\frac{1}{2}}$, 0.22-MeV, and $2d_{\frac{3}{2}}$, 0.03-MeV states in ^{125}Sn, and 56% for the $1h_{\frac{11}{2}}$, 0.31-MeV state in ^{117}Sn. Under the same conditions, the change in spectroscopic factor is 20% for the $3s_{\frac{1}{2}}$, 2.39-MeV state in ^{117}Sn, showing a slight lessening of the effect for lower neutron binding energy. Approximately the same information on the effect of varying r_n is given in Table 8, which lists the percent change in the calculated cross section for the (d,p) reaction to seven states in ^{125}Sn, when r_n is changed from 1.29 to 1.27 fm. One will recall that a radius parameter of 1.27 fm was used to calculate the neutron wave function for ^{123}Sn and ^{125}Sn, and 1.25 fm was used for ^{117}Sn.

Returning to Table 7, one can see that the inclusion of the correction in the local energy approximation for non-locality in the bound state potentials has a sizable effect on the spectroscopic factors ranging from -18% for the $3s_{\frac{1}{2}}$ and $2d_{\frac{3}{2}}$ states in ^{117}Sn to -23% for the $1h_{\frac{11}{2}}$ state. Since the spectroscopic studies of neutron well geometry on which we have relied did not include a non-local correction, and since it was thought at the time we started our analysis that there was major disagreement about the applicability of the correction to bound state wave functions, it was not included for our reported results. As can be deduced from a linear extrapolation of the figures for ^{117}Sn in Table 7, approximately the same spectroscopic factors would result if the non-local correction with $\beta = 0.8$ were included and r_n were reduced from

Table 8.. The change in calculated cross sections with a 0.02 fm decrease in r_n.[a]

$^{124}Sn(d,p)^{125}Sn$	r_n = 1.29 to 1.27	E_d = 5.55 MeV
$n,\ell,2\cdot j$	E_x	$\%\Delta\sigma$
3s1	0.22	-7
3s1	2.25	-6
3p3	4.03	-5
2d3	0.03	-8
2d5	1.54	-8
2f7	2.76	-8
1h11	0.00	-13
1g7	1.36	-12

[a]Listed is the percent change in the calculated cross section for the $^{124}Sn(d,p)^{125}Sn$ reaction to several states in ^{126}Sn when r_n is changed from 1.29 to 1.27 fm.

1.25 to 1.21 fm. The spectroscopic factors for the $3s_{\frac{1}{2}}$ and $1h_{\frac{11}{2}}$ states would be changed by about -2% and +5% respectively. Relative spectroscopic factors would be almost unchanged for states in the different isotopes with the same orbital and total angular momentum.

One may observe in Table 7 that the effects of varying the neutron radius over this range and including spin-orbit or non-local corrections are approximately independent of each other. Also, the effects of these changes are quite independent of the incident deuteron energy in the range from 4.5 to 5.5 MeV. In fact, Powell et al. [19] have shown that similar changes in r_n, VSOR, and β cause approximately the same change in calculated cross sections for the $^{124}Sn(d,p)^{125}Sn$ reaction at 12 MeV as at 5.1 MeV incident deuteron energy. Thus, they have disproved the argument that Coulomb stripping is more dependent on the neutron well parameters than stripping somewhat above the Coulomb barrier.

Based on proton elastic scattering data, we estimated the uncertainty in r_n to be 0.03 fm for a_n=0.65 fm. This is also a reasonable uncertainty from extrapolation of the parameters based on spectroscopic factors in Pb. The uncertainty in r_n yields an uncertainty in spectroscopic factors due to neutron well parameters of approximately 25% for the $1h_{\frac{11}{2}}$ and $1g_{\frac{7}{2}}$ states and approximately 13% for the other states. If, however, by comparison with theory or with (p,d) experiments using the same neutron well geometry one is convinced that the spectroscopic factor for the $1h_{\frac{11}{2}}$ state is known to better than 25%, then the spectroscopic factors for the s, d, and f states are probably known quite well.

That is assuming the whole approach of treating the states as single-particle states and keeping a fixed neutron well geometry for all states is valid. At the end of the next chapter, we argue on the basis of a sum rule that we do indeed know the $1h_{\frac{11}{2}}$ spectroscopic factor for ^{117}Sn to better than 25%, probably to the accuracy attained for relative spectroscopic factors. The variation of spectroscopic factors with the deuteron and proton optical-model parameters and with neutron well parameters suggests that the spectroscopic factors for the different states are correct relative to each other, to better than 15%.

For a given state in Table 7, the reduced width varies by less than 2% for any listed combination of the parameters. Excluding the $1h_{\frac{11}{2}}$ state, the variation in reduced width is less than 0.5%. This indicates that the stripping is occurring well outside the nucleus and is dependent only on the normalization of the asymptotic tail of the neutron wave function.

Deduced Spectroscopic Factors and Reduced Widths

Clearly the spectroscopic factor and reduced width obtained for a given level should be independent of the incident-particle energy in the reaction used to measure those quantities. Consistent determination of spectroscopic factors at several different incident-particle energies is a good indication that relative cross sections are being measured accurately, that the optical-model parameters for the incident and outgoing particles are suitable, and that the basic assumptions of the analysis such as assuming pure stripping, are suitable.

Spectroscopic factors were extracted for the first $s_{\frac{1}{2}}$ state and $d_{\frac{3}{2}}$ state in ^{117}Sn, ^{123}Sn, and ^{125}Sn from data at each of the three or four incident deuteron energies used to study each nucleus. These spectroscopic factors are listed in Table 9, along with the spectroscopic factor for the $h_{11/2}$, 0.31-MeV state in ^{117}Sn obtained at E_d = 5.35 and 5.15 MeV, and the spectroscopic factor taken at three energies for the $p_{\frac{1}{2}}$, 4.03-MeV level in ^{125}Sn. Beside each spectroscopic factor is its percent deviation from the energy-averaged value for that state.

The variation of the spectroscopic factors with energy is approximately within statistical uncertainties in the experimental cross sections for all the states listed in Table 9, except for the $d_{\frac{3}{2}}$, 0.03-MeV state and $p_{\frac{1}{2}}$, 4.03-MeV state in ^{125}Sn. There is a very slight tendency toward smaller spectroscopic factors at lower incident deuteron energy. This trend could be reversed by rather substantial changes in the optical-model parameters [27]. Reduced widths would show the same variation with incident deuteron energy as the spectroscopic factors since the neutron wave function is independent of the incident energy.

The variations shown in Table 9 are considerably less than the variation of spectroscopic factors with bombarding energy, when those energies are above the Coulomb barrier [15,58]. Except for the uncertainties from the neutron well geometry, our spectroscopic factors for states listed in Table 9 seem reliable to better than 10%.

Listed in Table 10 are the spectroscopic factors obtained in the $^{116}Sn(d,p)^{117}Sn$ reaction at E_d = 5.35 MeV for all of the identified s, d, g, and h states, and the more prominent f states in ^{117}Sn. Reduced

Table 9. Deduced spectroscopic factors at several incident deuteron energies. (%D = % deviation of S from the average value. $\%D = 100\ (S-S_{avg})/S_{avg}$.)

	E_d	0.0 MeV $s_{\frac{1}{2}}$ S	%D	0.16 MeV $d_{\frac{3}{2}}$ S	%D	0.31 MeV $h_{\frac{11}{2}}$ S	%D
$^{116}Sn(d,p)^{117}Sn$	5.35	0.52	0	0.76	0	0.79	0
	5.15	0.54	4	0.78	3	0.79	0
	4.55	0.50	-4	0.74	-3		
	Avg.	0.52		0.76		0.79	
	E_d	0.15 MeV $s_{\frac{1}{2}}$ S	%D	0.03 MeV $d_{\frac{3}{2}}$ S	%D		
$^{122}Sn(d,p)^{123}Sn$	5.15	0.30	3	0.45	2		
	4.75	0.28	-3	0.43	-2		
	4.55	0.29	0	0.44	0		
	Avg.	0.29		0.44			
	E_d	0.22 MeV $s_{\frac{1}{2}}$ S	%D	0.03 MeV $d_{\frac{3}{2}}$ S	%D	4.03 MeV $p_{\frac{1}{2}}$ S	%D
$^{124}Sn(d,p)^{125}Sn$	5.55	0.25	4	0.43	8	0.25	9
	5.15	0.23	-4	0.42	5		
	4.75	0.24	0	0.38	-5	0.22	-4
	4.55	0.23	-4	0.36	-10	0.23	0
	Avg.	0.24		0.40		0.23	

Table 10. Spectroscopic factor and reduced width for states in ^{117}Sn.[a]

E_x (MeV)	n,ℓ,2·j (assumed)	γ (keV)	S 5.35 MeV	S[b] 15 MeV	S[b] renorm.
0.0	3s1	2.17	0.52	0.65	0.49
0.157	2d3	1.57	0.76	0.55	0.65
0.313	1h11	0.277	0.79	0.81	
0.705	1g7	0.043	0.11	0.13	0.13
1.015	2d5	0.219	0.064	0.061	0.079
1.178	2d5		0.039	0.033	0.043
1.302	2f7	0.107	0.037	0.029	
1.499	2d5		0.028	0.020	0.026
1.668	2d5		0.007	0.007	0.009
2.046	2f7		0.027	0.025	
2.076	3s1		0.009		
2.146	2d3		0.005		
2.31	2d5	0.023	0.004	0.012	0.016
2.39	3s1	0.045	0.004		
2.461	2f7		0.044	0.030	
2.545	2f7	0.087	0.019	0.017	
2.770	2d3		0.006		
3.113	2d3	0.089	0.013		
3.235	2f7		0.12	0.120	
3.785	2f7	0.437	0.058	0.030	

[a] Results of the analysis of the ^{116}Sn(d,p)^{117}Sn reaction at E_d = 5.35 MeV are compared with the spectroscopic factors from the same reaction at 15 MeV [8].

[b] See Ref.[8]. S_{renorm} = their $S_{measured}$ times the renormalization coefficient in their Table 9.

widths for R_o = 11 fm are given for most of those states and a comparison is made with the experimental and renormalized spectroscopic factors from the (d,p) reaction at 15 MeV [8].

It should be noted that there is no uniform upper limit on the value of reduced widths comparable to the unit upper limit on spectroscopic factors. The statistical weight factors for the (d,p) spectroscopic factors are such that, neglecting the effects of spin-orbit forces, (2j+1)S is independent of the assumed angular momentum j of the state. Spin-orbit effects in the neutron bound state are non-negligible but may be estimated using Table 7. If the 1.499-MeV level were $d_{\frac{3}{2}}$ instead of $d_{\frac{5}{2}}$ as some of the evidence in Chapter 3 indicates its spectroscopic factor would be 0.049. The relation of the spectroscopic factors to theory and other experiments including Ref.[8] will be discussed in the next chapter.

Spectroscopic factors and reduced widths were extracted for three states in ^{123}Sn from the ^{122}Sn(d,p)^{123}Sn reaction at E_d = 5.15 MeV. Spectroscopic factors and reduced widths were extracted for ten states in ^{125}Sn from the ^{124}Sn(d,p)^{125}Sn reaction at E_d = 5.55 MeV. The results for ^{123}Sn and ^{125}Sn are listed in Tables 11 and 12, respectively. Included in these tables are related spectroscopic factors from other experiments. In the next chapter a comparison will be made between these listed sets of spectroscopic factors.

Table 11. Spectroscopic factor and reduced width for states in ^{123}Sn.[a]

E_x (MeV)	$n,\ell,2\cdot j$ (assumed)	γ (keV)	S 5.15 MeV	S[b] 15 MeV	s[b] renorm.	S_{pp}[c]
0.025	2d3	1.73	0.45	0.43	0.52	0.28
0.150	3s1	2.27	0.30	0.36	0.27	0.18
2.716	2f7	2.39	0.25			0.60

[a]Results of the analysis of the ^{122}Sn(d,p)^{123}Sn reaction at E_d = 5.15 MeV are compared with spectroscopic factors for the same states and the same reaction at 15 MeV [8] and for the isobaric analog states from the ^{122}Sn(p,p)^{122}Sn reaction.

[b]See Ref. [8]. S_{renorm} = their $S_{measured}$ times the renormalization coefficient in their Table 9.

[c]See Refs. [35,36].

Table 12. Spectroscopic factor and reduced width for states in ^{125}Sn.[a]

E_x (MeV)	$n,\ell,2\cdot j$ (assumed)	γ (keV)	S 5.55 MeV	S^b 15 MeV	S^b Renorm.	S^c 5.1 MeV	S^c 12 MeV	S_{pp}[d]
0.000	1h11	0.186	0.29				0.315	
0.028	2d3	1.64	0.43	0.34	0.41		0.212	0.24
0.0 + 0.028	2d3		0.48			0.336		
0.217	3s1	2.12	0.25	0.25	0.19	0.186	0.168	0.19
0.936	2d3	0.129	0.023			0.008 (2d5)	0.014 (2d5)	
1.261	2d5	0.318	0.040	0.039	0.051	0.032	0.034	0.040
1.364	1g7	0.024	0.022				0.032	
1.540	2d5	0.181	0.022	0.023	0.030	0.016	0.021	0.014
2.254	3s1	0.133	0.006	0.009	0.007			
2.760	2f7	4.35	0.53					0.79
4.03	3p3	12.5	0.25	0.24				
	3p1	25.4	0.53					

[a]Results of the analysis of the ^{124}Sn(d,p)^{125}Sn reaction at E_d = 5.55 MeV are compared with spectroscopic factors for the same states and the same reaction [8, 19] and for the isobaric analog states from the ^{124}Sn(p,p)^{124}Sn reaction [35].

[b]See Ref.[8]. S_{renorm} = their $S_{measured}$ times the renormalization coefficient in their Table 9.

[c]See Ref.[19].

[d]See Refs.[35,36].

CHAPTER V

COMPARISON OF SPECTROSCOPIC FACTORS WITH THEORY AND WITH OTHER EXPERIMENTS

Comparison with Other Experimental Determinations

Most spectroscopic factors from other experiments which may be compared directly with the present values are listed for the appropriate nucleus in Tables 10, 11 and 12. The results of Schneid et al. [8] from the (d,p) reaction at 15 MeV may be compared with our results for all three nuclei, ^{117}Sn, ^{123}Sn, and ^{125}Sn. As discussed in the previous chapter, this comparison is particularly valid since the neutron well parameters used in the analysis of both experiments are approximately the same.

Schneid et al. [8] also obtained complementary (d,t) cross sections but were not able to obtain spectroscopic factors directly from DWBA calculations because accurate triton optical-model parameters were not available for tin. In order to obtain (d,t) spectroscopic factors they used DWBA calculations to remove the Q value dependence of the (d,t) cross sections. A simple result of pairing theory, Eq. (30) in the next section, was used for each state, $s_{\frac{1}{2}}$, $d_{\frac{3}{2}}$, $d_{\frac{5}{2}}$, and $g_{\frac{7}{2}}$, over all the isotopes studied to normalize the (d,t) spectroscopic factors and renormalize the (d,p) spectroscopic factors. The renormalized (d,p) spectroscopic factors, S_{renorm} in Tables 10, 11 and 12, are then consistent on an average basis over the isotopes with the (t,d) results and the relation of Eq. (30).

In the next section, a comparison is made between the spectroscopic factors for the lowest $s_{\frac{1}{2}}$, $d_{\frac{3}{2}}$, $g_{\frac{7}{2}}$, and $h_{\frac{11}{2}}$ states that we have in common with the 15-MeV experiment of Schneid et al. [8]. For the main $s_{\frac{1}{2}}$ and the main $d_{\frac{3}{2}}$ states in ^{117}Sn, the renormalized 15-MeV spectroscopic factor is in much better agreement with our result than the experimental 15-MeV value. The 30% renormalization change for the $d_{\frac{5}{2}}$ states seems a factor of two too large. In ^{123}Sn and ^{125}Sn, both 15-MeV sets agree with our spectroscopic factors about equally well.

The $f_{\frac{7}{2}}$ spectroscopic factors for ^{117}Sn from the experiment at 15 MeV are noticeably lower than the present values, considering the fact that the 15-MeV results for the 2.046-, 3.235-, and 3.785-MeV levels include unresolved levels. In the present analysis, spectroscopic factors were not extracted for the $p_{\frac{3}{2}}$ levels in ^{117}Sn, however, our value agrees with the 15-MeV result for the large isolated p level in ^{125}Sn.

The spectroscopic factors S_{pp} listed in Tables 11 and 12 are for isobaric analogs in ^{123}Sb and ^{125}Sb to some of the states we have observed in ^{123}Sn and ^{125}Sn. They are preliminary results obtained by Boyd and Arking from study of resonances in the ^{122}Sn(p,p)^{122}Sn and ^{124}Sn(p,p)^{124}Sn reactions [35], using methods described in Ref. 36.

The S_{pp} may be compared with spectroscopic factors S_n calculated by a different method in the same references for the same data and with spectroscopic factors from an earlier experiment, using the same reaction on many isotopes of tin [59]. The S_{pp} listed in Tables 11 and 12 resemble our spectroscopic factors for the analogous states in Sn. Since Boyd reported very few resonances in the region of the analogs to

the 2.760-MeV level in ^{125}Sn, and the 2.716 in ^{123}Sn, we might assume that the S_{pp} for the analogs to the 2.760- and 2.716-MeV levels are affected by the nearby states. States within ± 50 keV have cross sections in our spectra totaling 11% of the 2.760 cross section, and 53% of the 2.716 cross section.

A rather complete comparison of spectroscopic factors S_{pp} extracted by resonance analysis with those from DWBA methods is reported in Ref.[60]. In a study of many states in the Ba isotopes, they used the same optical-model parameters and well parameters for both methods. The agreement between the two approaches was fairly good, but large discrepancies existed for some states.

The spectroscopic factors in Table 12 marked 5.1 MeV and 12 MeV are from the study of the ^{124}Sn(d,p)^{125}Sn reaction at those energies by Powell, Dallimore, and Davidson [19]. The listed spectroscopic factors are based on local, zero-range (LZR) calculations. Powell et al. also included spectroscopic factors based on calculations including, in the local energy approximation, corrections for non-local and finite range effects in all potentials. The calculations were performed with the DWBA code DWUCK with similar neutron potential parameters to those we used.

Making corrections for the slight differences in the calculations, our spectroscopic factors should be approximately 10% smaller than their LZR values listed in Table 12, at least for their 5.1-MeV results. To the contrary, their 5.1-MeV LZR spectroscopic factors are from 20-30% smaller than ours. One may compare the experimental cross

sections from their figures for the 0.217-MeV level and the 0.028 plus ground state with our cross sections at 5.15 MeV, interpolated to 5.1 MeV. This shows that the difference is almost entirely in the experimental cross section. The most likely sources of the difference are an error of 150-200 keV in incident deuteron energy, or an error in target thickness and detector solid angle determination, both of which seem quite unlikely in our experiment with the procedures described in Chapter II. Powell et al. [19] used approximately the same elastic scattering method as we did for determining target thickness and detector solid angle; however, they may have normalized against beam current, and may have evaporated some of their target with the beam.

Comparison of Experimental and Theoretical Occupation Parameters

The single-particle shell model assumes that a certain number of valence nucleons move in a common potential produced by an inner core of nucleons which is comprised of pairs of identical particles coupled to zero spin and magnetic moment. The number of particles not so coupled is the seniority of the system. Varying residual interactions may be included between the active nucleons. Calculations of this type can predict many properties of a wide range of nuclei. The extreme single-particle model treats only one nucleon moving in an average (shell model) potential due to the remaining even-even core. This model, with a spin-orbit term in the potential yields the familiar single-particle wave functions and single-particle energy levels. Relatively large gaps exist between some of the single-particle levels. Nucleons filling

levels up to a gap are often considered to form a closed shell for more complete single-particle shell models.

Such a gap exists in the single-particle energies when levels up through the $1g_{\frac{9}{2}}$ are filled with fifty nucleons. Thus in the tin isotopes with fifty protons, the protons are expected to form a rather inert spherical core for the ground and lowest excited states, and the neutrons are expected to be filling the $1g_{\frac{7}{2}}$, $2d_{\frac{5}{2}}$, $2d_{\frac{3}{2}}$, $3s_{\frac{1}{2}}$, and $1h_{\frac{11}{2}}$ levels in the N=50 to 82 shell in that approximate order. The above ordering of levels is followed in the excitation energies of the low-lying states of ^{111}Sn, indicating a particle-like configuration for that nucleus, and the inverse ordering is followed in the excitation energies of the states of ^{125}Sn, indicating a hole-like configuration [12].

In the following general description of the application of pairing theory to the isotopes of tin, we rely greatly on a recent review article by E. U. Baranger [9]. Clearly, the number of active neutrons and single-particle states in the intermediate mass tin isotopes such as ^{117}Sn is too great to be handled by conventional shell-model programs, which include interactions between the active neutrons, nor have such shell-model programs yet been applied to the lightest and heaviest tin isotopes. The main residual interaction between the active neutrons is the pairing force. The BCS theory of superconductivity handles a pairing force in a simple, approximate way. Applications of the BCS theory to single closed-shell nuclei such as the tin isotopes have been fairly successful for over a decade. The ground state of an even number of active identical particles spread over a chosen number of single-particle levels is assumed to consist of pairs of particles coupled to

zero angular momentum, i.e., seniority-zero. The "gap equations" of the theory are used to determine the set of occupation probabilities of the single-particle levels which yields the lowest energy for the system.

A transformation is made to quasi-particle states which are linear combinations of single-particle and single-hole states. In this linear expansion, the square of the coefficients for the particle- and hole-states are the "emptiness" and "fullness" parameters u_j^2 and v_j^2 of the QP state, where $(2j+1)v_j^2$ equals the expectation value of the number of identical spin j particles in the QP state and

$$u_j^2 + v_j^2 = 1 \quad . \tag{30}$$

There is a one-quasi-particle (1QP) state for each single-particle state. Interactions between quasi-particles may be transformed from single-particle interactions and handled in an analogous way to single-particle interactions.

The lowest states of the odd isotopes are 1QP states. Higher excited states are 3QP and 5QP states or, if collective vibrations of the core are included explicitly, 1QP plus phonon states. The simple excited states of even isotopes are 2QP and 4QP states with excitation energies equal to the sum of appropriate 1QP energies. Thus, the excitation of the first simple excited state in even isotopes is twice the lowest 1QP energy. This is the energy gap observed in even spectra.

The occupation parameters v_j^2 and u_j^2 may be measured experimentally by stripping and pickup reactions. In pairing theory, for even 0^+ targets, stripping and pickup reactions to a state of spin j have cross

sections proportional to u_j^2 and v_j^2, respectively [61,62]. For odd targets in a state of spin j, stripping and pickup cross sections to the even ground state are proportional to v_j^2 and u_j^2, respectively. In accordance with these relations, we have equations analogous to Eqs. (15) and (16) of the previous chapter.

If we again let nucleus B be the heavier of the two nuclei rather than being the residual nucleus, then simple pairing theory (pure 1QP states) predicts

$$S_j = (2j+1)\, v_j^2(B), \qquad \text{for even B,} \tag{31}$$

and

$$S_j = u_j^2(A), \qquad \text{for even A [61].} \tag{32}$$

Eqs. (31) and (32) may be compared with exact sum rules which do not depend on pairing theory, but only on the assumption that just neutrons are active. The general non-energy-weighted (NEW) monopole sum rule for stripping is

$$\sum_{\alpha_B J_B} \frac{2J_B+1}{2J_A+1}\, S(\alpha_A J_A, lj \,|\, \alpha_B J_B) = \langle \text{neutron holes, A} \rangle_j \ , \tag{33}$$

where the right side, the expectation value of the number of neutron holes of spin j, is equal to $(2j+1)\, u_j^2(A)$ of pairing theory. Any additional quantum numbers needed to fully specify the state are represented by α, and the quantity after S is just an identifier.

For pickup transitions,

$$\sum_{\alpha_A J_A} S(\alpha_A J_A, \ell j | \alpha_B J_B) = \langle \text{neutrons, B} \rangle_j \quad , \tag{34}$$

where the expectation value of the number of neutrons of spin j is equal to $(2j+1)\, v_j^2(B)$ of pairing theory. French and Macfarlane [63] have shown that if protons are active in the same orbit, j, then Eq. (34) must include a term on the left side for pickup to states with isospin $T_A = T_B + 1/2$. The additional term is $C^2 \sum_{\alpha_A J_A} S_+$, where C^2 is $1/(2T_B+2)$. For an even, seniority-zero target nucleus, the sums in Eqs. (33) and (34) are over all final states of spin j.

In the event the entire S sum is concentrated in a single final state, Eq. (33) becomes identical with Eq. (32) for stripping, and Eq. (34) reduces to Eq. (31) for pickup. This is approximately the case for the $s_{\frac{1}{2}}$, $d_{\frac{3}{2}}$, $h_{\frac{11}{2}}$, and $g_{\frac{7}{2}}$ states in the odd tin isotopes with A=115 to 125. In these nuclei, the lowest level with each of the above assignments has greater than 9 times the yield of any other level with the same assignment [8,12]. The same is true for ^{111}Sn and ^{113}Sn except for some strength in a higher $s_{\frac{1}{2}}$ state in ^{111}Sn and some fairly strong higher $s_{\frac{1}{2}}$ and $d_{\frac{3}{2}}$ states in ^{113}Sn. Using just the main four low levels in each odd nucleus, the experimental occupation parameters u_j^2 and v_j^2 are obtained from Eqs. (31) and (32) for $j^\pi = 1/2^+$, $3/2^+$, $7/2^+$, and $11/2^-$. The experimental and theoretical occupation parameters are compared in Fig. 21, which is taken largely from a similar figure in the review work of E. U. Baranger [9], which is in turn taken in part from Ref.[5]. The theoretical curve of Ref.[9], and the (p,d) results for v_j^2 of Cavanagh [64,65],

Fig. 21. Comparison of theoretical and experimental occupation parameters.

Occupation parameters based on the lowest level of each indicated spin are shown. The theoretical curve is from Ref. [9]. The experimental values are based on the spectroscopic factor for stripping or pickup to or from the lowest state of spin j. The symbol □ and x are from the present experiment and Ref. [8], respectively. They represent values of u_j^2 from the (d,p) reaction on even isotopes. The triangles indicate values of v_j^2 from the (d,p) reaction on odd isotopes [8]. The circles represent values of v_j^2 from the (p,d) spectroscopic factors of Refs. [64] and [65].

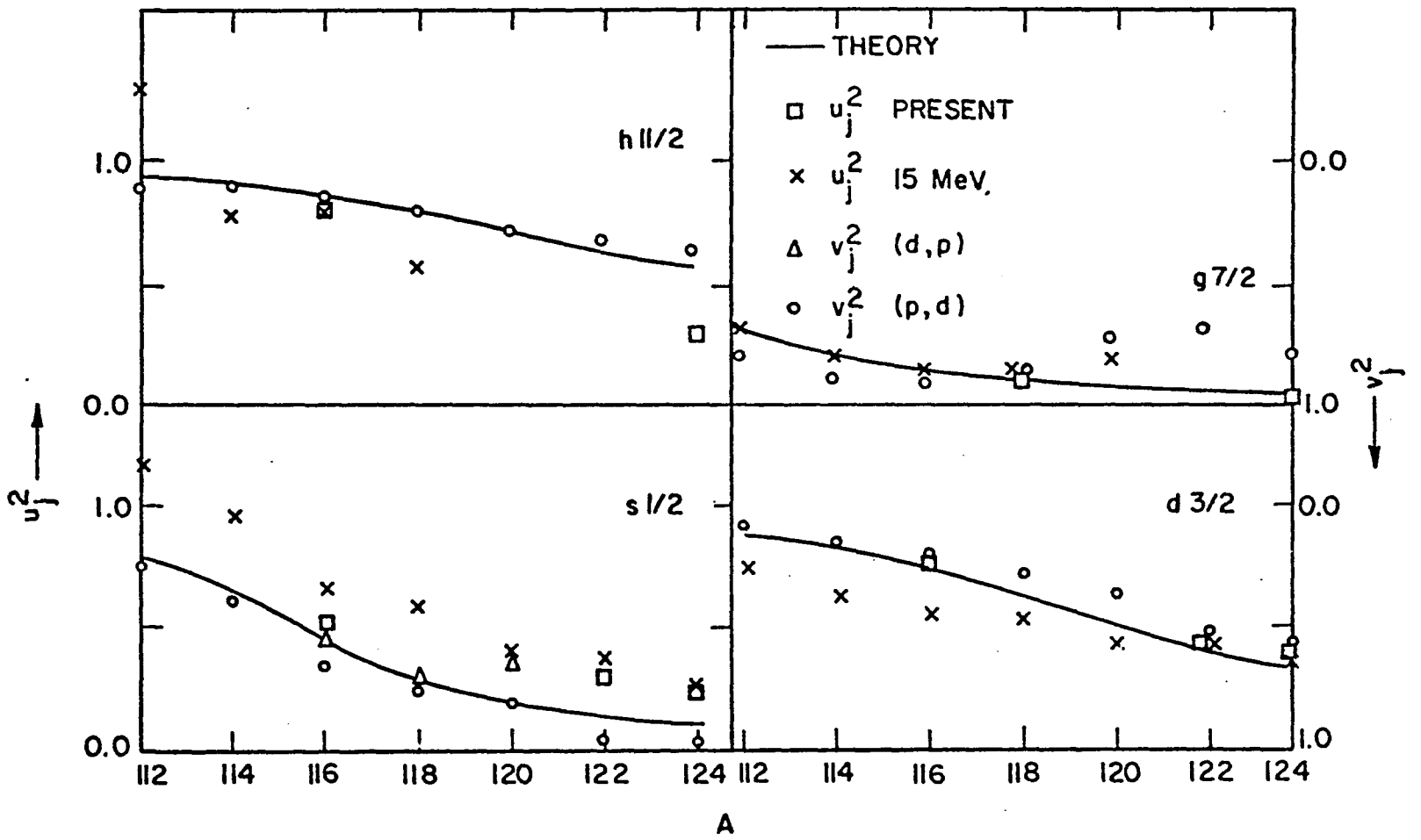

Fig. 21. Comparison of theoretical and experimental occupation parameters.

which we have not seen, are taken from Ref.[9]. The u_j^2 from earlier (d,p) data [8] are the same as in Ref.[9], except for $u^2_{\frac{11}{2}}$ for ^{112}Sn. We have added the present experimental values of u_j^2 as well as the $v_{\frac{1}{2}}^2$ from the (d,p) transition to the ground state of even isotopes [8]. Our values are based on the energy averaged spectroscopic factors of Table 9 for levels included in that table. Other appropriate experimental results for one nucleus [19,30], and unpublished results for ^{123}Sn shown in Ref.[9], have been omitted for clarity. In comparing results in cases such as the $s_{\frac{1}{2}}$ state in ^{124}Sn, or the $g_{\frac{7}{2}}$ state in all the isotopes, where one occupation parameter is near zero, and the other near unity, it is more appropriate to think of the difference in results in terms of a percentage of the larger occupation parameter.

The theoretical values shown in Fig. 21 are for 1QP states. If the states were pure 1QP states and the experiments and DWBA theory were correct, the experimental points and the theory would coincide for each nucleus. In fact, they do fairly well.

Calculations using a Gaussian residual interaction with phenomenological parameters indicate 3QP admixtures to the same states affect the occupation parameters by less than 10% except for the $g_{\frac{7}{2}}$ state in the heavier isotopes [4]. This is consistent with the small cross sections observed for any higher levels with the same configuration. Other experiments more sensitive to slight deviations from pure 1QP states indicate some admixture of other configurations [9].

Except for the 0.02 fm increase in our value of r_n for ^{122}Sn and ^{124}Sn, and an almost negligible difference in the spin-orbit potential,

the neutron well parameters used in the present work are the same as those used by Schneid et al. [8]. Major differences in u_j^2 between the two experiments then should be due to some nonstripping reaction strength in either experiment or to the rather great sensitivity to optical-model parameters at the higher energy of Ref.[8]. A significant difference between the two experiments is apparent for ^{116}Sn with their $u_{\frac{1}{2}}^2$ larger than ours and $u_{\frac{3}{2}}^2$ smaller than ours. Thus, each experiment would give a different slope to the u_j^2 versus isotope curve for those two states.

If the real central well parameters for the neutron were chosen correctly, assuming pure 1QP states, then u_j^2 from the (d,p) reaction on the even isotopes should equal $(1-v_j^2)$ from the (d,p) reaction on the appropriate odd isotopes and the (p,d) reaction on the appropriate even isotopes. This is approximately the case. Unfortunately, not having obtained Refs.[64] and [65], we do not know any details of the DWBA analysis of the (p,d) data; so only a comparison of the relative change of the occupation parameters with A is meaningful. In that respect our agreement with their results is at least as good as with the (d,p) data of Ref.[8]. The fairly large separation between the (p,d) results and ours on the $s_{\frac{1}{2}}$ levels indicates inaccuracy of some type considering the relative insensitivity of the ℓ_n=0 spectroscopic factors to neutron well parameters. It is interesting to note that the theoretical u_j^2 for the $s_{\frac{1}{2}}$ states are higher, in better agreement with our measurements, when second-order corrections in the matrix elements are not included in the calculations [5]. The $d_{\frac{3}{2}}$ occupation parameters are only slightly affected by the second-order corrections.

In renormalizing their occupation parameters, Schneid et al. [8] made u_j^2 from their (d,p) data equal $1-v_j^2$ from their (d,t) data as much as was possible through choosing for all isotopes a renormalization constant for each angular momentum j. Plotted as in Fig. 21, their renormalized occupation parameters for the $d_{\frac{3}{2}}$ and $s_{\frac{1}{2}}$ states give clearly better agreement with our experimental u_j^2 results than did their experimental u_j^2. For the $s_{\frac{1}{2}}$ states there is better agreement of the renormalized values with our results than with the theory or the (p,d) results.

Although our cross section for the $h_{11/2}$ ground state of ^{125}Sn may be somewhat uncertain, it is unlikely that the cross section is as large as would be necessary for agreement with the (p,d) data or the theory. This would require the ground state to contribute as much as 30% of the total ground state plus first excited state doublet cross section. This seemed clearly unlikely in looking at the spectra. Our value of $u^2_{\frac{7}{2}}$ for ^{124}Sn is from the 1.364-MeV level in ^{125}Sn. The $g_{\frac{7}{2}}$ assignment for this level is tentative [19], and it is not clear that there are no $g_{\frac{7}{2}}$ levels in ^{125}Sn with larger yields, but obscured by even stronger peaks such as the one at 1.261 MeV.

The general agreement of the simple experimental and theoretical occupation parameters indicates that the pairing theory description of the ground state of the even tin isotopes is fairly accurate, and it indicates that the lowest levels of the odd tin isotopes can be described by predominantly 1QP states. Or, as E.U. Baranger [9], concluded, at least the lowest levels of the odd tin isotopes are predominantly 1QP states with respect to the ground state of the even tin isotopes.

One can almost say that the experimental data displayed in Fig. 21 is consistent within the uncertainties arising from just the choice of optical-model parameters. This might serve as inducement for a series of experiments on the isotopes of tin involving both stripping and pickup reactions at subcoulomb energies to see just how closely the occupation parameters from stripping and pickup can be matched, and to try to explain the difference. The (d,t) and (t,d) reactions would be ideal since the Q values are much closer to zero for those reactions than for the (d,p) and (p,d) reactions. This is important because the neutron binding energies are high for the even tin isotopes, so Coulomb stripping conditions will be hard to realize for (p,d) reactions to the lowest states of the odd isotopes.

If we include in Eq. (33) a summation over j for all the orbits in the N=50 to 82 shell, then we should obtain from the sum of weighted spectroscopic factors the number of holes from that shell in the target ground state,

$$\sum_{\alpha j} (2j+1)\, S_{\alpha j} = \sum_{j} \langle \text{neutron holes} \rangle_{j} \,, \tag{35}$$

where we have taken $J_A = 0$ and $J_B = j$. For ^{116}Sn this should be 82-N = 16 holes to a high degree of accuracy, since the spectrum is fairly well known, and pickup reactions show no evidence of filling the next higher shell while stripping reactions show no evidence of holes from the next lower shell. Also, in the calculations of Ref.[5], $v_j^2 \cong 0.99$ for states of the next lower shell, and $u_j^2 \cong 0.98$ for states of the next higher

shell. The deviation of these quantities from unity is somewhat higher for ^{124}Sn than for ^{116}Sn.

The sum of our weighted spectroscopic factors is 15.4 for states in the N=50 to 82 shell in ^{117}Sn. The $h_{\frac{11}{2}}$ state contributes 9.5 to this sum, so it seems that on theoretical grounds we can say the absolute error in the $h_{\frac{11}{2}}$ spectroscopic factors in ^{117}Sn is considerably less than 30%. Perhaps 15% is a reasonable estimate for the absolute spectroscopic factors on all the low-lying states, wherever statistics permit. The sum in Eq. (35) for our results on the ^{124}Sn(d,p)^{125}Sn reaction is 6.4 rather than 8, the expected number of holes. This is consistent with our disagreement with theory for the spectroscopic factor for the $h_{\frac{11}{2}}$ ground state in ^{125}Sn as indicated in Fig. 21, and is fairly strong evidence that our measured ground state cross section is too low. If the same value of the neutron radius parameter were used for ^{124}Sn as was used for ^{116}Sn, then the spectroscopic sum would be increased from 6.4 to approximately 7.2. It is quite possible that our error in the ground state cross section is large enough to bring the sum of weighted spectroscopic factors down from 8.0 to 7.2.

The $d_{\frac{5}{2}}$ levels in the heavier odd isotopes are quite fragmented and lie at excitation energies near 1 MeV and higher, above the other main single-particle levels which we have just discussed, except for the $g_{\frac{7}{2}}$ in several cases. The level schemes above 1 MeV are complex and not well understood. Considerable theoretical effort has gone into attempts to explain many higher levels on the basis of weak or intermediate coupling models in which 1QP states are coupled to the first or second

vibrational states of the even-even core [2,3]. Higher states were also predicted in a more microscopic approach [4].

Several comparisons have been made between experiments and the predictions of these models especially for ^{117}Sn [8,9,28,30]. We will not add to the comparisons at this time, but hope that our more detailed (d,p) spectra including the new levels below 2 MeV in ^{125}Sn, and our more easily interpreted cross sections and spectroscopic factors will be useful in future attempts at understanding this region of the energy spectra of ^{117}Sn, ^{123}Sn, and ^{125}Sn.

It is interesting to note that in expanding their model space to obtain the odd-even mass difference with realistic interactions, Kuo, Baranger, and Baranger [66] included levels from the next neutron shell, so perhaps in the not too distant future there will be a possibility of some detailed understanding of the $f_{\frac{7}{2}}$ and p levels that dominate the (d,p) spectra at higher excitation energies in the odd tin isotopes.

CHAPTER VI

SUMMARY AND CONCLUSION

In order to obtain accurate spectroscopic factors and reduced widths for stripping to odd tin isotopes, we have studied the reactions $^{116}Sn(d,p)^{117}Sn$, $^{122}Sn(d,p)^{123}Sn$, and $^{124}Sn(d,p)^{125}Sn$ at incident deuteron energies between 4.35 and 5.55 MeV.

Despite the generally low cross sections and interference from low mass contaminants attendant with the low bombarding energies, many previously unreported levels were observed in all three residual nuclei. Most of the new levels are at excitation energies above 4 MeV. In ^{125}Sn, however, we have observed a new level at 0.859 MeV, and determined that the level at approximately 1.80 MeV is a doublet. Between 2- and 4-MeV excitation in ^{117}Sn, six levels are previously unreported and six are new to stripping reactions. Comparison is made between our results and those of other experiments to help establish the orbital and total angular momentum of the observed levels. The Q value for the reactions to the ground states of ^{117}Sn, ^{123}Sn, and ^{125}Sn is 4.720, 3.716, and 3.515 MeV, respectively.

Excitation functions for the $^{116}Sn(d,p)^{117}Sn$ reaction at 160° and deuteron energies between 4.35 and 5.35 MeV were measured for the first three states in ^{117}Sn. These showed relatively smooth variations with energy and were fitted well with DWBA calculations.

The angular distribution of the differential cross section was extracted for all levels resolved in the $^{116}Sn(d,p)^{117}Sn$ reaction at 5.35 MeV and the $^{124}Sn(d,p)^{125}Sn$ reaction at 5.55 MeV. The differential cross section at 160° was determined for all observed levels in the $^{122}Sn(d,p)^{123}Sn$ reaction at 5.15 MeV. Angular distributions were extracted for three levels populated in that reaction.

DWBA calculations with the computer code DWUCK were fitted to the experimental angular distributions to obtain spectroscopic factors for the reaction to twenty states in ^{117}Sn, three states in ^{123}Sn, and ten states in ^{125}Sn. Reduced widths were calculated for most of these states. The reduced widths are of value because they are independent of the rather large uncertainties in the calculation of the bound state wave function for the neutron.

Angular distributions of the differential cross section at several incident deuteron energies were extracted for certain states of interest in all three odd nuclei studied. Deduced spectroscopic factors for a given level were consistent at all energies to better than 10%.

Good fits to the angular distributions were obtained with DWBA calculations. The variation of the theoretical cross sections with reasonable variations in the optical-model parameters was observed to be less than about 12% in the worst cases. At higher energies, the variation in S is often much larger using parameter sets that fit the elastic scattering data equally well [15,55].

The absolute value but not the shape of calculated angular distributions are quite sensitive to the method of calculating the neutron

bound-state wave function. The separation energy prescription was used to determine the depth of the potential well for the neutron including a volume Woods-Saxon potential and a Thomas spin-orbit potential. If this common prescription is appropriate for the levels studied, then our analysis in Chapter IV indicated the major uncertainty in the calculated cross sections arises from the uncertainty in the geometrical parameters of the potential well for the neutron. However, application of the sum rule, Eq. (35), indicated that the geometrical parameters were chosen correctly for ^{116}Sn; so the absolute errors in spectroscopic factors are approximately the same as the uncertainty in the relative spectroscopic factors. The relative spectroscopic factors are probably accurate to better than 15%

For ^{122}Sn and ^{124}Sn the radius parameter r_n for the neutron well was increased 0.02 fm over the value for ^{116}Sn to 1.27 fm. This increase was based on recent determinations of relative rms neutron radii for the tin isotopes [57]. The sum of weighted spectroscopic factors, Eq. (35), for states in ^{125}Sn from the N=50 to 82 shell was 6.4 instead of the number of neutron holes, 8. This suggests that the increase in r_n for ^{122}Sn and ^{124}Sn was inappropriate, or that our somewhat uncertain cross section for the $h_{\frac{11}{2}}$ ground state of ^{125}Sn is much too small.

We have compared our spectroscopic factors with those obtained from other (d,p) experiments and from experiments using different reactions. The agreement is generally within the expected uncertainties, with one exception. The spectroscopic factors of Powell et al. [19] from the ^{124}Sn(d,p)^{125}Sn reaction at E_d = 5.1 MeV, and from DWBA

calculations similar to ours, are 20-30% smaller than our spectroscopic factors for the same states. The difference appears to be in the measured differential cross sections. The uncertainty in our absolute cross sections is approximately 7%.

The shell model states filling most rapidly in the tin isotopes are the $1h_{\frac{11}{2}}$, $2d_{\frac{3}{2}}$, $3s_{\frac{1}{2}}$, and to some extent, the $1g_{\frac{7}{2}}$ states. The occupation parameters for these states in the ground state of even tin isotopes are obtained approximately from experimental spectroscopic factors for the lowest state of the appropriate spin in the odd tin isotopes. The present experimental occupation parameters and those of other stripping and pickup experiments are compared with results from recent pairing theory calculations. There is general agreement of the experimental values with each other and the theory, although not always within the 15% accuracy we claim for the present results. It is concluded that pairing theory can describe fairly accurately the filling of the shell model states in the ground state of the even tin isotopes, and that the lowest levels of the odd tin isotopes can be described by predominantly one-quasi-particle states.

A particularly interesting test of the structure of tin isotopes and of the DWBA reaction theory at subcoulomb energies would be provided by comparison of u_j^2 and v_j^2 from (t,d) and (d,t) reaction studies similar to our (d,p) experiment.

LIST OF REFERENCES

1. Kisslinger, L. S., and R. A. Sorensen, Mat. Fys. Medd. Dan. Vid. Selsk. 32, No. 9 (1959).

2. Sorensen, R. A., Nucl. Phys. 25, 674 (1961).

3. Yoshida, S., Nucl. Phys. 38, 380 (1962).

4. Kuo, T. T. S., E. U. Baranger, and M. Baranger, Nucl. Phys. 79, 513 (1966).

5. Clement, D. M., and E. U. Baranger, Phys. A120, 25 (1968).

6. Alzetta, R., and J. Sawicki, Phys. Rev. 173, 1185 (1968).

7. Lee, H. C., and K. Hara, Phys. Rev. C3, 325 (1971).

8. Schneid, E. J., A. Prakash, and B. L. Cohen, Phys. Rev. 156, 1316 (1967).

9. Baranger, E. U., in Advances in Nuclear Physics, Vol. IV, ed. by M. Baranger and E. Vogt, (Plenum Press, New York, 1971), p. 261.

10. Posner, M., Phys. Rev. 158, 1018 (1967).

11. Gibson, F. P., and A. K. Kerman, Phys. Rev. 145, 758 (1966).

12. Cavanagh, P. E., C. F. Coleman, A. G. Hardacre, G. A. Gard, and J. F. Turner, Nucl. Phys. A141, 97 (1970).

13. Samour, C., J. Julien, J. M. Kuchly, R. N. Alves, and J. Morgenstern, Nucl. Phys. A122, 512 (1968).

14. Goldfarb, L. J. B., Nucl. Phys. 72, 537 (1965).

15. Jeans, A. F., W. Darcey, W. G. Davies, K. N. Jones, and P. K. Smith, Nucl. Phys. A128, 224 (1969).

16. Rapaport, J., and A. K. Kerman, Nucl. Phys. A119, 641 (1968).

17. Dost, M., and W. R. Hering, Phys. Rev. Letters 19, 488 (1965).

18. Torti, R., and R. Graetzer, Nucl. Phys. A171, 305 (1971).

19. Powell, D. L., P. J. Dallimore, and W. F. Davidson, Report No. ANU-P/511, (Australian National University, 1971, to be published).

20. Yamaya, T., Y. Nakagome, Y. Hiratate, S. M. Lee, S. Iwasaki, T. Tohei, and S. Morita, Nucl. Phys. A126, 449 (1969).

21. Reich, C. W., G. C. Phillips, and J. L. Russel, Phys. Rev. 104, 143 (1956).

22. CN Van de Graaff Log Book, 1971, (University of Arizona), p. 92.

23. Andersson-Lindstroem, G., Nucl. Instr. and Meth. 56, 309 (1967).

24. Zurstadt, D., Utilization Report No. CYC-6833, University of Colorado, 1969 (unpublished).

25. Endt, P. M., and C. van der Leun, Nucl. Phys. A105, 1 (1967).

26. Maples, C., G. W. Goth, and J. Cerny, Report No. UCRL-16964, (University of California, Lawrence Radiation Laboratory, 1966).

27. Dally, E. B., J. B. Nelson, and William R. Smith, Phys. Rev. 152, 1072 (1966).

28. Beery, D. B., G. Berzins, W. B. Chaffee, W. H. Kelly, and W. C. McHarris, Nucl. Phys. A123, 649 (1969).

29. Baedecker, P. A., A. Pakkanen, and W. B. Walters, Nucl. Phys. A158, 607 (1970).

30. Yagi, K., Y. Saji, T. Ishimatsu, Y. Ishizaki, M. Matoba, Y. Nakajima, and C. Y. Huang, Nucl. Phys. A111, 129 (1968).

31. Robinson, R. L., F. K. McGowan, P. H. Stelson, W. T. Milner, and R. O. Sayer, Nucl. Phys. A123, 193 (1969).

32. Cohen, B. L., and R. E. Price, Phys. Rev. 121, 1441 (1961).

33. Yamazaki, T., and G. T. Ewan, Nucl. Phys. 134, 81 (1969).

34. Nealy, C. L., and R. K. Sheline, Phys. Rev. 135, B325 (1964).

35. Boyd, R. N., and R. Arking, private communications.

36. Arking, R., R. N. Boyd, J. C. Lombardi, A. B. Robbins, and B. Gonsior, Nucl. Phys. A155, 480 (1970).

37. Borello, T., O. Dietzsch, E. Frota-Pessoa, E. W. Hamburger, and C. Q. Orsini, in Proceedings of the International Conference on Properties of Nuclear States, Montreal, Canada, (Les Presses de l'Universite de Montreal, 1969), p. 739.

38. Kunz, P. D., private communication.

39. Kunz, P. D., Report No. COO-535-613, University of Colorado, 1969 (unpublished).

40. Kunz, P. D., Report No. COO-535-606, University of Colorado, 1969 (unpublished).

41. Austern, N., Direct Nuclear Reaction Theories, (Wiley-Interscience, New York, 1970).

42. Perey, F. G., Phys. Rev. 131, 745 (1963).

43. Austern, N., Phys. Rev. 136, B1743 (1964).

44. Pinkston, W. T., and G. R. Satchler, Nucl. Phys. 72, 641 (1965).

45. Sugawara, Kazuko, Nucl. Phys. A110, 305 (1968).

46. Hutton, J. L., Nucl. Phys. A120, 657 (1968).

47. Prakash, A., and N. Austern, Ann. Phys. (N.Y.) 51, 418 (1969)

48. Perey, F., and B. Buck, Nucl. Phys. 32, 353 (1962).

49. Ulrici, W., and W. R. Hering, Nucl. Phys. A110, 281 (1968).

50. Dost, M., W. R. Hering, and W. R. Smith, Nucl. Phys. A93, 357 (1967)

51. Dar, A., A. de-Shalit, and A. S. Reiner, Phys. Rev. 131, 1732 (1963)

52. Perey, C. M., and F. G. Perey, Phys. Rev. 132, 755 (1963).

53. Dickens, J. K., and F. G. Perey, Phys. Rev. 138, B1086 (1965).

54. Durish, J. E., and R. R. Johnson, Phys. Rev. 137, B904 (1965).

55. Robertshaw, J. E., S. Mecca, A. Sperduto, and W. W. Buechner, Phys. Rev. 170, 1013 (1968).

56. Greenlees, G. W., G. J. Pyle, and Y. C. Tang, Phys. Rev. 171, 1115 (1968).

57. Boyd, R. N., J. Fenton, M. Williams, T. Kruse, and W. Savin, Nucl. Phys. A162, 497 (1971).

58. Lee, L. L., J. P. Schiffer, B. Zeidman, G. R. Satchler, R. M. Drisko, and R. H. Bassel, Phys. Rev. 136, B971 (1964).

59. Richard, P., C. F. Moore, J. A. Becker, and J. D. Fox, Phys. Rev. 145, 971 (1966).

60. Williams, N., D. von Ehrenstein, J. A. Nolen, Jr., and G. C. Morrison, in Proceedings of the Conference on Nuclear Isospin, Asilomar-Pacific Grove, California, 1969, ed. by J. D. Anderson, D. Bloom, J. Cerney, and W. W. True, (Acad. Press, New York, 1969), p. 695.

61. Yoshida, S., Phys. Rev. 123, 2122 (1961).

62. Bes, D. R., and R. A. Sorensen, in Advances in Nuclear Physics, Vol. II, ed. by M. Baranger and E. Vogt, (Plenum Press, New York, 1969), p. 165.

63. French, J. B., and M. H. Macfarlane, Nucl. Phys. 26, 168 (1961).

64. Cavanagh, P. E., Report No. AERE-R 5801, United Kingdom Atomic Energy Authority Research Group, 1968 (unpublished).

65. Cavanagh, P. E., Report No. AERE-R 5901, United Kingdom Atomic Energy Authority Research Group, 1968 (unpublished).

66. Kuo, T. T. S., E. U. Baranger, and M. Baranger, Nucl. Phys. 81, 241 (1966).